METHODS OF IMPROVING HIGH FREQUENCY DIRECT INJECTION TESTING

Dr. Jane Lehr
Mr. Roy Sizemore
Maj. Paul Barre
Lt. Eric Johnson

Fiore Industries, Inc.
5301 Central Ave. NE, Suite 900
Albuquerque, New Mexico 87108

January 1997

Final Report

DTIC QUALITY INSPECTED 3

PHILLIPS LABORATORY
Advanced Weapons and Survivability Directorate
AIR FORCE MATERIEL COMMAND
KIRTLAND AIR FORCE BASE, NM 87117-5776

19970516 078

PL-TR-97-1057

PAUL R. BARRÉ, Maj, USAF
Project Manager

FOR THE COMMANDER

JAMES J. ROONEY, JR, Lt Col, USAF   WILLIAM G. HECKATHORN, Col, USAF
Chief, Electromagnetic Effects Division   Director, Advanced Weapons
                                             and Survivability Directorate

REPORT DOCUMENTATION PAGE

Public reporting burden for this collection of information is estimated to average 1 hour per response, including the time for reviewing instructions, searching existing data sources, gathering and maintaining the data needed, and completing and reviewing the collection of information. Send comments regarding this burden estimate or any other aspect of this collection of information, including suggestions for reducing this burden, to Washington Headquarters Services, Directorate for Information Operations and Reports, 1215 Jefferson Davis Highway, Suite 1204, Arlington, VA 22202-4302, and to the Office of Management and Budget, Paperwork Reduction Project (0704-0188), Washington, DC 20503.

1. AGENCY USE ONLY (Leave blank)	2. REPORT DATE	3. REPORT TYPE AND DATES COVERED
	31 January 1997	1 January 1996 through 31 January 1997

4. TITLE AND SUBTITLE
Methods of Improving High Frequency Direct Injection Testing

5. FUNDING NUMBERS
C: F29601-95-C-0025
PE: 62601F
PR: 5797
TA: AL
WU: 03

6. AUTHOR(S)
Dr. Jane Lehr
Mr. Roy Sizemore
Maj. Paul Barre and Lt. Eric Johnson

7. PERFORMING ORGANIZATION NAME(S) AND ADDRESS(ES)
Fiore Industries Inc.
5301 Central Avenue NE, Suite 900
Albuquerque, New Mexico 87108

8. PERFORMING ORGANIZATION REPORT NUMBER

9. SPONSORING/MONITORING AGENCY NAME(S) AND ADDRESS(ES)
Phillips Laboratory
3550 Aberdeen Ave. SE
Kirtland AFB, NM 87117-5776

10. SPONSORING/MONITORING AGENCY REPORT NUMBER

PL-TR-97-1057

11. SUPPLEMENTARY NOTES

12a. DISTRIBUTION AVAILABILITY STATEMENT
Approved for public release; distribution is unlimited.

12b. DISTRIBUTION CODE

13. ABSTRACT (Maximum 200 words)

Direct injection testing is a valuable tool for identifying electromagnetic effects and critical subsystems prior to expensive, labor intensive free-field testing. However, as the frequencies of interest increase, the method becomes less reliable and the measurement techniques become more difficult. A major problem has been the frequency response of the voltage probes. This effort has identified the cause of the degradation of the voltage dividing ratio with frequency, through experiment and circuit simulation, as a capacitive effect. Moreover, the effective capacitance has been quantified, and constraints on the resistive element have been devised. An improved compact voltage probe is demonstated which shows a flat frequency response to 3 GHz.

Other issues which have been addressed are the importance of measuring the node impedance to ground; comparison of direct injection vulnerability levels with those obtained with free field testing; the practice of using incident power as a metric; using a transmission line as a voltage probe; and probe loading effects.

14. SUBJECT TERMS
RF, Electromagnetics Effects, Direct Injection Testing, Voltage Probes

15. NUMBER OF PAGES
120

16. PRICE CODE

17. SECURITY CLASSIFICATION OF REPORT	18. SECURITY CLASSIFICATION OF THIS PAGE	19. SECURITY CLASSIFICATION OF ABSTRACT	20. LIMITATION OF ABSTRACT
Unclassified	Unclassified	Unclassified	UL

i

Table of Contents

Figures

Tables

EXECUTIVE SUMMARY

Direct injection testing is a valuable tool for identifying electromagnetic effects and critical subsystems prior to expensive, labor intensive free field testing. However, as the frequencies of interest increase, the method becomes less reliable, and the measurement techniques become more difficult.

This team was tasked with identifying and addressing key sources of error in the present methods of conducting direct drive testing. Many variations of experimental procedures exist, and the information contained in this document will not necessarily be pertinent to every testing scenario. Alternately, in addition to direct injection testing, much of the material covered herein is general, and hence, pertinent to a wide variety of experimental efforts, including free field electromagnetic effects testing.

Three major areas of direct drive testing have been addressed: the correlation between direct drive and free field power levels for upset, the relevant power quantities, and measurements using voltage dividing probes.

The most extensive treatment was given to the voltage probe. Both capacitive and resistive loading of the circuit is discussed. Criteria for choosing the probe input impedance is given. A subtlety of the impact of the choice of probe is that the closer the input impedance is to its minimum acceptable value, the more sensitive the probe will be. Thus, it is imperative that the node impedance be known prior to probe selection.

Various probes were evaluated, both experimentally and through simulation. It was found that the most commonly used probes suffer from capacitive degradation, with a capacitance which is much higher than commonly believed. We demonstrate the operation of probes which have no discernable degradation in its transfer function to 3 GHz. Additionally, a calibration fixture has been designed which allows for quick and easy pretest probe characterization.

Although many test engineers measure incident power only, the absorbed power is the relevant quantity. The crux of this assertion was expanded to derive a correlation factor to adjust power levels for upset obtained through direct drive experiments with free field power levels causing the same upset.

1

1.0 INTRODUCTION

The development of microwave weapons is currently a promising research area. In conjunction with High Power Microwave (HPM) source development, programs to detect the vulnerabilities of electronic systems to high frequency electromagnetic radiation have been implemented. In addition to electromagnetic hardening technique development, a strong interest has arisen in developing economical methods to obtain system vulnerability information. One of the more successful techniques has been direct drive experiments, where a voltage signal is injected directly onto a node of the device under test (DUT). The critical parameters are the frequency and power level at which an asset is susceptible. Thus, direct injection experiments can be combined with low power free field coupling measurements to determine the incident power density for asset susceptibility. At frequencies below 100 MHz, good agreement between test results obtained in free field tests and direct injection experiments has been shown. *

While the reliability of test data in the frequency range 100-400 MHz is debatable, the techniques currently being used at frequencies above 400 MHz are known to be unreliable. Currently, the frequencies of interest, common to both the electromagnetic susceptibility and HPM source communities, are approaching the 10 GHz range. While this effort was limited to frequencies up to 3 GHz, the techniques outlined in this report are anticipated to also be valid in the higher frequency regime. Testing procedures in this report are also valid in the lower frequency regime, but may not be critical since high frequency techniques depend largely on the reactive parameters, which have a negligible effect at low frequency.

It is the mission of this team to develop a reliable and technically sound methodology to perform direct injection tests at frequencies above 400 MHz.

---

* Hector del Aguilar (PL/WSM), private communication.

1.1 Objectives

The primary objectives of this preliminary test effort are:

1.) Determine the issues in the current state of the art direct drive techniques.

2.) Examine these issues in the frequency range of 400 MHZ to 3 GHz.

3.) Develop improved experimental techniques which will result in the development of a reliable high frequency direct drive test methodology.

2.0   OVERVIEW OF DIRECT INJECTION TESTING TECHNIQUES

The direct injection of signals into an electronic system allows economical testing of electromagnetic immunity, and several variations of this testing technique are currently in use. For clarity, a brief discussion of the two dominant techniques of conducting direct injection tests are elucidated.

The direct injection technique of system vulnerability testing was initially developed by the Electromagnetic Pulse (EMP) community as a simulation of a free field EMP test. ** Since aircraft are a main target of an EMP strike, the direct injection methods developed around the testing of avionic subsystems. The "bulk current injection" method uses inductive coupling to transfer current from an external source onto the wire bundles that connect the avionic systems. A representative test arrangement is shown in Figure 1.
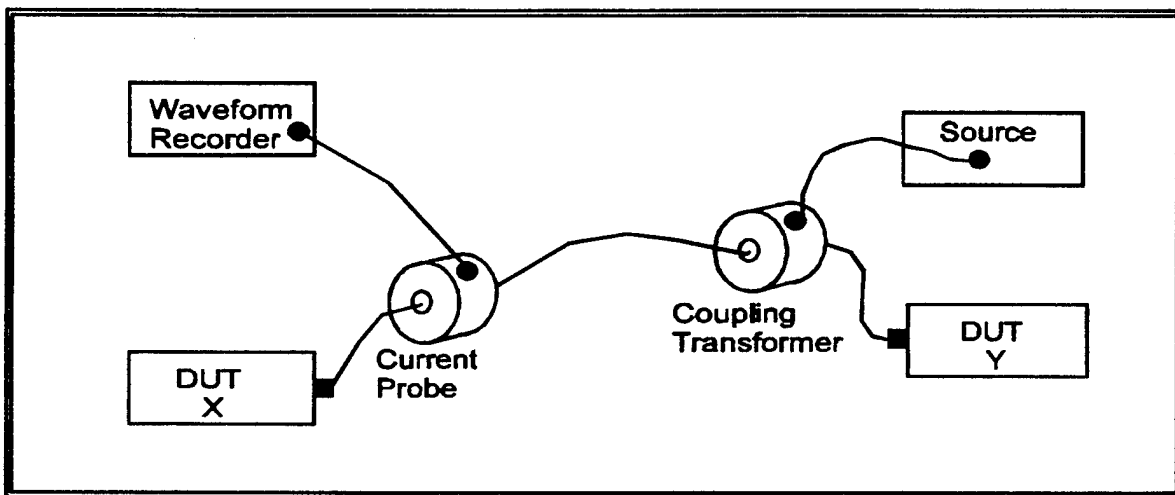
Figure 1.   Typical experimental arrangement of a bulk current injection into an avionics system for the simulation of electromagnetic effects.

The advantages of bulk current injection onto a wire bundle are numerous. Low power signals can be inductively coupled to induce currents that would require very high radiated power to achieve. Since surface currents induced on the skin of the aircraft are reactively coupled to

---

**   William D. Prather, (PL/WSQ), private communication.

4

internal wiring, the coupling is linear and the resonances determined at low power can extrapolate to high power.[1] Although this testing technique is generally valid to within a factor of two of the free field data, this is strongly dependent on the implementation of the technique. For instance, one comparative study[1] injected one wire of a bundle through bulk current injection and found large variations between the susceptibilities due to bulk current injection and free field radiation. The authors concluded that multiple or distributed coupling techniques should be investigated in hope that better agreement could be attained. A theoretical investigation of the currents induced by bulk current injection and free field radiation indicate that the two testing procedures differ significantly when the lengths of the wire bundles are long. However, when these leads are kept electrically short ($kL \ll 1$), the currents induced via bulk current injection and free field radiation are comparable.[2]

While the method of bulk current injection is an important implementation of the technique, particularly for avionics systems, its applicability is severely limited in frequency. Bulk current injection couplers use a magnetic core, which resists the passage of high frequencies. Bulk current injection probes have been extended to 1 GHz[3] using air core couplers with limited success: the air couplers are useful for receivers, but not as injection couplers.[**]

In an effort to expand the direct drive test methodology to more complex systems and higher frequencies, testing is being conducted by connecting a source directly to the system under test. A representative experimental setup is shown schematically in Figure 2.

This arrangement, if properly conducted, is capable of identifying high frequency vulnerability data, if any. Moreover, this technique of directly injecting of an electric signal into a device under test is suitable for compact and complex systems which may have limited physical accessibility. To date, reliable high frequency direct injection data for electromagnetic susceptibility has been sparse. This report identifies several key issues within the testing procedure for the measurements to be believable. Many of the issues concerning direct drive experiments, particularly the design of invasive voltage probes, are of a general nature and apply to a variety of testing techniques, including free field HPM testing.

**   William D. Prather, (PL/WSQ), private communication.
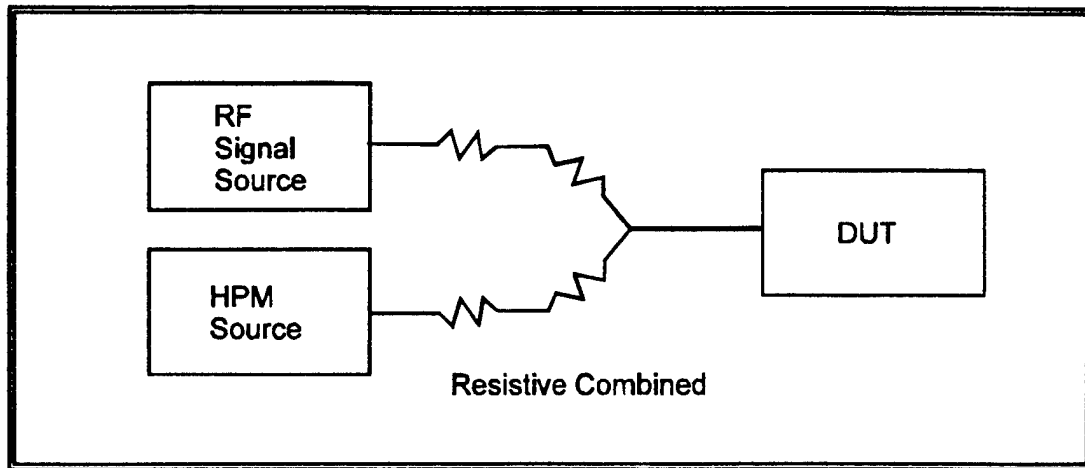
Figure 2a. Illustration of a direct drive experiment where two signals are combined resistively.
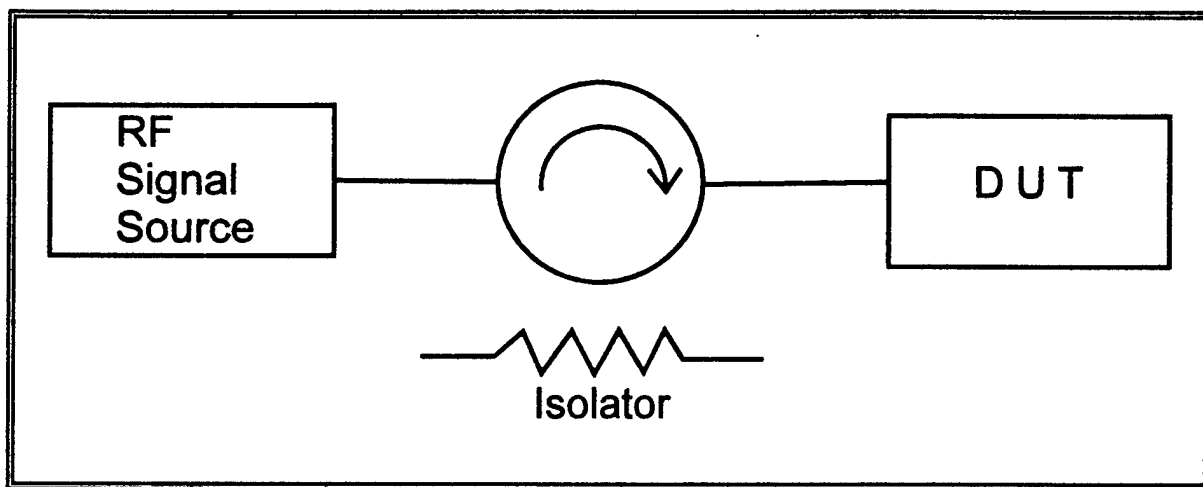
Figure 2b. A direct drive experiment in which the RF signal source injection directly into the node of the DUT. Typically, the voltage is monitored at the injection site.

3.0 VOLTAGE PROBES

The paradox of probe design is the development of a method which invades in order to obtain knowledge about a system without perturbing the system. Of course, the introduction of any probe into any system necessarily perturbs the system. Thus, the crux of probe design is to minimize the effect of the probe on the system, while gaining information with sufficient sensitivity to be useful.

3.1 General Conditions on Invasive Probe Design

Electrical measurements can be made with a variety of techniques which can be described as either invasive (voltage dividers, current viewing resistor) or noninvasive (inductive couplers, B-dot and Rogowski coils). This treatise will be limited to issues concerning invasive probes.

The following are general criteria[4, 6] which all suitable voltage probes will meet. The consequence of not meeting these requirements is incorrect measurements. For a voltage probe to be satisfactory for the observation and measurement of electrical characteristics the requirements are:

- The input impedance of the voltage divider is sufficiently high, so that no appreciable disturbance is introduced in the circuit under test. In a circuit sense, the probe draws only a minimum of current from the circuit for measurement purposes. Thus, the probe impedance must be high in comparison to the node impedance of the circuit under test.

- The probe has a linear uniform transient response over a wide range of frequencies. That is, the probe must not distort the waveforms under investigation.

- The divider should be capable of precise calibration with standard laboratory methods and apparatus.

3.2 Voltage Divider Fundamentals

Voltage division is a frequently used and reliable method of measuring voltage without perturbing the system under test. The basic voltage divider circuit is shown in Figure 3.
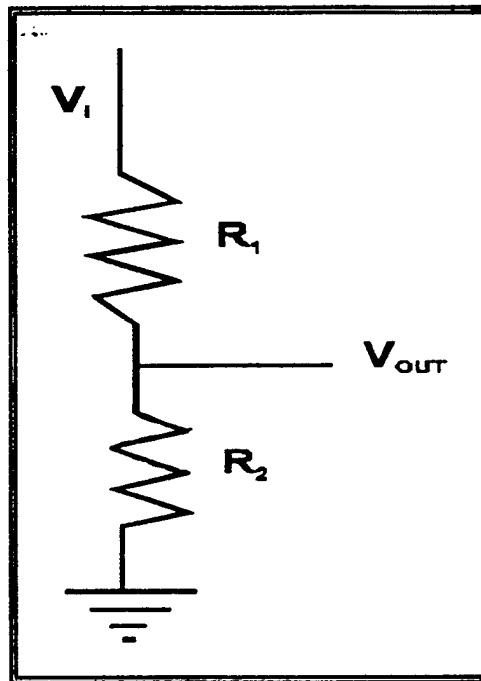
Figure 3.   The equivalent circuit of a basic voltage divider circuit.

3.2.1   Derivation of the Voltage Divider Relation

The derivation of the voltage divider relation is based on the schematic of Figure 3. Implementation of Kirchhoff Voltage Laws yield,

$$V_i = I (R_1 + R_2) ,$$

and

$$V_{out} = I R_2 ,$$

where I is the current flowing through the circuit. Thus,

$$I = \frac{V_{out}}{R_2} \quad .$$

Substituting this expression for the current into the equation for V_i yields an expression for the voltage division ratio, V_i/V_{out},

$$\frac{V_i}{V_{out}} = \frac{R_1 + R_2}{R_2} \quad .$$

This ratio is the fundamental basis for a voltage divider circuit. When a voltage divider probe is constructed from real, nonideal components, additional assumptions for its operation surface. This will be examined later in Sections 4.2 and 4.4.2.

Figure 3 refers only to the voltage divider itself. The current though the voltage divider is provided by the node of the circuit being monitored. As elucidated in Section 3.1, the input impedance of the voltage divider is assumed to be much greater than the impedance of the node under test. This condition limits the current drawn from the circuit being monitored. If an excessive amount of current is drawn from the circuit, the probe is said to "load the circuit." Circuit loading will result in measurement errors.

To avoid circuit loading with a voltage divider the input impedance of the probe, R_p, which is given by

$$R_p = R_1 + R_2 \quad ,$$

should exceed the impedance of the node under test, R_n, by a factor of at least 10.[4-6] Thus, the condition to insure for proper voltage divider probe operation is expressed mathematically as,

$$R_p \geq 10 \, R_n \quad .$$

3.2.2 Validation of the Loading Criteria

If the condition $R_p \geq 10\, R_n$ is not met, then the circuit being monitored is loaded by the probe, and the measurement, V_i does not accurately reproduce the generator voltage, V_n, at the oscilloscope or other measuring device. To examine the origin of the condition $R_p \geq 10\, R_n$, suppose that $R_p = 10\, R_n$. The experimental setup and the equivalent circuit is shown in Figure 4, with $R_p = R_1 + R_{Scope}$.

A voltage divider is formed by the combination of Rp and Rn. The effect of the relative values of R_p and R_n will be evaluated using both the voltage divider relation and the Thevenin equivalent circuit. Substituting the relative values, $R_p = 10\, R_n$ into the voltage divider relation yields,

$$V_n = V_i \frac{10 R_n + R_n}{10 R_n} = \frac{11}{10} V_i$$

and the measured voltage, V_i, is approximately that of the circuit node.
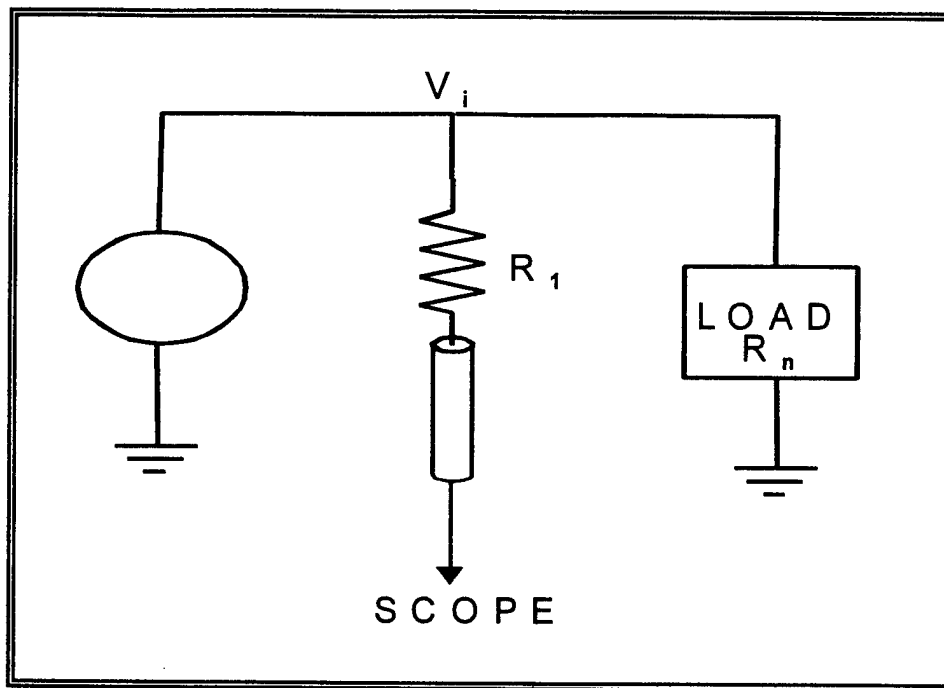
Figure 4a. The experimental setup of a voltage divider measuring a circuit node of impedance, R_n.
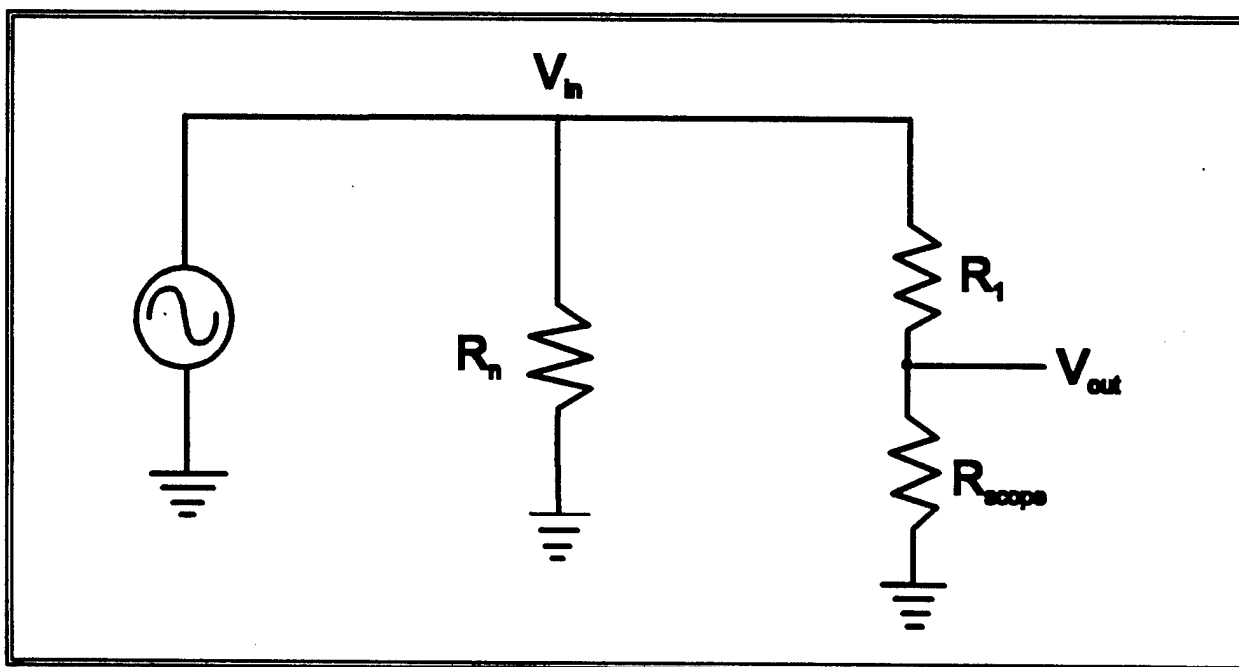
Figure 4b. The equivalent circuit of the experimental setup of Figure 4a.

The same conclusion can be reached using the Thevenin equivalent circuit for the circuit of Figure 4. The addition of the probe impedance, R_p effectively modifies the source impedance and reduces the amplitude of the signal at the viewing port. The effect of loading can be evaluated using Thevenin's theorem. The equivalent Thevenin source voltage, V_{TH}, is

$$V_{Th} = V_n \frac{R_p}{R_p + R_n}$$

As previously stated, the industry standard for an acceptable probe input resistance, R_p, to measure a node resistance, R_n, is

$$R_p \geq 10 R_n$$

Using the minimum value of the above criteria, the Thevenin equivalent circuit parameters becomes,

$$V_{Th} = V_n \frac{R_p}{R_p + R_n} = V_n \frac{10 R_n}{11 R_n} \quad ,$$

•and

$$V_{TH} \approx V_n$$

Thus, the industry standard,[5] $R_p > 10 \ R_n$, is justified.

3.3   Overview of Voltage Divider Probe Designs

A common method of observing and measuring a transient signal is to insert a voltage divider between the circuit under test and the transient signal recorder, such as an oscilloscope or network analyzer. Voltage division is a popular technique since the magnitude of the signals of interest may exceed the rating of the measuring apparatus. For the measurement to be useful, the voltage divider must accurately reproduce the voltage waveform at the node of the circuit under test, without perturbing the normal operation of the circuit. Of course, the introduction of an additional component into a circuit necessarily perturbs it. Thus, a good probe design reproduces the true signal parameters at the node of the DUT while minimizing the effect of its introduction into the circuit. A probe which loads a circuit will register a faulty reading by drawing excessive current. Circuit loading is an insidious effect which can easily go undetected by the experimenter.

3.3.1   The Capacitively Compensated Voltage Divider Probe

High impedance voltage dividing probes which are designed for parallel connection to a pulse generator are generally either resistive or capacitive dividers. In practice, however, stray reactance and intrinsic resistance values must also be incorporated into the design. The inductance, which causes a lag in the voltage, should be minimized for high frequency and pulsed voltage divider probe designs. In addition to a low inductance probe design, the inductance is minimized by keeping the connecting leads short and making the ground connections directly to the chassis. Capacitive reactance is often ignored, since the capacitance components can be incorporated into a compensated resistive voltage divider. In compensated voltage divider designs, high quality capacitors are used to enhance performance.[4] The schematic for a capacitively compensated voltage divider is shown in Figure 5.
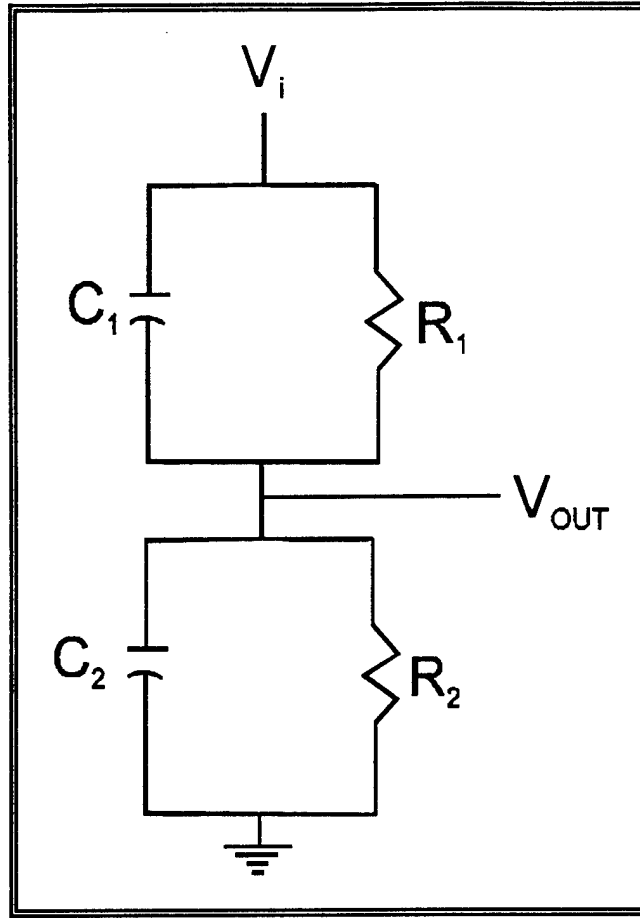
Figure 5. **Equivalent circuit of a capacitively compensated voltage divider.**

Kirchoffs voltage law for the parallel capacitively compensated divider provides the expression for the output voltage, V_{Out}, as

$$V_{Out} = V_i \left[\frac{R_2}{R_1 + R_2} + \left(\frac{C_1}{C_1 + C_2} - \frac{R_2}{R_1 + R_2} \right) e^{-\frac{t}{R_iC_i}} \right]$$

where R_i and C_i are the parallel combination of the respective components. For the condition when

$$R_1 C_1 = R_2 C_2 \quad ,$$

14

•then

$$\frac{R_2}{R_1 + R_2} = \frac{C_1}{C_1 + C_2} \quad ,$$

and

$$\frac{V_{Out}}{V_I} = \frac{R_2}{R_1 + R_2} = \frac{C_1}{C_1 + C_2} \quad .$$

Thus, the capacitively coupled voltage divider provides a perfect voltage divider whose voltage division ratio is the same at all frequencies. However, the basic assumption, $R_1 C_1 = R_2 C_2$, implies the charging time constants for each leg of the circuit of Figure 5 is the same. For very high frequency signals, the required charge time constant, τ, may not allow the replication of the signal with a capacitively compensated divider. For instance, the time constant necessary to measure a signal of frequency, f, is given by,

$$\tau = \frac{1}{5f} \quad .$$

This equation is derived from the signal period, T = 1/f, and the definition of the time constant of a circuit. That is, it takes five time constants to fully charge a circuit. If a 10 GHz signal is to be measured, with a 1 kΩ resistor, the time constant is on the order of 10^{-11}s. The capacitance value is obtained from the relation,

$$\tau = RC \quad ,$$

and is computed to be 0.01 pF. This value is the equivalent capacitance which includes the stray capacitance as well as the cable capacitance. A capacitance value of 0.01 pf generally exceeds the stray capacitance. Thus, this is an unrealistically small value for a reasonable length of cable.

Commercially available capacitively compensated voltage probes are limited to below frequencies of 150 MHz and risetimes of 1.0 ns.[5]

3.3.2 The Z_0 Voltage Divider Probe

In view of the brief treatise on capacitively coupled voltage dividers for high frequency applications, a purely resistive divider is desired. The capacitance which is associated with high frequency recording devices, such as network analyzers and oscilloscopes, is necessarily small, and the capacitance of the purely resistive probe should be minimized; this avoids the need for capacitive compensation and permits the measurement of higher frequencies.

Z_0 voltage divider probes are so called because they use a "lossless" transmission line to connect to the measuring device. The schematic of a Z_0 probe is shown in Figure 6.

$$\frac{V_I}{V_{OUT}} = \frac{R_{SCOPE} + R_1}{R_{SCOPE}}$$
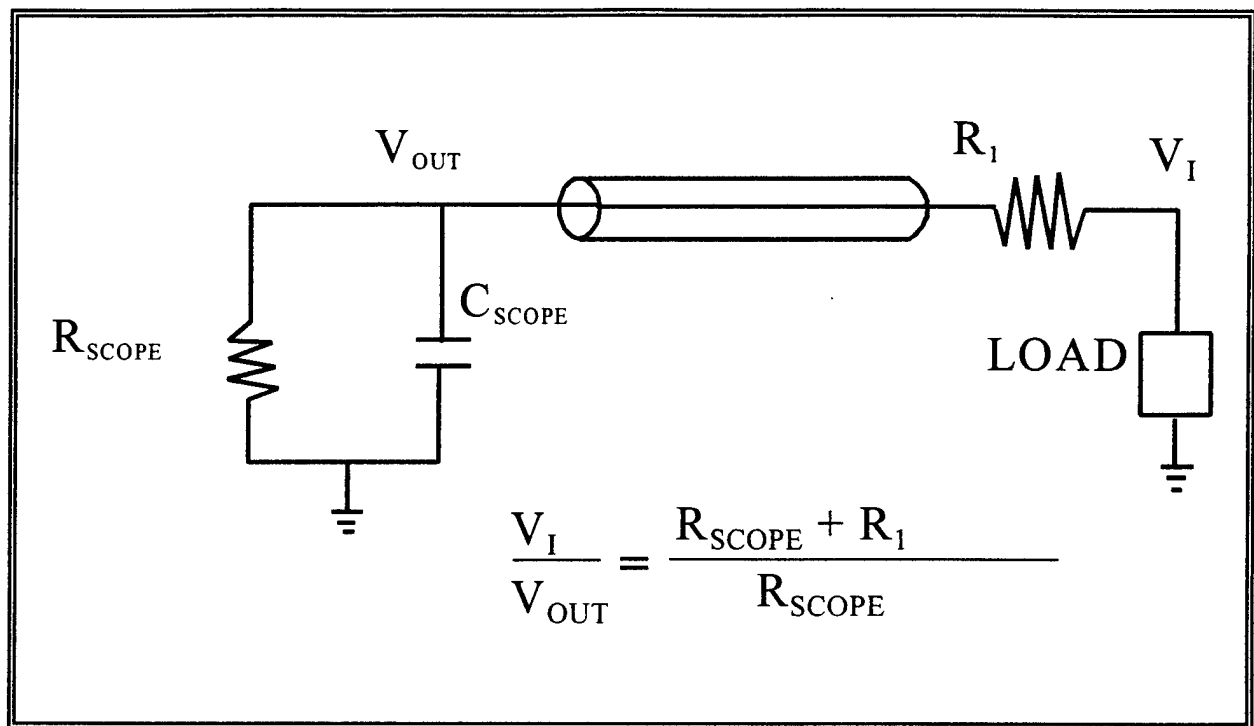
Figure 6. **The schematic of a Z_0 voltage divider probe.**

The Z_0 probe is designed to drive a 50 Ω input impedance on the measuring device. When using an oscilloscope as the waveform recorder, the 50 Ω termination must be used for two reasons: the low impedance (1) has an intrinsically low shunt capacitance and (2) provides the voltage division. The high impedance resistor, R_1, fully determines the voltage division

ratio. The voltage division ratio is

$$\frac{V_i}{V_{out}} = \frac{R_1 + R_{Scope}}{R_{Scope}} \quad,$$

and the input impedance of this probe is,

$$R_P = R_1 + R_{Scope} \quad.$$

Thus, both the input impedance and the voltage dividing ratio, when used with standard waveform recording devices, is fully determined by the resistor value, R_1.

The Z_0 probe has a low input capacitance which is desirable for high speed signals. Because this probe is relatively low impedance, care must be taken to avoid circuit loading. The value of the resistor, R_1, is limited to 5 kΩ in commercial Z_0 probes which is due to stray capacitance at the probe head.

Since R_1 is typically a ½ W resistor, the DC input voltage is limited to 16 V. Allowable sine wave peak voltage is 45 V. The use of a DC block, with typical capacitance value of 4700pF, will allow the measurement of signals with DC components of up to 500 V, but will limit the frequency response. The frequency for which the probe's response is 30% down (the 3dB point) can be calculated from

$$f = \frac{1}{2\pi C (R_P + R_{node})} \quad,$$

where C is the capacitance of the DC block.

In general, Z_0 probes have faster risetimes than capacitively compensated probes and are used primarily for the measurement of high frequency signals because they provide a low capacitance load. Moreover, the simplicity of the design allows for their easy construction, even for use in challenging experimental arrangements.

17

3.3.3   The Coaxial Transmission Line as a Voltage Probe

Recently, the 50 Ω voltage probe has become popular in direct injection testing because of its excellent frequency response. A coaxial commercially available transmission line can be used in this manner. However, the applicability of this type of probe is limited to circuits with very small node impedances. However, if the condition $R_p < 10\ R_{node}$ is met, this is an excellent choice. Many high frequency 50 Ω commercial voltage probes are available for digital circuit testing.

The experimental arrangement for testing with this type of probe is shown in Figure 7.
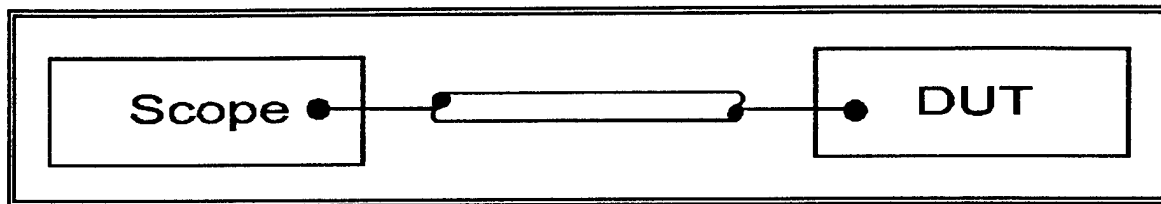
Figure 7.   **A coaxial transmission line inserted into a circuit for use as a voltage probe.**

The lossless transmission line is soldered directly onto the node under test and measured on a recording device. This arrangement provides no voltage division and care must be taken not to exceed the voltage rating of the measuring device. Thus, the signal which is recorded is the actual measurement, and the voltage division ratio is 1. Since this type of probe has an intrinsically low capacitance, the frequency response is excellent. Experimental verification of both the frequency response and the effect of node impedance is illustrated in Section 7.2.

3.4   Ranking of Probe Performance on EMPTAC tests

The problem of measuring waveforms during direct drive tests has long been known. To aid in testing, a team of test engineers had evaluated the performance of various types of probes.[7] The results are reproduced in Table 1. The probes are ranked with explanatory comments.

Rank ordering of probes

Rank	Probe	Rationale
1	Passive Probe	The measurement errors were small, the costs low and the probes easy to use for large to moderately sized LRUs. If the probes were repackaged to make them smaller, their usefulness would be extended.
2	Coax with Series Resistor	The measurement errors were small as long as the series resistor was significantly greater than the load resistance. They take little space; however, they are fragile and difficult to install. If this type of probe would be commercially produced to improve the operational problems with soldering and mechanical stress, this sensor would rank with the commercial passive voltage probes. They are relatively inexpensive.
3	Current Probe	The measurement errors were small. The measurement can be made external to the LRU. Impedance measurements are not easy to make; however, in some instances, a simple constant load impedance can be used. The effectiveness of the probe can be noise limited depending on the induced wire currents. The costs for the probes are low. This technique could be combined with a voltage measurement as indicated above to calculate an equivalent load impedance. This could then be used with current measurements to speed up testing.
4	Active Differential Probe	The measurement errors were assumed to be very small. A full-up system (rather than the adapted system used) should provide measurements with the lowest noise. The installation of the probe is very difficult. The probe head and the associated fiber-optic link will not fit into small spaces. The probe is very expensive and requires a differential input NanoFast fiber-optic link to derive its power. Use of this probe should be very limited.
5	Coax	Largest errors. Easy to install and use.

Table 1.   The ranking of probes used in testing the EMPTAC[7]

19

The passive probes are deemed the best by the authors of this ranking, particularly for large line replaceable units (LRUs). These commercially available probes, however, can be too large for some systems and have a limited voltage range. Commercially available voltage probes are typically capacitively compensated, and therefore, have a limited bandwidth. For lower frequency applications, similar (capacitively coupled) probes could be constructed, on site, using very small components, thereby extending their usefulness. The bandwidth of the commercially available version of this probe is such that it is not applicable for high frequency applications.

The probe which is ranked second is the one that is typically used in direct drive testing, and has been discussed in Section 3.3.2. The "rationale" comments state that the impedance of the asset relative to the probe input impedance determines the accuracy of the measurement. This is true for all voltage divider measurements and, more precisely, the probe input impedance should be greater than ten times the asset impedance. That is to be contrasted with the inaccurate measurements obtained with the coax probe. Although the coax probe has an excellent frequency response, accurate measurements are obtained only if the node impedance is less than 5Ω. That is, the coax has an input impedance of 50Ω, and thus, accurate measurements can be obtained for load impedances whose value is less than 5Ω.

4.0 PROBE LOADING EFFECTS

Network theory provides a valid model to portray the complicated systems under test by the direct injection method of HPM simulation. In general, any system can be represented by a n-port network, where each circuit node is a potential port. In direct injection testing, the device under test is represented by at least a 1-port, which is the case where the signal is monitored at the node being driven. Moreover, a model can be generated in which the direct drive source is part of the network, and the asset is a one port with the voltage probe as the load. This model is represented by Figure 8.
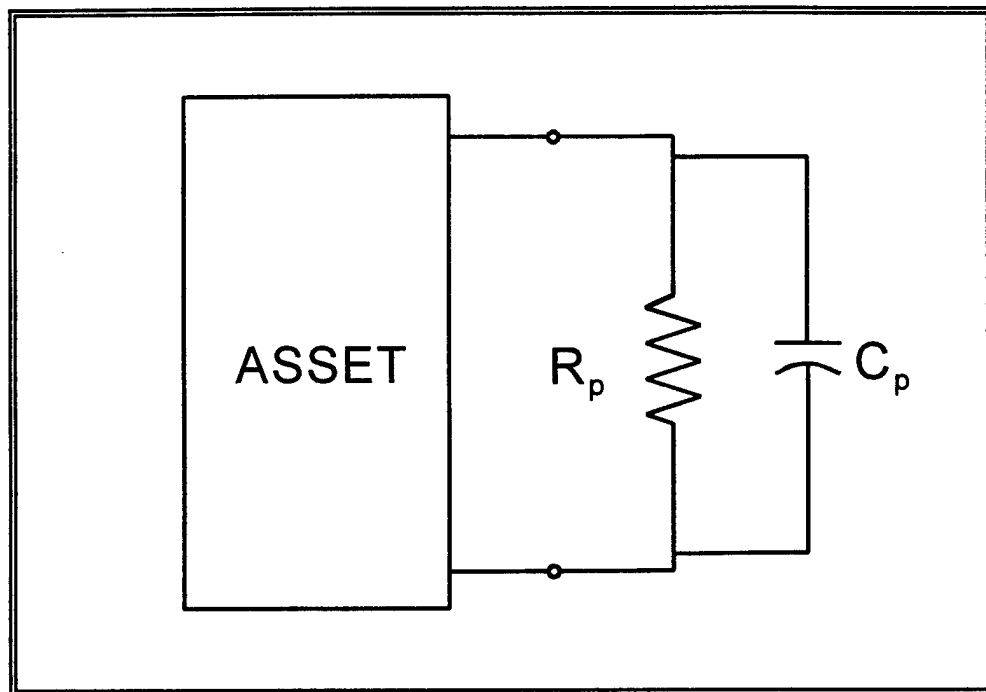
Figure 8.   The model of a circuit as a one port network. The voltage probe is shown schematically as a load to the one port circuit.

Of course, the quantity of interest is the voltage at a circuit node. Since the node has an impedance to ground and a voltage of arbitrary waveshape, the node can be fully represented by a voltage source with an equivalent impedance. This equivalent voltage source, represented by V_n, will be referred to as the "node voltage" to distinguish it from the physical voltage generator, although the loading effects outlined here are also relevant.

The node can be modeled as a waveform generator with a series resistance and a shunt capacitance. If the asset is a linear system, then this model reduces to an application of Thevenin's theorem. This model is fully justified by nodal analysis of circuit topology for a general network. That is, any branch cut will have an associated voltage and an equivalent impedance to ground.[8,10] Thus, the 1-port model of an asset can be modeled as shown in Figure 9.
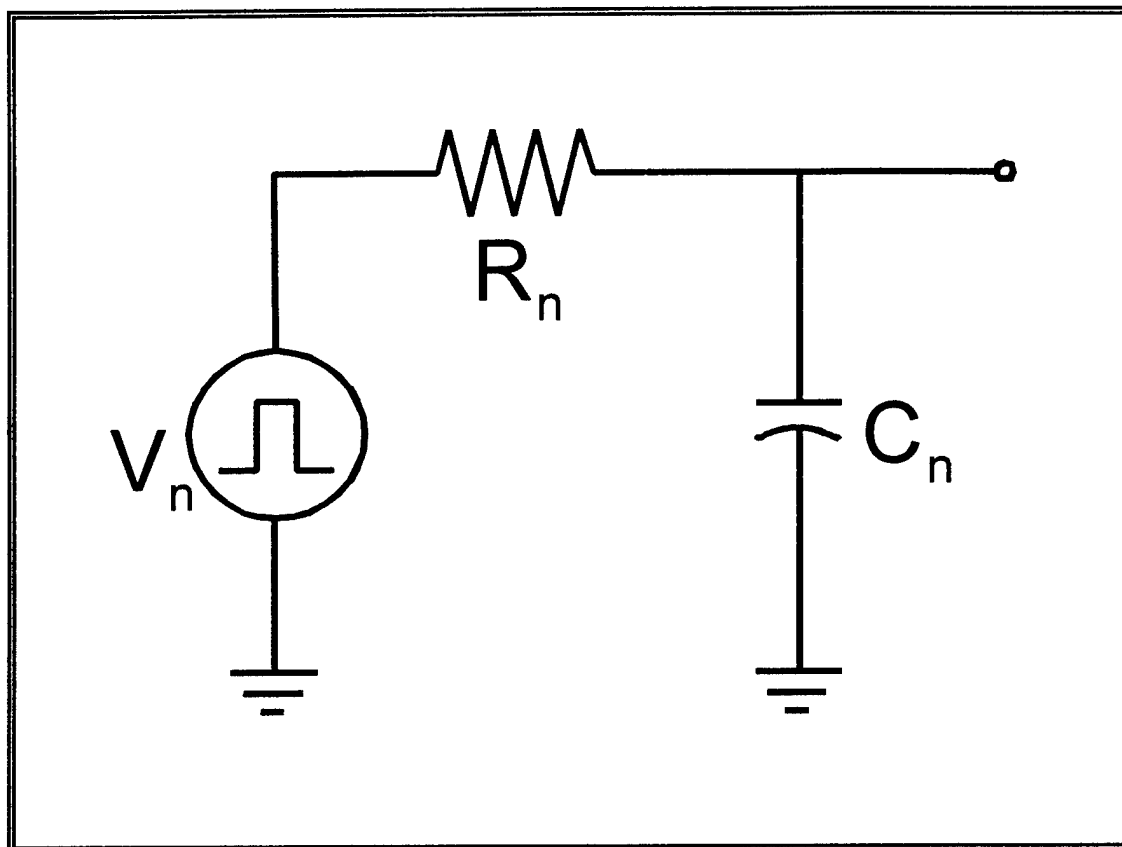
Figure 9. **Model of the circuit node as a node voltage source with an associated impedance.**

Loading effects manifest differently when measuring signals from pulse and continuous wave sources. The parameters relevant to pulse sources are amplitude, risetime, transient response, and time distortions. Narrowband sources are concerned with amplitude and phase distortion. Typically, a signal source is portrayed as purely resistive, and the probe is evaluated

via degradation associated with probe input capacitance. In reality, however, the source has some output capacitance which shunts the series source resistance.[10] This relationship is shown schematically in Figure 9 and conveys the relationship between the shunt capacitance and the source output waveform. Typical values of source capacitance are in the range of one to 100 pF and source resistance may be anywhere in the range of a few mΩ to several hundred ohm, and is circuit specific.

When the probe is connected across the output terminals of the source, as shown in Figure 10, the probe's input parameters, both resistive and reactive, add to the source parameters. An investigation of the relative size of the perturbance of the source output, for both narrowband and ultrawideband sources, follows.
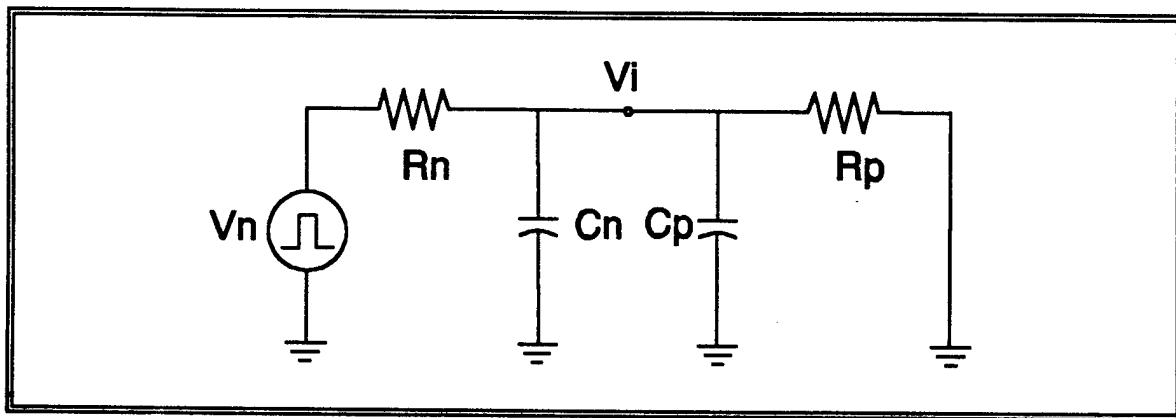
Figure 10. **The equivalent circuit of the voltage source, which respresents the node of the circuit under test, being monitored with a voltage probe. The voltage probe also has an associated shunt capacitance.**

4.1   Resistive Loading of a Node Voltage

Using the circuit of Figure 10, the circuit can be analyzed. If the input resistance of the probe, R_p, is greater than 10 times the node resistance, R_n, the probe resistance can be ignored. The probe capacitance, C_p, adds to the shunt capacitance of the node.

23

To evaluate the effect of resistive loading on the circuit by the probe consider a pulse node voltage whose series resistance is such that it does not meet the criteria, $R_p \leq 10 \ R_n$. Thevenin's Theorem can be used to evaluate the effect of resistive loading on the node voltage. The Thevenin equivalent resistance, R_{TH}, is the parallel combination of R_n and R_p,

$$R_{TH} = \frac{R_p \, R_n}{R_p + R_n},$$

and the Thevenin equivalent voltage, V_{TH}, is given by,

$$V_{TH} = \frac{V_{n0}}{R_n} R_{TH} = V_{n0} \frac{R_p}{R_n + R_p}.$$

To quantify the the effect of loading the circuit by the probe, consider a node with the following parameters:

R_n	C_n	R_p	C_p	R_{TH}	V_{TH}
200 Ω	20 pF	1 kΩ	1 pF	166 Ω	0.833 V_{no}

Note that the Thevenin equivalent resistance, 166.7Ω, is less than the node resistance, 200 Ω. Thus, the voltage measured by the probe, V_{TH}, is only 83% that of the true voltage, V_{no}.

$$t_r^L = 2.2 R_{TH} C_n = t_r \frac{R_p}{R_p + R_n}.$$

4.2 Capacitive Loading of UWB Sources

The result of resistive loading by the probe results in a reduced peak voltage in both NB and UWB sources. However, the effect of probe capacitance on the measured signal manifests differently for UWB and NB voltage sources.

The capacitive component of the probe impedance, C_p effectively adds to the node capacitance, C_n, in a pulse voltage node source, as shown in Figure 11.
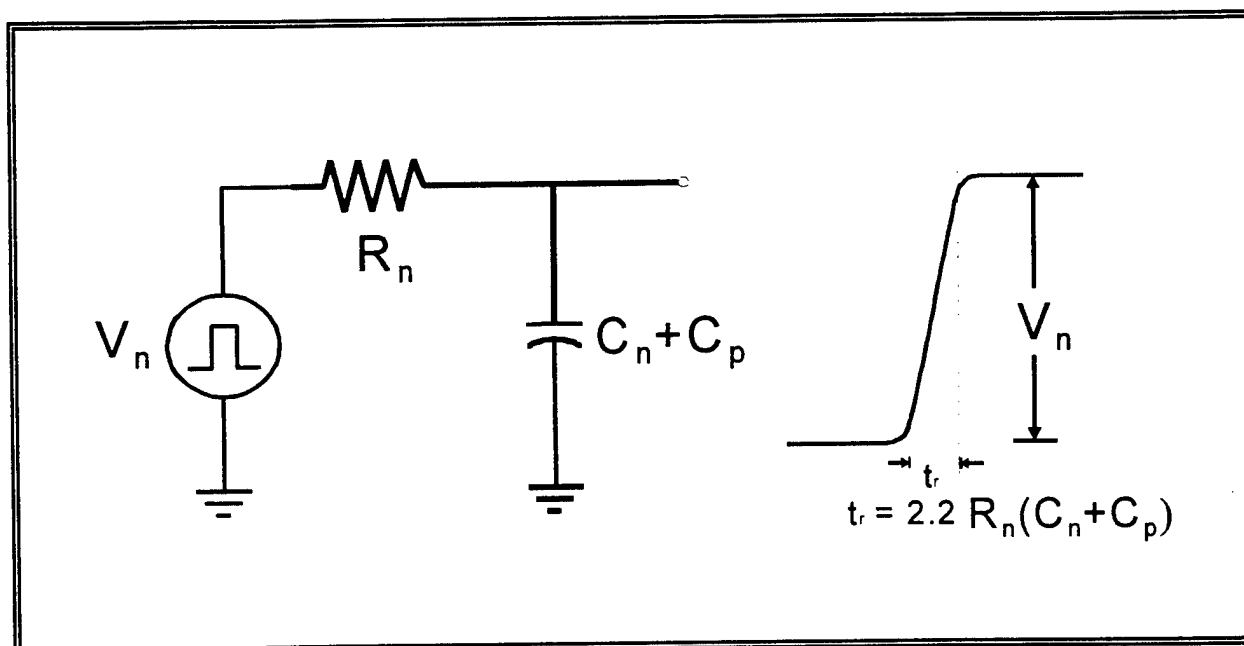
Figure 11. The effect of probe capacitance, C_p on a pulse node source of amplitude V_{no}. The probe capacitance is in parallel with the node capacitance, C_n.

If the probe does not resistively load the circuit, the probe resistance, R_p, may be excluded. As illustrated in Figure 11, the effective risetime of the pulse, τ_r^{eff}, is

$$\tau_r^{eff} = 2.2 \ R_n \ (C_n + C_p) \ .$$

It should be noted that the probe capacitance adds to the node capacitance regardless of its relative size. Thus, it is imperative that the probe capacitance be kept to a minimum.

4.3 Exploiting Resistive Loading to Increase the Risetime of UWB Sources

In some experimental situation, an increased risetime is desirable. Since direct injection work uses UWB sources for testing, the following treatise is included to illustrate how deliberately loading the UWB source can result in an increased pulse risetime, with a cost in peak amplitude. That is, a pulse source with a specified risetime and maximum amplitude can be altered by intentionally loading the source output. An example of a loaded source output is shown in Figure 12.
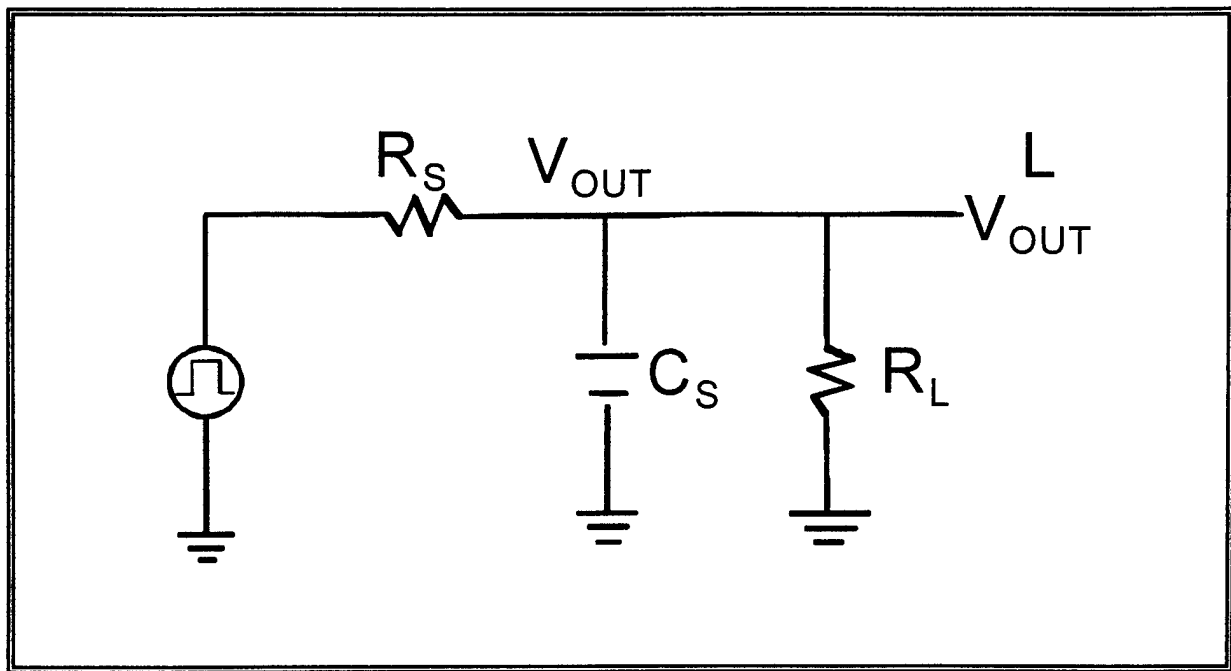
Figure 12.   Equivalent circuit of a loaded source.

The resistance, R_s, is the series load resistance of the pulse generator. The addition of a shunt resistor, R_L, to the pulse generator changes the effective series output resistance. To illustrate the effect of a shunt resistor on the performance of a generator, let the following values in Table 2 apply, where the superscript 'L' denotes the values upon loading. The Thevenin equivalent source resistance, R_{TH}, is 10 Ω. Thus, by loading the generator circuit with a 50Ω shunt resistor, a significantly faster risetime can be achieved at the expense of peak generator amplitude.

26

Parameters	Specifications	Effective Loaded Specifications
R_s	450Ω	450Ω
V_{out}	100V	10V
R_L	-----------	50Ω
t_r^L	100nsec	10nsec

Table 2.   The source, with a series resistance of 450 Ω and a risetime of 100 ns can be loaded with a 50 Ω shunt resistance to decrease the effective source risetime to 10 ns.

The peak amplitude, V_{out}, and effective generator risetime, t_r^L, may be calculated using the value of the Thevenin equivalent source resistance. The pulse generator is current limited, and, thus, the peak voltage is determined from the effective series resistance of the source. The maximum value of current, is determined from the specified values of the unloaded generator,

$$I = \frac{V_{out}}{R_s}$$

Under loaded conditions, the loaded peak voltage, V_{out}^L, decreases to accommodate the effective impedance, R_{TH}, of the loaded generator. The loaded peak voltage, V_{out}^L, can be calculated in terms of the specified peak voltage, V_{out}, from

$$V_{TH}^L = IR_{TH} = V_{out} \frac{R_s R_L}{R_s + R_L} \quad .$$

If the intrinsic shunt capacitance of the loading resistor is small, the effective risetime of the loaded generator will increase due to the reduced effective series resistance. The specified risetime of the generator, t_r, can be used to determine the new risetime, t_r^L of the pulse generator via the following relation,

$$t_r^L = \frac{R_{TH}}{R_S} t_r \quad .$$

27

4.4   Capacitive Effects on NB Sources

Because capacitance effects on narrowband signals are so important, the effects of the internal capacitance and capacitive loading from the probe will be treated separately.

4.4.1   Effects of Internal Source Capacitance

To illustrate the effects of capacitive loading of a NB node voltage source, the circuit of Figure 13 will be used as the source model. The capacitance, C_n, is the internal capacitance of either a node voltage source or an external NB source.
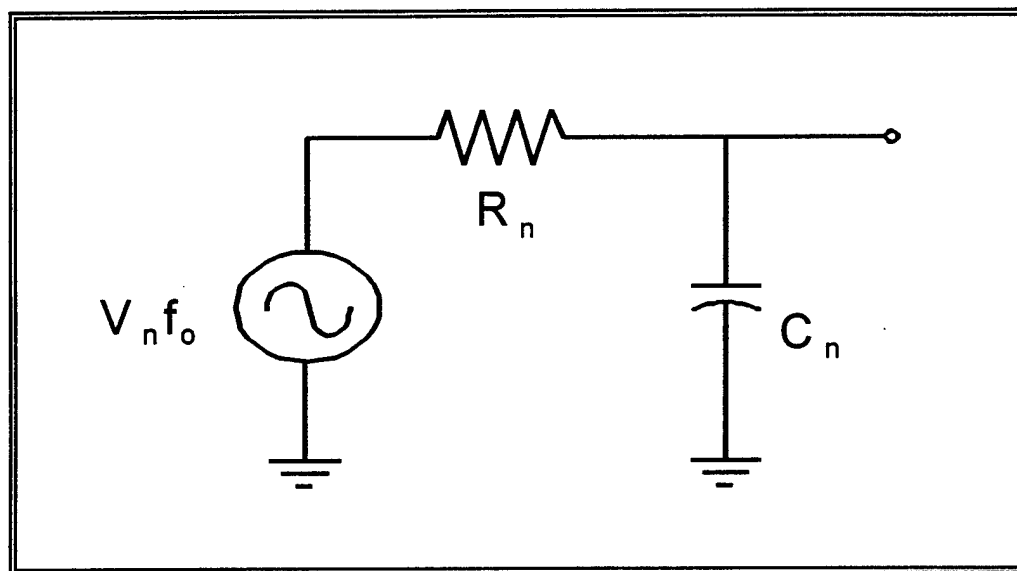
Figure 13.   The model of a narrowband source.

For an narrowband source, the shunt capacitance at frequency, f_{n0}, is an equivalent reactance, X_n, which adds to the equivalent output impedance of the source. The reactance, X_n, is computed from

$$X_n = \frac{1}{2\pi f_{n0} C_n}$$

The equivalent impedance and phase angle is calculated using phasors. The impedance at a given frequency is

$$Z_n = \sqrt{R_n^2 + X_n^2} \ ,$$

and angle of the phase shift can be computed from

$$\tan\phi = \frac{R_n}{Z_n} \ .$$

The relationship between the phasor components is illustrated in Figure 14.
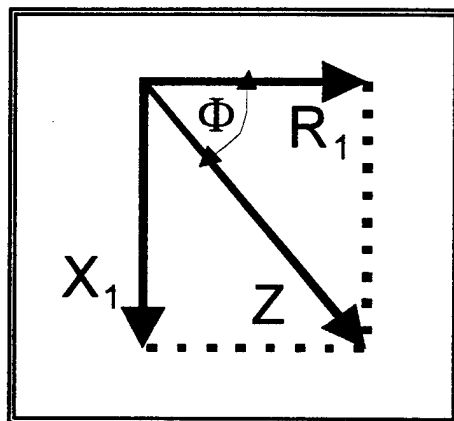
Figure 14.   The phaser relationship between the node impedance components

The voltage is measured with an ideal probe, that is, with no capacitance and infinite impedance, and is given by

$$V_I = V_{n0} \frac{X_n}{Z_n} \ ,$$

where V_I is the voltage which is registered on the recording device. Note as the reactance changes with frequency, the peak signal voltage will drop. This is commonly seen when using a NB signal generator at a given power level: as the frequency is changed, the voltage which is registered on the recording device drops.

29

The point at which the voltage drops to 3dB of its DC value is called the bandwidth of the source. In terms of percentage, on a plot of peak voltage, V_{n0}, and frequency, the bandwidth is determined to be the point at which the measured voltage, V_1 falls to 70.7% of its initial value, V_{n0}, as illustrated in Figure 15.
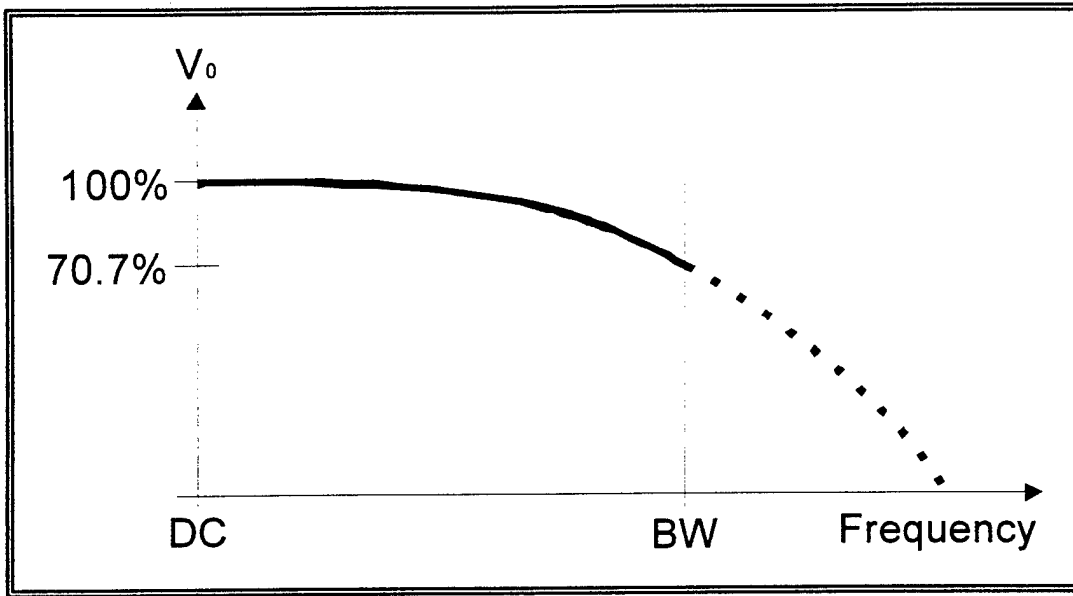
Figure 15.   Effect of NB source capacitance on the bandwidth, bw.

To illustrate the effect of the intrinsic source capacitance on the source output, the following table has been constructed.

f_{n0}	R_n	C_n	X_n	Z_n	V_I/V_I^{DC}
10MHz	200Ω	20pF	796Ω	820Ω	97%
100 MHZ	200Ω	20pF	79.5Ω	215.5Ω	37%
500 MHZ	200Ω	20pF	16Ω	200	8%
1 GHz	200Ω	20pF	8Ω	200	4%

Table 3.   The effect of frequency on the measured voltage, V_I, at constant source resistance, R_n and capacitance, C_n.

Note that almost the full signal is delivered at a frequency of 10 MHZ despite the magnitude of the resultant impedance, Z_n, being far in excess of the series resistance, R_n. The magnitude of the impedance is dominated by the reactive term, X_n.

4.4.2 Capacitive Loading by a Probe

The addition of a probe to a narrowband source also affects node voltage source performance, in a similar fashion to that seen in pulse sources. The model for a narrowband source and a probe is shown in Figure 16.

The relative magnitude of the equivalent circuit components, R_n, C_n, R_P, and C_P determine the loading on the CW source. If the probe does not resistively load the node voltage source, then R_P may be disregarded in the model. The capacitance of the source adds to the probe capacitance. Of course, the equivalent reactance could also be combined via the relation,

$$X_n^{\text{eff}} = \frac{1}{2\pi f_{n0} (C_n + C_p)} \quad .$$

and the measured voltage, V_I, is reduced by the fraction, (X_n^{eff} / Z_n).
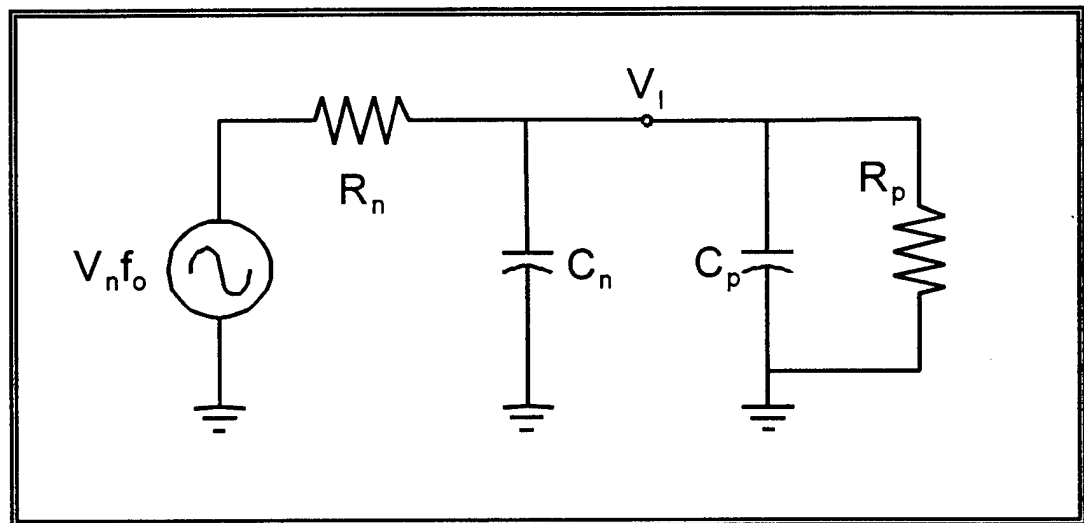
Figure 16. **Model of a narrowband source which is being monitored by a voltage probe.**

4.5   Complex Loading of a Node Voltage Source

4.5.1   Capacitive and Resistive Loading on a NB Node Voltage Source

If, $R_p < 10 R_n$, the probe will resistively load the source circuit and will effect the source voltage amplitude and series resistance. If the probe also has a significant capacitance, the probe will affect both the amplitude and phase relationship of the measured signal.

The equivalent resistance, R_{TH}, is the parallel combination of R_p and R_n. That is,

$$R_{TH} = \frac{R_n R_p}{R_n + R_p} \quad .$$

Note the effective resistance replaces the specified series source resistance, and the peak voltage amplitude, V_I, is a fraction of the specified generator amplitude V_{no}.

To illustrate the impact of probe loading on a narrowband signal measurement, let the following values apply: $R_I = 200\Omega$, $C_I = 20pF$, $R_P = 1k\Omega$, $C_P = 20pF$ as shown in Figure 17.

The effects of excessive reactive and resistive loading act in collusion to degrade the signal output. Under resistively loaded conditions, the percentage of voltage output must be referenced back to the effective Thevenin voltage. Thus, the percentage degradation of the signal output under complex loaded conditions can be expressed as,

$$V_I = V_{no} \frac{X_n^{eff}}{\sqrt{R_{TH}^2 + (X_n^{eff})^2}}$$

where X_n^{eff} is given by

$$X_n^{eff} = \frac{1}{2 \pi f_{no} (C_n + C_p)} \quad .$$

Thus, as shown in Figure 17, the effect of loading of a voltage node source by the probe can cause serious measurement errors which can be eliminated by careful measuring techniques.
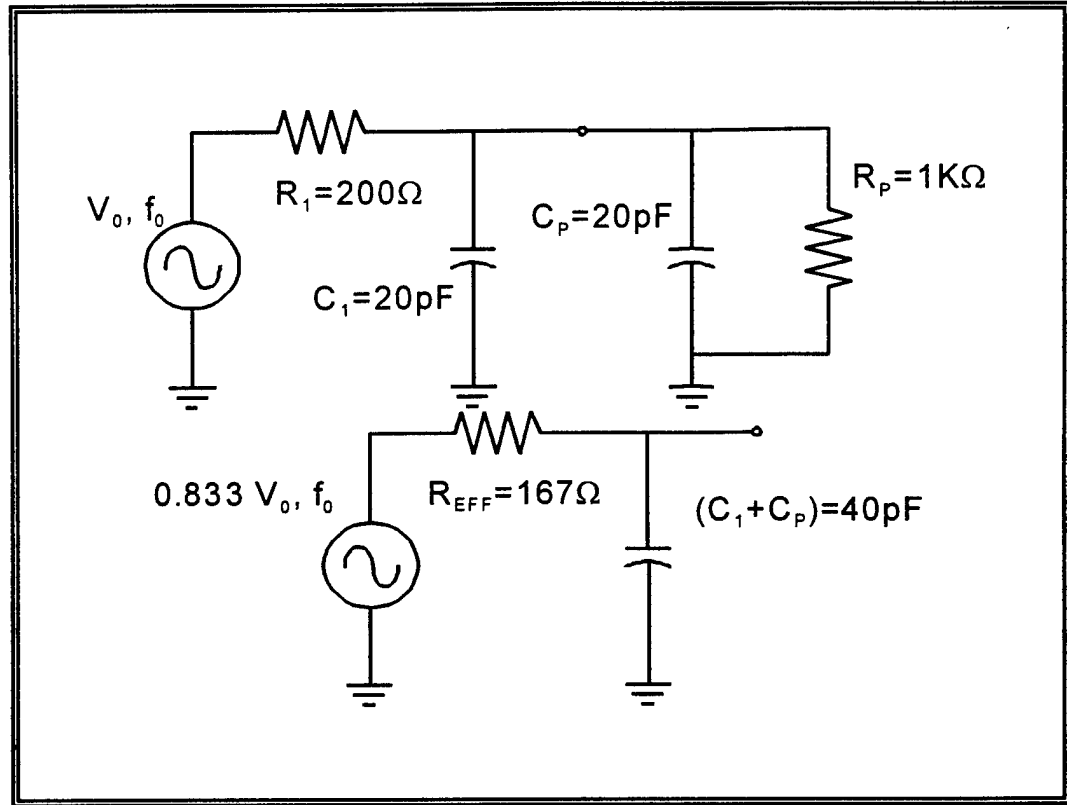
Figure 17.   An example to illustrate the effect of complex probe loading on a narrowband signal. Note that both the effective resistance and capacitance is altered from the unloaded signal.

4.5.2   Capacitive and Resistive Loading on an UWB Node Voltage Source

For UWB sources, the reduced effective node resistance, R_{TH}, which results from resistive loading of the probe, affects the risetime of the loaded node voltage pulse. The measured pulse risetime, t_r^L, for the loaded source is altered, and can be calculated from the Thevenin equivalent parameters from

$$t_r^L = 2.2 \ R_{Th} \ (C_g + C_p) \ .$$

33

This value is altered from the unloaded value, since the equivalent Thevenin resistance is reduced from the node resistance, but the capacitance is increased. Thus, the effective risetime of the complexly loaded node depends on the relative size of the resistive and reactive loadings.

4.6   Predictions of system measurements

This treatise has dealt explicitly with the change in a signal source with the addition of a measurement probe. The results show that the ideal probe has an infinitely high resistance and no reactance. Thus far, no mention has been made of system considerations. In general, the risetime of a system is determined by the response capabilities of the system components. To determine the measurement system capability, the displayed risetime, $t_{r\,system}$, is obtained from,[10]

$$t_{r\,system} = \sqrt{t_{r\,source}^2 + t_{r\,probe}^2 + t_{r\,scope}^2}$$

where $t_{r\,source}$ is the effective risetime, including any probe loading.

For a narrowband signal generator, the source risetime, $t_{r\,source}$ is not applicable, of course, and a zero can be substituted in the above equation. With a specific sinewave signal, the bandwidth of the probe and viewing device also plays a strong role in its ability to predict the waveform. The system bandwidth, bw, can be related to the system risetime, $t_{r\,system}$, by combining the equations for a RC network.[11] The 10-90% risetime is given by

$$t_{r\,system} = 2.2RC$$

and the 3dB bandwidth, bw, is given by

$$bw = \frac{1}{2\pi RC}$$

Combining these relations, yields,

$$t_{r\,system} = \frac{0.35}{bw} \quad .$$

34

5.0   MEASURING THE NODE IMPEDANCE WITH A VECTOR NETWORK ANALYZER

It has been established in Sections 3.1 and 3.2 that the input impedance of the probe, R_p, must be ten times greater than the impedance to circuit ground of the node under test, R_n. That is, the measurement will accurately reflect the voltage at the node providing

$$R_p \geq 10R_n \ .$$

The node impedance to ground is, in general, a function of frequency. Hence, the above criteria must be met for the frequencies of interest for the measurements to be valid in the test frequency range. For clarity, the procedure for measuring the node impedance to ground as a function of frequency is elucidated.

The circuit node impedance to ground is recorded by performing a S11 measurement using a network analyzer. This is a standard calibration of a one port circuit. The network analyzer has an appropriate calibration kit for the connectors of the device under test which is used to perform the S11 measurements over the frequency range. The measurement is referenced to a chosen plane. If the node under test contains a DC signal, a DC block is included in the test setup, and must be incorporated into the calibration procedure.

The calibration set uses the wave travel time between the circuit and the network analyzer to determine the wave reflection properties. The network analyzer uses a default reference dielectric constant for calibration, unless specified otherwise. The true calibration is calculated from the length and dielectric constant, ϵ_r, of the connecting cable between the network analyzer and circuit under test. Some network analyzer models allow for a change in the velocity of propagation (Vp) of the electrical conduit from the default value; otherwise, the time delay can be calculated. The calculation of the delay time, caused by the addition of the connecting cable, extends the reference plane.

Select the S11 measurement on the vector network analyzer and then choose the phase format for displaying information. Using the electrical delay, flatten the trace on the Cartesian format. Alternately, one can make the smallest cluster with a polar or smith chart format. Note, several transitions in phase may occur because of the device.

35

The length which is displayed on the network analyzer's CRT is a two way wave travel time. The true electrical length is this value divided by two, a one way travel time. One anticipates this value by the physical length of the cable. If the expected and measured values do not agree, the electrical length of the circuit under test must also be measured. This manifests in the Cartesian format that a flat response is not possible and in the Smith chart format a small cluster is not possible. If the device interferes with the measurement, the time domain should be used. To determine the electrical length, insert a short circuit at the node of the circuit under test. Turn on a marker on the analyzer display and read the two way propagation time to the short. This is value is the electrical length of the line to the circuit.

When the electrical length has been determined, the display should be changed to the Smith Chart format. If the marker is not already turned on, do so at this point. Enter the frequencies of interest in the calibrated band while in the marker mode (active display) and read the real and imaginary impedance values for each frequency point entered.

6.0   PRELIMINARY NARROWBAND EXPERIMENTS

It has long been suspected that techniques used in low frequency direct drive experiments yield inaccurate results at higher frequencies. One of the objectives of this project is to develop direct drive techniques which will provide reliable data at frequencies exceeding 400 MHZ.

To this end, the first task was to assess the current techniques involved in direct drive experiments. Although both current and voltage measurements are used in low frequency direct drive techniques, voltage probes are more suitable for high frequency testing and are easily modified for insertion into physically constrained spaces.

In evaluating the techniques currently used in direct injection testing, two fundamental assumptions of the methodology were identified as suspect and worthy of investigation. The first assumption is the voltage probe's invariance with frequency, and the second is the contention that the impedance of the asset is 50 ohms at all nodes. To evaluate these assumptions the circuit of Figure 18 was constructed.
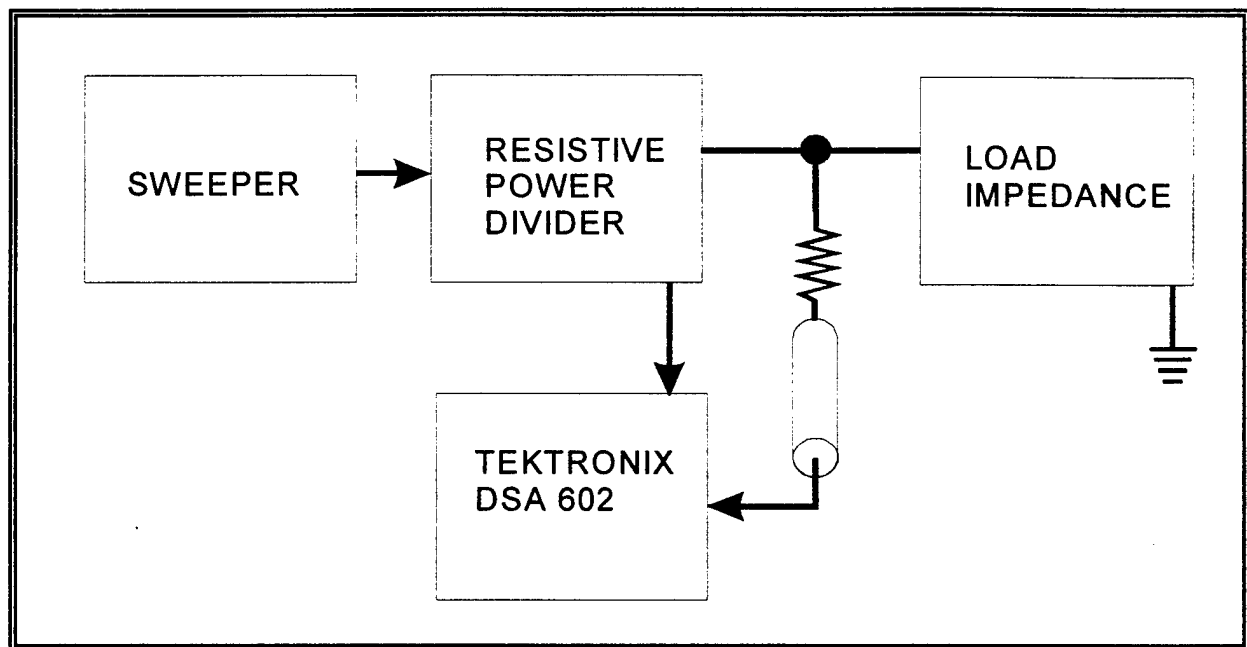
Figure 18.   **The experimental test setup. The load impedance was alternately the NATO cylinder and a commercially available coaxial termination which was rated to 18 GHz.**

The voltage dividing ratio is used as a metric in the exploration of probe performance because it is the most fundamental quantity associated with the voltage probe. The voltage division ratio is the ratio of the voltage being measured (the "source"),V_i, to the voltage output of the probe, V_{out}. If the fundamental assumptions of probe design are valid, the voltage division ratio will be constant with respect to frequency. To investigate if the validity of the fundamental assumptions, an experiment was configured to test the operation of the probe while measuring, separately, an ideal 50Ω impedance load and a real asset node.

6.1   The Asset Description

The objective of this research effort was to develop a testing methodology, and so, the test object used was of secondary importance. A "NATO SNR cylinder" was chosen as a test device. At a North Atlantic Treaty Organization workshop on HPM testing, the participants agreed that measurement of microwave coupling to a generic test object would provide a standard from which comparisons could be made.[12] Toward this end, a generic thin walled cylinder, the "NATO cylinder," with the option of an installed standardized circuit board was chosen as the common test item for the participating countries. For this research, only the circuit board portion of the NATO cylinder was utilized for the direct injection tests, and will be referred to as the NATO cylinder.

6.2   Test Point Selection

Generally, test point candidates are chosen on the basis of the circuitry involved. For this test, the two nodes used were chosen solely on the basis of prior tests. The results of that test are documented in "Direct Injection Test Report for the SNR Cylinder".[12] The two nodes are:

Component	Pin	Function
NSC800 Microprocessor	33	Reset In
NSC800 Microprocessor	25	Interrupt

Table 4.   **Test point selection.**

In these narrowband experiments, the applied frequency was generally set at 10, 30, 50 MHZ, then from 100 MHZ to 1 GHz in 100 MHZ increments.

6.3   Measurement of the Voltage Division Ratio under Two Load Conditions

In these preliminary experiments, the load being measured was varied between the circuit under test and an ideal 50 Ω load. This ideal load is a 50 Ω RF termination, which simulates the assumption of a 50 Ω ohm asset impedance.   The effect of these loads on the voltage dividing ratio is shown in Figure 19.

The voltage probe is designed to give a voltage division ratio of '21', which is shown in Figure 19 as a reference. The experimental data designated "probe with 50 ohm termination" shows that the probe itself responds to a high frequency signal. The degradation of the voltage division ratio in this case is attributed solely to probe performance. Probe performance is documented separately in Section 7.

The experimental data labeled "Probe with asset termination" is obtained by attaching the probe output to Pin 33 of the NATO cylinder board. It is abundantly clear that the asset affects the performance of the probe. The voltage division ratio varies from a value of 0 at 10 MHZ to 100 at 500 MHZ in an erratic fashion. This experimental data is a combination of the variation in probe response with frequency and the variation of the asset input impedance with frequency. The convoluted relationship between the complex impedance of the asset and the degradation of the voltage probe with frequency creates a challenging experimental task.

The large variations of the probe voltage with the asset as the terminating load has been identified as a result of the voltage standing wave ratio (VSWR) . To illustrate the effect of a VSWR on a measurement, assume a lossless transmission line, with characteristic impedance Z_0, is terminated in an arbitrary load of impedance, Z_L.   When a narrowband signal, in the form $V_0{}^+e^{-j\beta z}$, is generated at $z < 0$, the incident wave is partially reflected. This reflected wave interferes with the incident wave. The reflected wave is given as $V_0{}^-e^{+j\beta z}$. The resultant voltage along the line, then, is given by

$$V(z) \;=\; V_0^+\, e^{-j\beta z} \;+\; V_0^-\, e^{+j\beta z} \quad .$$

39
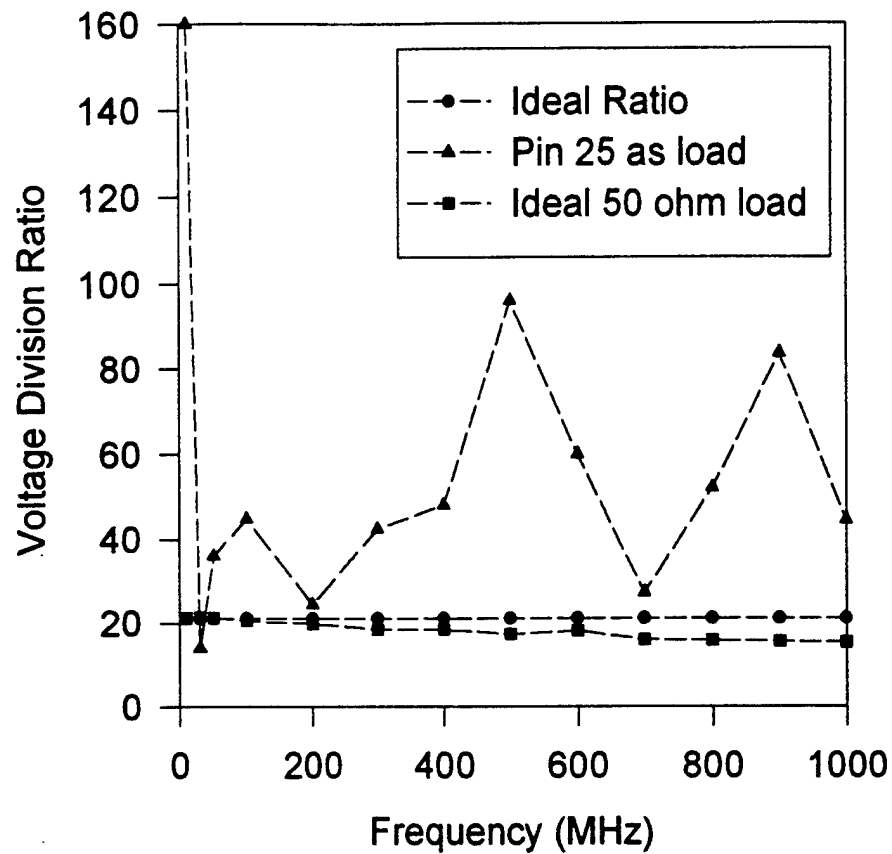
Figure 19. The effect of various loads on the voltage division ratio under narrowband excitation. The asset is mismatched to the RF feed line which results in a VSWR. This experiment illustrates the insidious result of an unknown DUT node impedance.

40

The relationship between the incident and reflected voltages is

$$V_0^- = \Gamma V_0^+ ,$$

where Γ, the reflection coefficient, is given by,

$$\Gamma = \frac{Z_L - Z_0}{Z_L + Z_0} .$$

The resultant voltage along the length of the transmission line is given by

$$V(z) = V_0^+ (e^{-j\beta z} + \Gamma e^{j\beta z}) .$$

The voltage, then, varies with position, z, along the transmission line. The maximum voltage which is measured, V_{Max}, is

$$V_{Max} = |V_0^+| (1 + |\Gamma|) ,$$

and the minimum voltage, V_{Min}, is

$$V_{Min} = |V_0^+| (1 - |\Gamma|) .$$

The voltage at any location, z_1, along the transmission line, is

$$V(z_1) = V_0^+ (e^{-j\beta z_1} + \Gamma e^{j\beta z_1}) .$$

Graphically, the voltage along the length of the transmission line is shown in Figure 20.
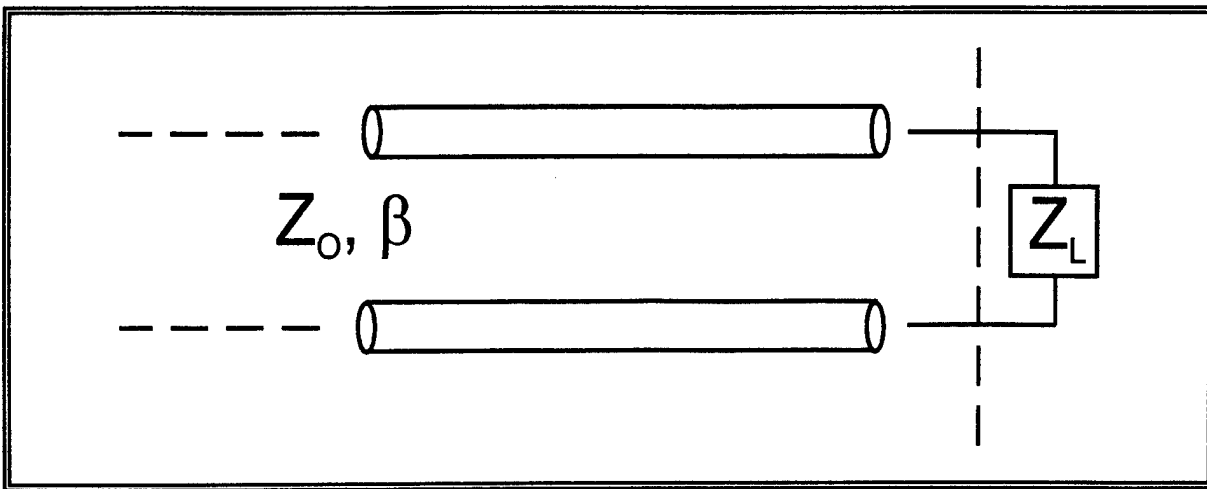
Figure 20a. The model of theRF excitation of the load impedance. If the load impedance and the transmission line impedance are mismatched, a standing wave will be establish.
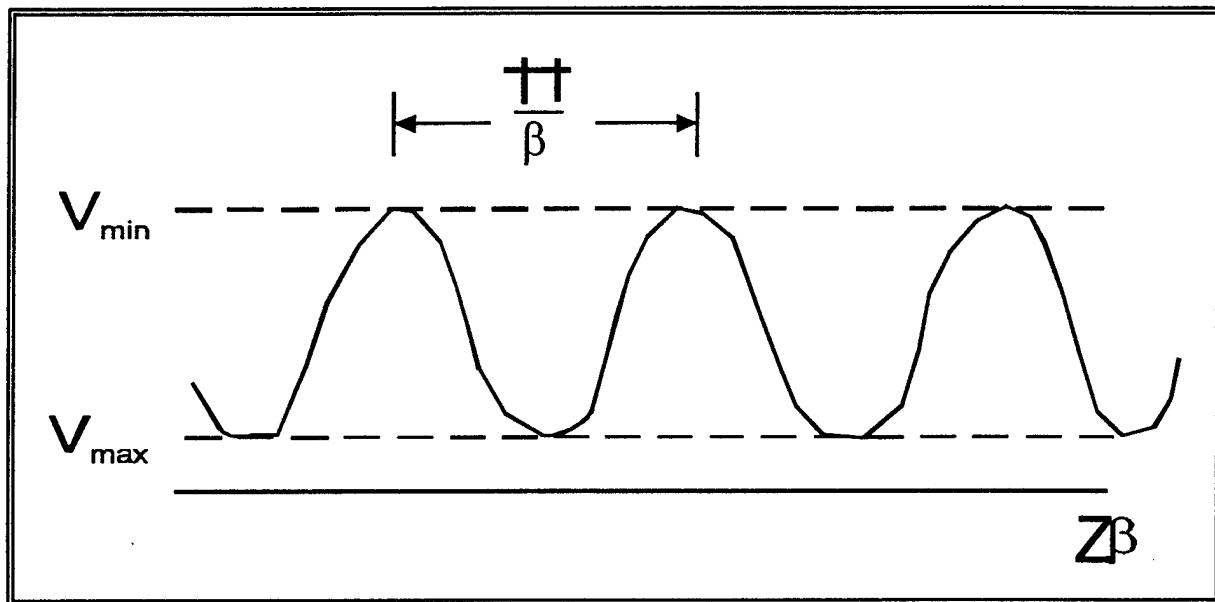
Figure 20b. The voltage along the length of a transmission line under narrowband excitation and impedance mismatched conditions.

The phenomena of standing waves along a transmission line are characterized by the voltage standing wave ratio, VSWR, which is given by

$$VSWR = \frac{|V_{Max}|}{|V_{Min}|} = \frac{1 + |\Gamma|}{1 - |\Gamma|} .$$

In this experiment, the source voltage is a narrowband signal, and as the frequency is changed, the positions of the location of the voltage maxima and minima shift. The voltage probe is located at a fixed position. Thus, the voltage measurement changes with frequency at least partially because the voltage at the measurement location changes with frequency. It is also suspected that the node impedance of the asset changes with frequency, yielding a reflection coefficient which changes with frequency. These two factors combine to yield the inconsistent voltage dividing ratios which were measured and shown in Figure 19. This experimental exercise illustrates the misleading results which are easily obtained without proper evaluation of the critical node points prior to testing.

7.0 Z_0 Voltage Probe Evaluation

The measurement of an electronic circuits response to a direct drive excitation requires that the probe not disturb the normal operation of the circuit while providing sufficient sensitivity to measure the circuit response. A Z_0 voltage divider can be designed which meets these requirements.

Typically, a Z_0 voltage probe is constructed by soldering a 1 kΩ resistor to the center conductor of a length of transmission line, which is terminated in the impedance of the measuring device. Solid shield coaxial cable, nicknamed CuJac, is often used to reduce impinging electromagnetic interference.

The choice of resistor type is controversial in the DIT community. Generally, either a chip resistor is chosen for its low inductance, or an 1/8 watt carbon composition resistor is used for its ease of handling. The physical size of the low wattage carbon composition resistor is very compatible with the physical size of the CuJac. The solid copper outer conductor is pulled over the resistor which minimizes the length of the wire, and therefore, the inductance to the local ground of the asset. Real resistors, however, have an intrinsic capacitance which is associated with their construction. Moreover, the inclusion of the probe into a circuit, with finite lengths of wire, result in the addition of stray reactance. Stray reactance becomes increasingly important at high frequency, and thus, a circuit simulation was performed to evaluate the effect of intrinsic reactances on Z_0 voltage probe performance. The simulation results are compared to measured voltage probe frequency responses.

Several currently used techniques for voltage probes have been tested to evaluate their performance as a function of frequency. First, a transmission line is used in the experimental setup to illustrate the pitfall one could fall into if using this probe improperly, and to evaluate its frequency response. The voltage probes which were constructed using carbon composition and chip resistors are evaluated. These are presently the resistors of choice for most voltage monitoring applications. Their performance is shown to be unacceptable for high frequency applications. However, specially designed resistors from which acceptable probes can be constructed are commercially available. This effort measures their frequency characteristics.

7.1   The Experimental Setup

It was found in preliminary experiments that the probe and circuit under test interact under narrowband excitation. An experimental effort was undertaken to investigate the frequency response of the voltage probes for use in DIT. The experiment is designed to be independent of the DUT, and thus, focuses solely on the probe performance . The experimental setup is given in Figure 21.
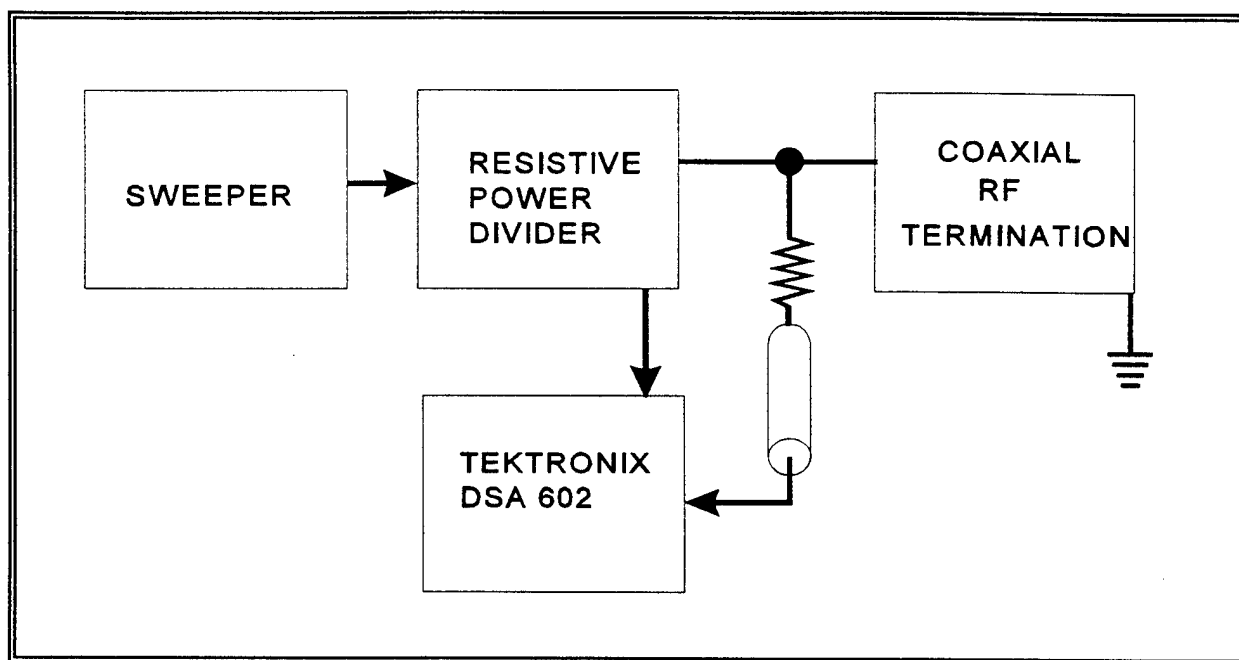
Figure 21.   The experimental setup for the evaluation of Z_0 voltage probes. The RF termination simulates a 50 Ω circuit node impedance.

The circuit is simulated by a 50 Ω load which is rated at high frequencies: a 50 Ω RF terminator. This resistive load provides a well characterized component which simulates the ideal, matched condition of a 50 Ω asset input impedance.

7.2   Transmission Lines used as 50 Ω Voltage Probes

The use of a "lossless" transmission line as a voltage probe has been discussed in Section 3.3.3, and was included in this series of experiments for completeness. Transmission lines are desirable for use as voltage probes because of their compactness and excellent frequency response. However, they are only appropriate for circuit nodes which have an impedance of less than 5 Ω. Many circuit types do have impedances this low. For instance, Cascade Microtech has commercially available, broadband 50 Ω probes for laser diode applications, multiport MMICs, low impedance power amplifiers and discrete transistors.

The results of using a transmission line to measure the voltage of a 50 Ω impedance is shown in Figure 22. The experimental setup of Figure 21 is used to investigate the voltage dividing ratio in the frequency range 10 MHZ to 1 GHZ. The ideal voltage division ratio is assumed to be 1:1. In this experiment, using a 50 Ω terminating load on the oscilloscope, the measured ratio is 1.5. The frequency response of the transmission line is very good as expected.
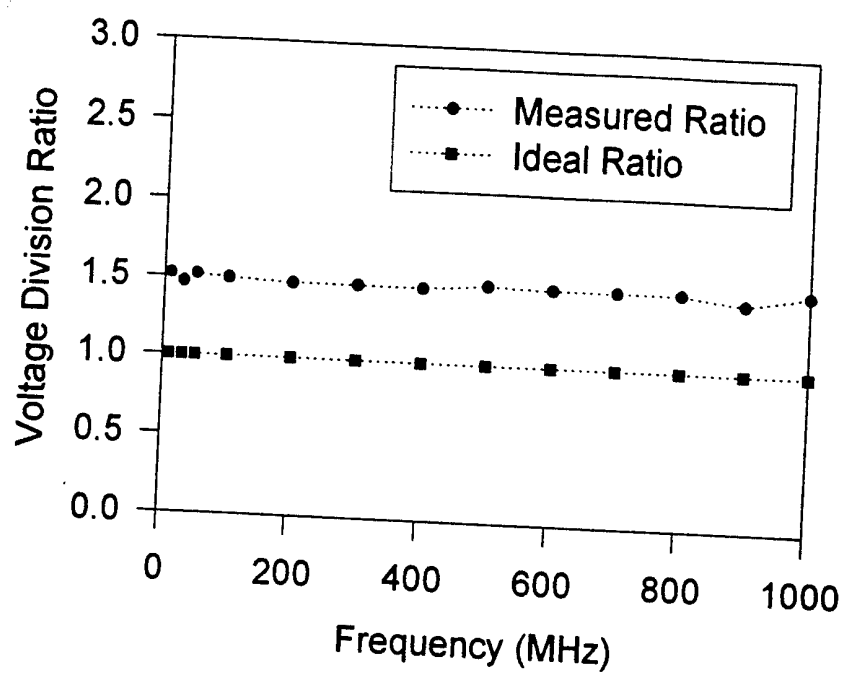
Figure 22. The frequency response of a 50 Ω transmission used as a voltage probe on a 50 Ω load. Note that a 50 Ω probe loads a circuit node with an impedence of 50 Ω.

The measured ratio of 1.5 is explained with the aid of Figure 23 which shows a circuit model of the cable probe measuring a 50 Ω asset. The transmission line voltage probe is modeled as its characteristic impedance, Z_0, which is 50 Ω. However, the transmission line which connects to the RF source also has a characteristic impedance of 50 Ω. The characteristic impedance is modeled as a resistor located between the center and outer conductors of the real transmission line. Hence, the equivalent resistance, Z_0, of the RF feed transmission line is in parallel with the 50 Ω RF load. The parallel combination of impedance is 25 Ω, which results in a voltage divider ratio of 1.5. Knowledge of the correct ratio is essential if a cable probe is used.

$$\frac{V_S}{V_P} = \frac{Z_0 R_T + R_S R_T + Z_0 R_S}{R_S (R_T + Z_0)} = \text{VOLTAGE DIVIDER RATIO}$$
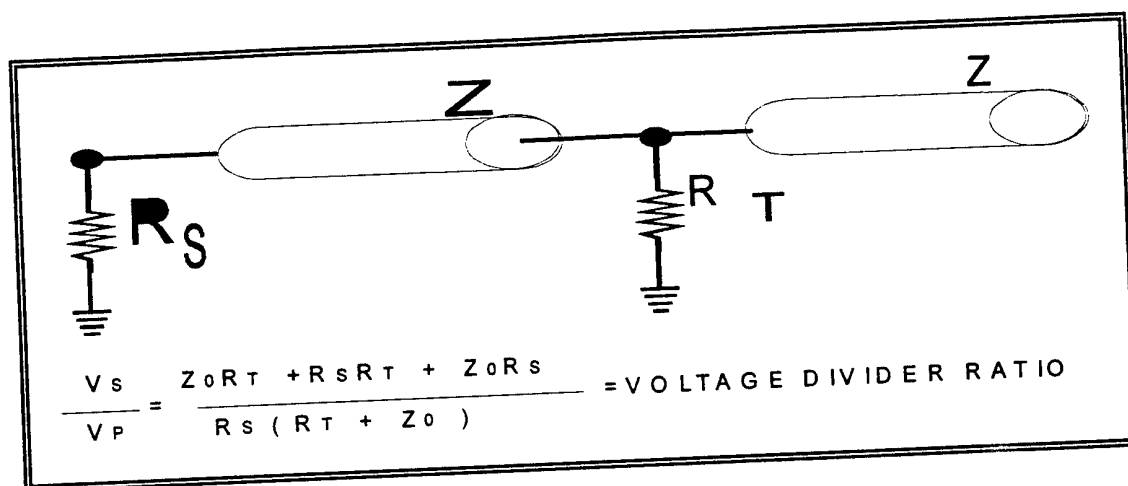
Figure 23.   The equivalent circuit model of the experimental setup of Figure 22. The model is analyzed to correctly predict the voltage divison ratio when using a 50 Ω transmission line to monitor the voltage on a 50 Ω load. The transmission line loads the circuit under test.

It should be noted that a transmission line is an inappropriate choice for measuring a 50 Ω load. Moreover, this cannot be corrected since the probe interferes with the circuit under test by drawing excessive current through the transmission line "probe". A transmission line, with an input impedance of 50 Ω, can only be used to accurately measure loads with impedances less than 5 Ω.

To illustrate this point, experimental verification of this criteria is provided. The electromagnetic coupling crossection of an electronic system was measured by the test engineer *** using two probes. One was a 1050 Ω Z_0 probe and the other was a transmission line (CuJac) probe. The crossection, as measured with the Z_0 probe was quickly recognized by the engineer as being unreasonably large over 1 GHz. The crossection which was measured with the CuJac probe is shown in Figure 24.
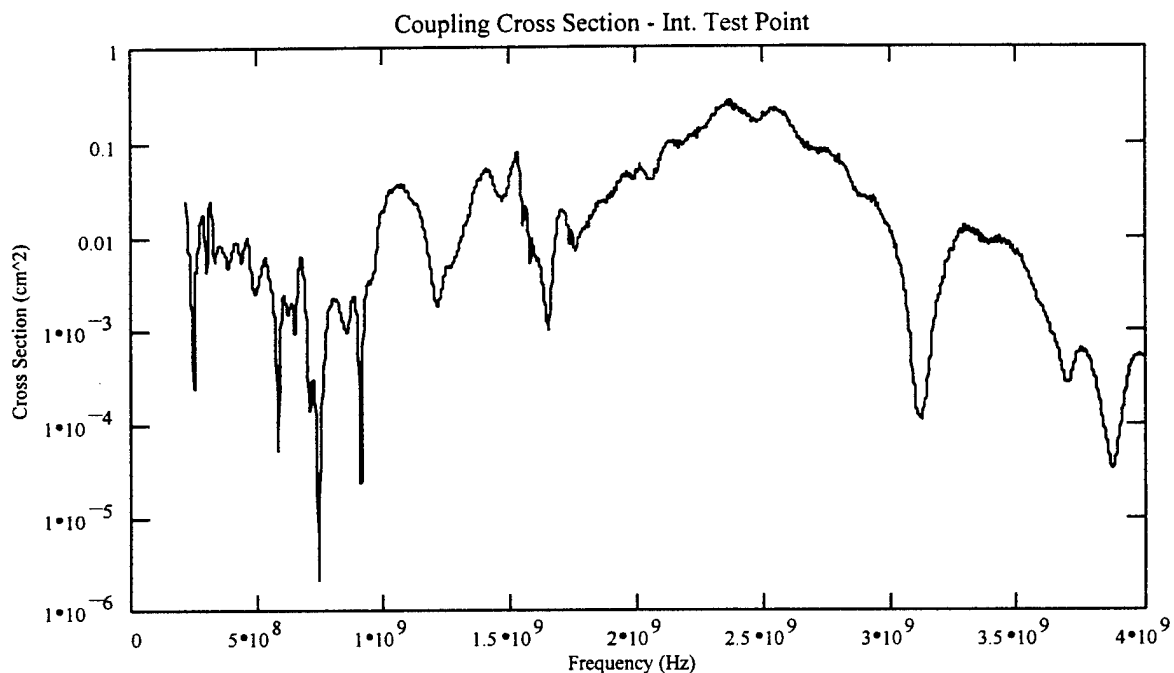
Figure 24.   The electromagnetic coupling crossection of a GPS receiver as measured with a transmission line used as a 50 Ω probe.***

After these measurements were made, the node impedance was measured. The resistive component of the node impedance is shown in Figure 25. The real part of the node impedance is shown to be near 5 Ω in the frequency range of 300 kHz to 3 GHz, thus validating the use of a transmission line as a voltage probe.

***   Ms. Julie Lawrence, private communication.
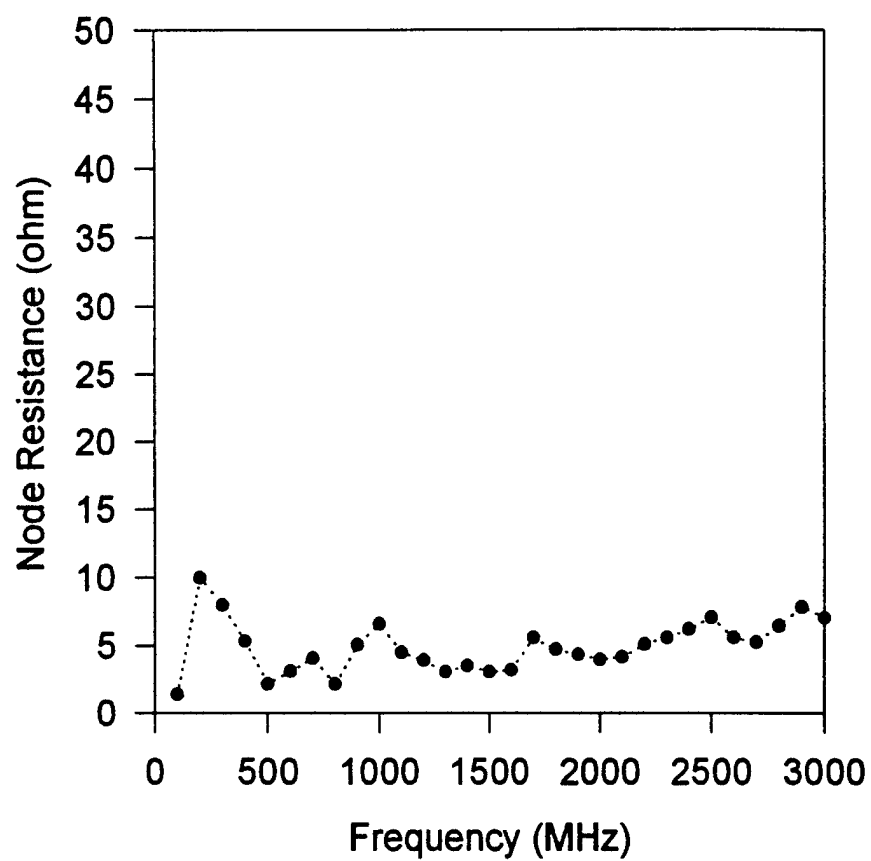
Figure 25. The impedence of the node of the electronic asset which was monitored in the electromagnetic coupling crossection experiments shown in Figure 24. The impedence is nearly always 5 Ω.

7.3   Pspice Simulations of High Frequency Z_0 Voltage Probes

The effects of the intrinsic reactance of the resistive component of Z_0 probes was evaluated by simulating the circuit with a Pspice code. The metric used was the voltage division ratio in the frequency range of 10 MHZ to 1 GHz. The simulation allows an estimation of the intrinsic reactance of the resistive elements of the measured probe response.

In a Z_0 probe, the voltage division exploits the resistance of the measuring device. The

$$\frac{V_1}{V_{Out}} = \frac{R + R_{Scope}}{R_{Scope}} \quad .$$

voltage divider ratio, V_1/V_{out}, is given by

For a resistor value of 1 kΩ and a voltage recorder internal impedance of 50 Ω, the voltage division ratio is 21. Thus, the ideal voltage division ratio for a resistive voltage probe, with an input impedance of 1050 Ω is 21.

The circuit of Figure 26 is used to evaluate the effects of intrinsic capacitance of the resistive element for a Z_0 probe. The capacitor shunts the resistor. The effect of various capacitance values on the voltage division ratio is shown in Figure 27.
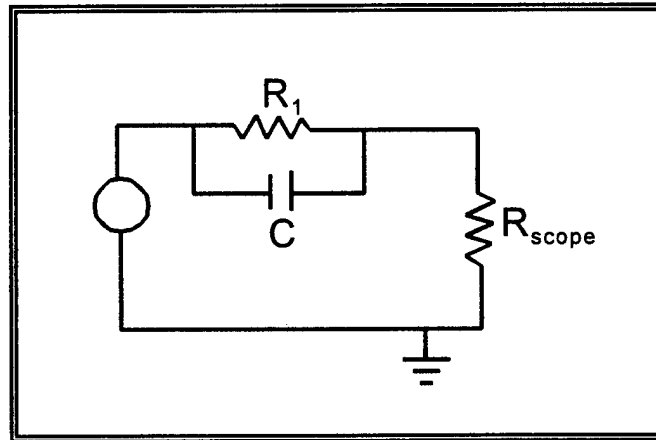
Figure 26.   The equivalent circuit of a resistive divider which has an intrinsic shunt capacitance across the resistive element R_1, whose value is chosen as 1 kΩ. The resistor R_{scope} does not have a shunt capacitor since it represents the 50 Ω termination of the oscilloscope which has negligible capacitance.
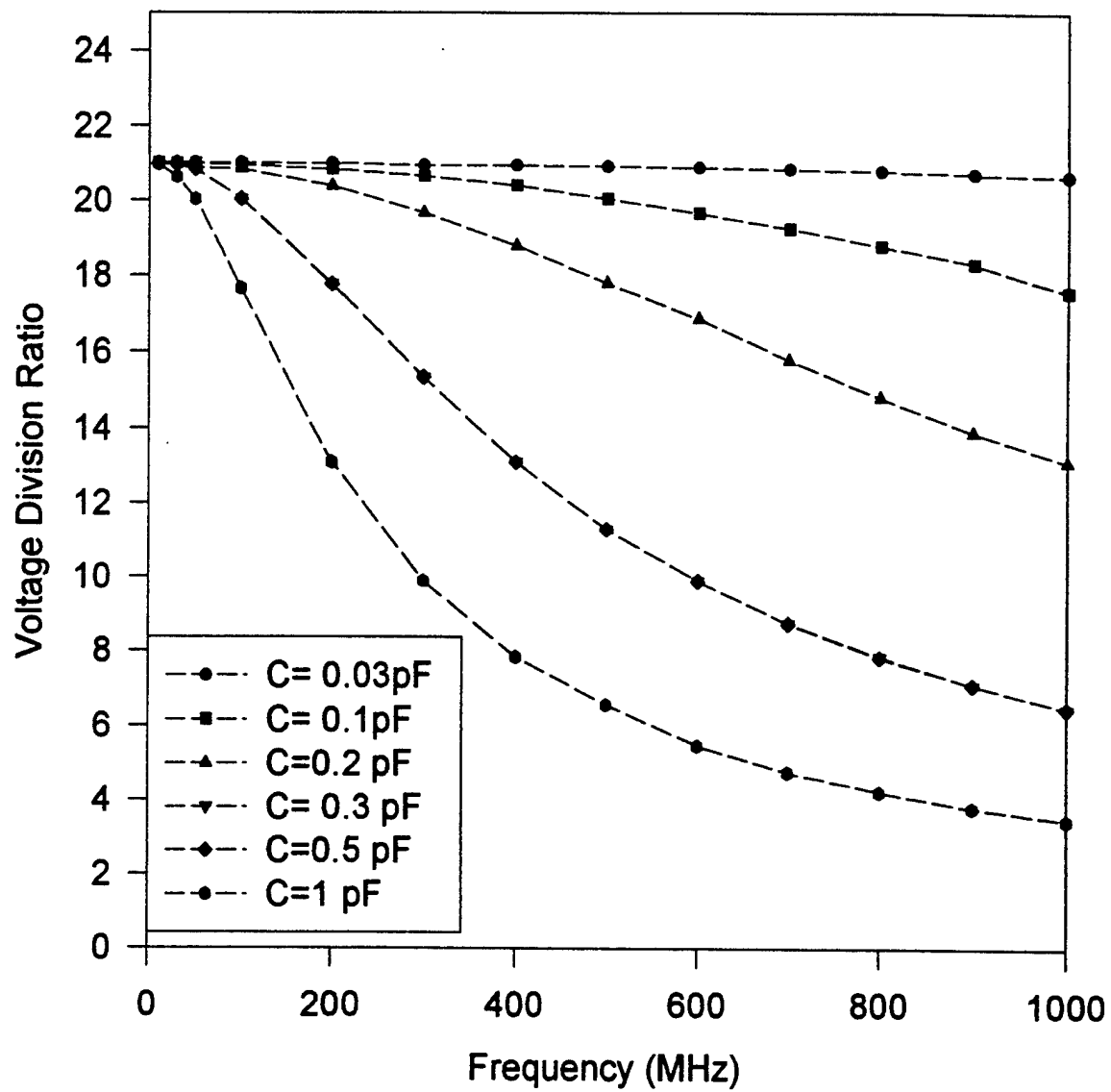
Figure 27. The effect of various values of shunt capacitance of resistor R_1 on the voltage dividing ratio, V_I/V_{out}. The initial value of 0.03 pF was chosen since it is the value of the shunt capacitance, as specified by the manufacturer, of a carbon composition resistor.

Thus, increasing capacitance tends to decrease the voltage dividing ratio, V_I / V_{out}. The larger the capacitance value, the larger the deviation from the ideal ratio. The simulation indicates that a capacitance value of 0.03 pF does not significantly change the voltage dividing ratio of a Z_0 probe for frequencies up to 1 GHz.

It has been established that the voltage dividing ratio decreases with an increasing shunt capacitance value. This trend is also strongly dependent on the input resistance of the Z_0 voltage probe. The circuit of Figure 26 was used to determine the effect of a 0.1 pF shunt capactance on the voltage division ratio as the input impedance of the probe is increased. The results of this Pspice simulation is shown in Figure 28. As the resistance value, R_1, is increased from 1 kΩ to 2 kΩ, the effect of the shunt capacitance on the voltage dividing ratio becomes more severe. For a 2 kΩ resitor shunted with a 0.1 pF capacitor, the voltage division ratio falls to 60 % of its design value at 1 Ghz. The voltage division ratio for a corresponding probe made with a 1 kΩ resistor falls to only 80 % of its ideal ratio. The results of this simulation indicate that the probe performance is maximized by choosing a resistor with the lowest acceptable value. That is, the resistor should meet the criteria,

$$R_p \sim 10 R_n \quad .$$

In addition to providing a probe in which capacitive effects have the least impact, the sensitivity of the probe will also be maximized.
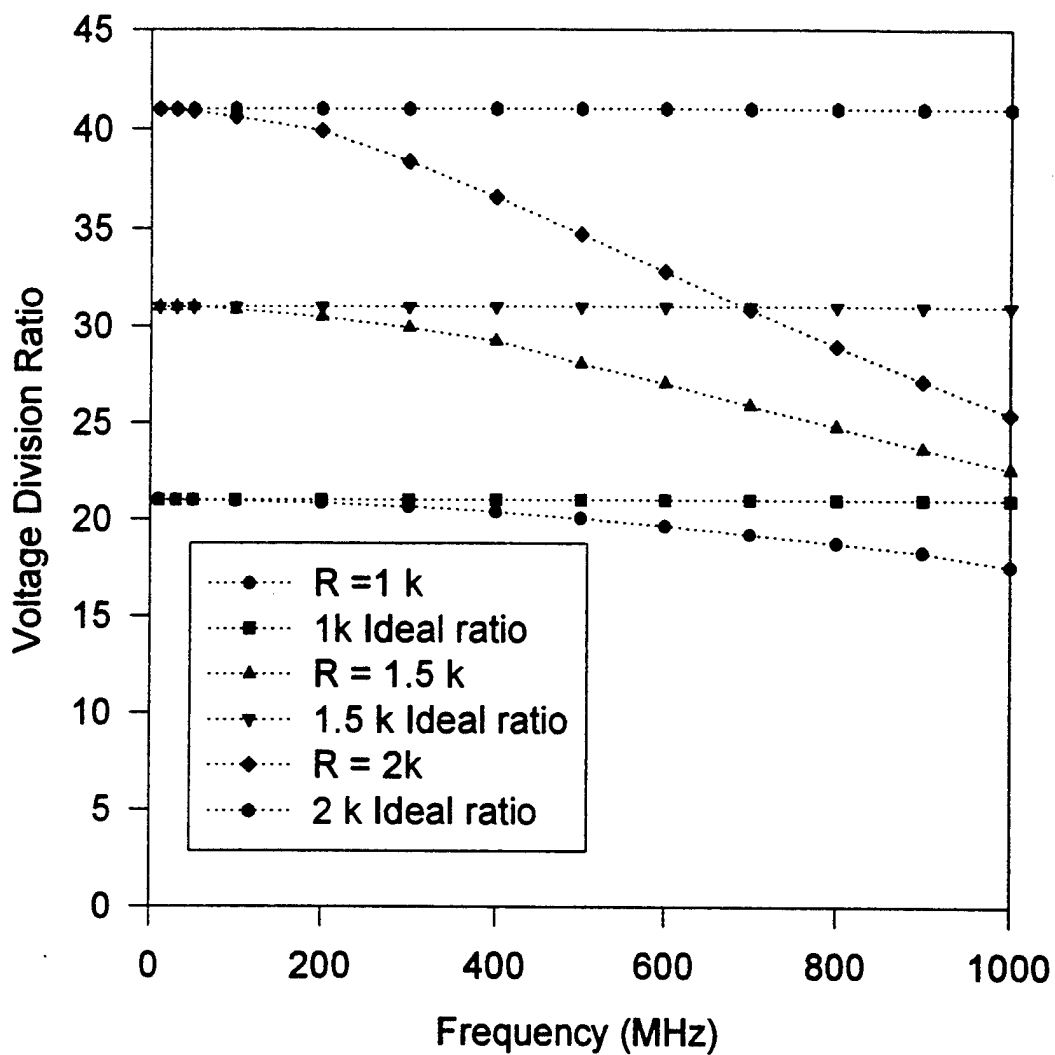
Figure 28. The effect of a 0.1 pF shunt capacitance on Z_0 probes of various input impedances. The capacitance has a much more severe effect on a probe with a 2050 Ω input impedence than on lower impedence probes. These results indicate the lowest acceptable value of resistor should be used.

The circuit of Figure 29 is used to evaluate the effects of intrinsic inductance of the resistive element for a Z_0 probe. The inductor is in series with the resistor because the same current flows through both components.
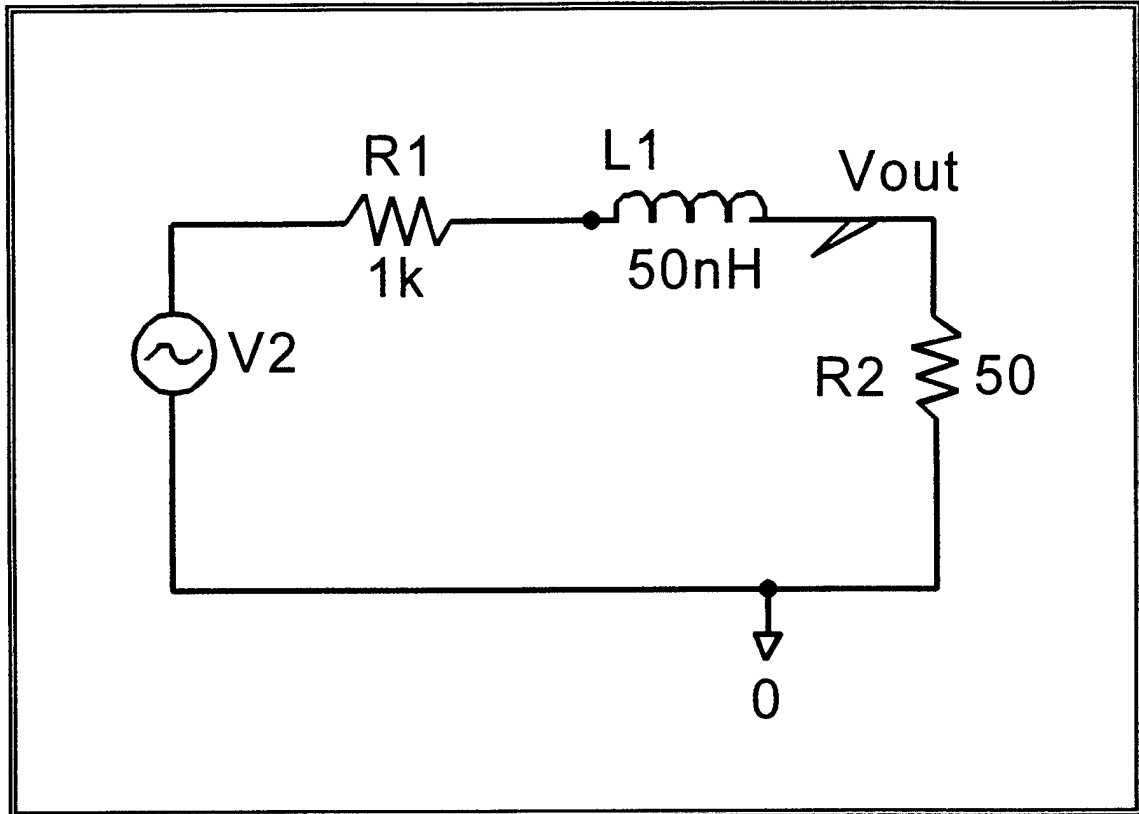
Figure 29.   The circuit used to simulate the effects of inductance on the voltage dividing ratio for a Z_0 probe with an input impedance of 1050 Ω.

The effect of various inductance values on the voltage division ratio is shown in Figure 30. The results of the Pspice simulation show that intrinsic inductance increases the voltage dividing ratio as the frequency increases. If care is taken to minimize the inductance in the experimental setup, inductive effects should not excessively affect measurements.
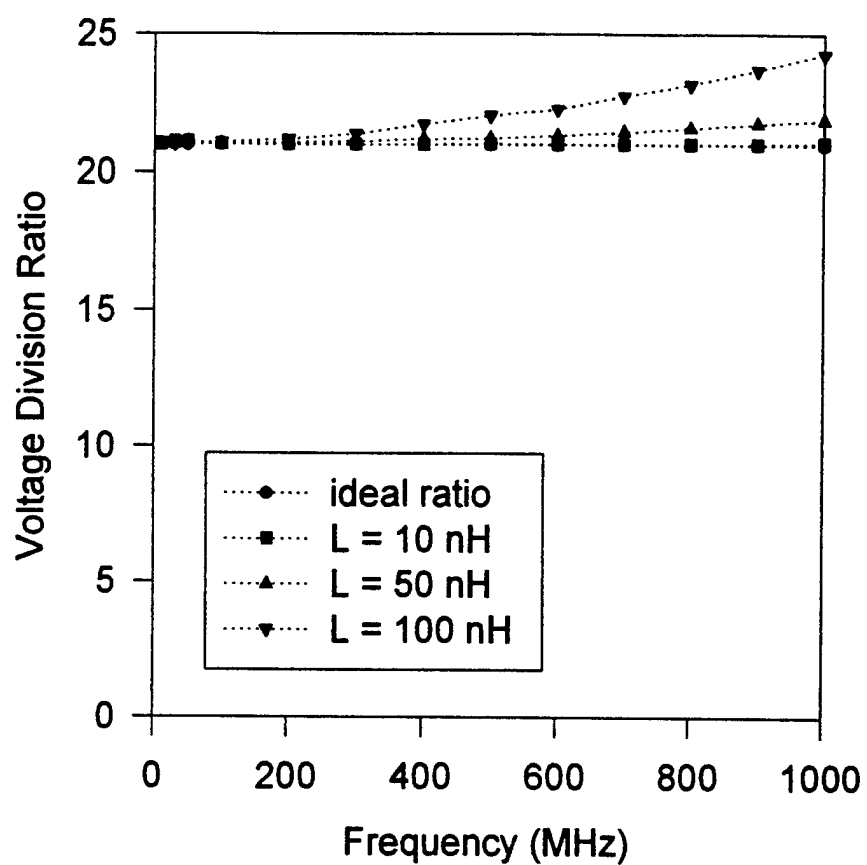
Figure 30. The effect of intrinsic inductance of a resistive element on the voltage dividing ratio of a Z_0 probe with an input impedance of 1050 Ω.

7.4   Resistor evaluation

An experiment was designed to investigate the voltage probes which are commonly used in DIT and their frequency limitations. The integrity of the experiment is insured by using the voltage division ratio as the parameter for comparison between resistor types. The experimental setup is that shown in Figure 21.

7.4.1   Commonly used Resistors in Z_0 Voltage Probes

Chip resistors and non-inductive carbon composition resistors are commonly used to make Z_0 voltage probes. These resistors have features which make them attractive for this type of probe. For instance, chip resistors are small, with a flat and broad geometry, and hence, intrinsically low in inductance. Their small size, especially at low wattage, make them ideal for circuits with limited space to insert a voltage probe. In surveying the DIT community, no constraints were made on the type of chip resistors which are used, although the designation "chip resistor" actually encompasses a large variety of manufacturing techniques. Carbon composition resistors, on the other hand, are cylindrical in shape and can be inserted on the end of a section of transmission line almost seamlessly. Carbon composition resistors have inductive leads, and provided the lead lengths are kept short, are low in inductance. To evaluate their use in Z_0 voltage probes, various probes were constructed as described in Section 3.3.2.

Representative data is shown in Figure 31. An ideal probe has a voltage division ratio of 21 for all frequencies and is shown by the straight line and designated "ideal probe." It is common for the ideal probe ratio to be assumed by test engineers when conducting direct drive tests. The curve labeled "Chip resistor" is the measured response of a commonly used 1kΩ chip resistor. The voltage dividing ratio degrades from 21 at 10 MHz to nearly 15 at 1 GHz. The frequency response of a 1.1kΩ carbon composition resistor is also shown to degrade with increasing frequency. The carbon composition resistor also indicates a voltage division ratio of approximately 15 at a frequency of 1 GHz.

The results of the Z_0 voltage probe circuit simulation indicate that a decreasing voltage dividing ratio with increasing frequency is a capacitive effect. By comparing the experimental and simulation results, the experimental results could reseanably be interpreted
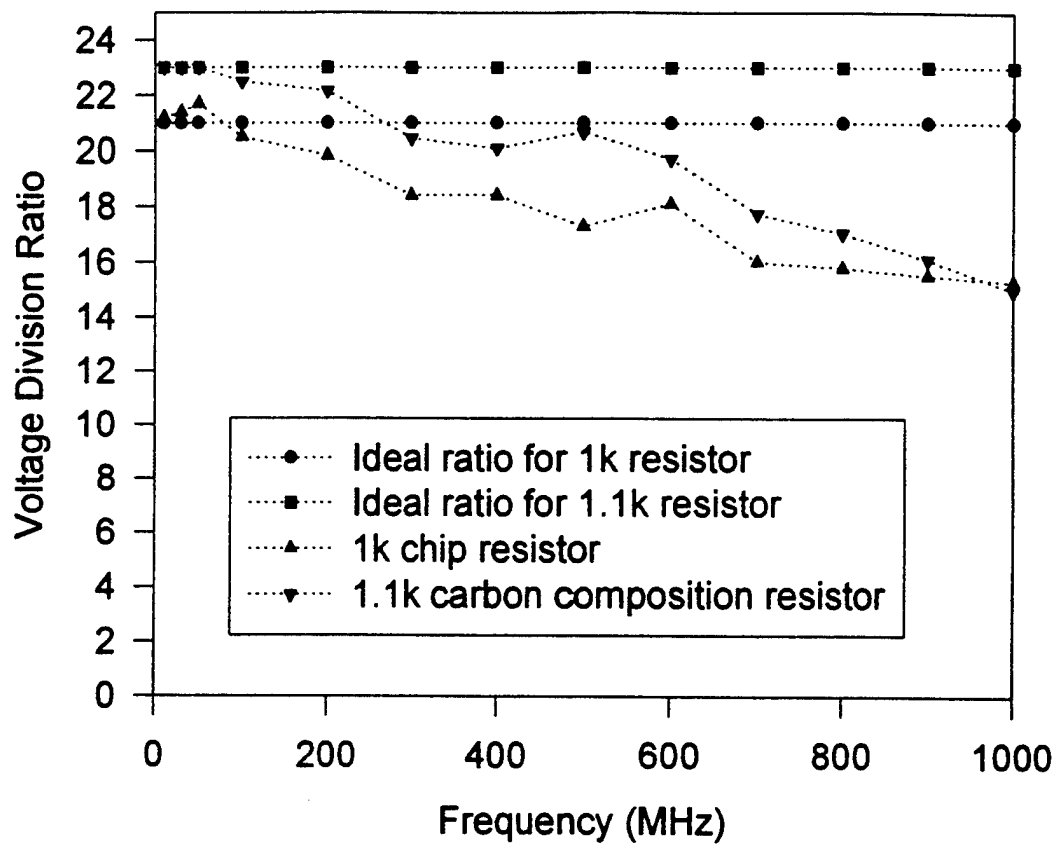
Figure 31. Measurements of the voltage dividing ratio on Z_0 probes made with carbon composition and chip resistors. These type of resistors are usually used to make these probes.

to be a capacitive effect. However, the capacitance of a carbon composition resistor is measured to be 0.03 pF. This capacitance should not alter with frequency. Comparing the frequency response of the probe made with a carbon composition resistor to the Pspice circuit simulation, the carbon composition resistor has an effective capacitance of approximately 0.2 pF.

A concern when dealing with high frequency is the current path through the component. At low frequency, the current penetrates fully through the material. As the frequency is increased, the current tends to travel towards the surface of the component, a phenomena which is well known as the skin depth. This altered current path may affect the actual resistance of the component by lowering the effective crossectional area.

To illustrate the effect of high frequency on the resistance of a material, examine the internal resistance of a cylindrical wire. At low frequency, the resistance of a wire of length, s, and radius, r, is given by[13]

$$R_{DC} = \rho s/A = \rho \frac{s}{(\pi r^2)}$$

For AC, the current travels along the surface to the skin depth, δ, and the AC resistance is

$$R_{AC} = \rho \frac{s}{(2\pi r \delta)}$$

The skin depth, δ, can be computed from

$$\delta = \frac{1}{\sqrt{\pi f \mu_r \sigma_r}} \quad .$$

Since the skin depth cannot exceed the wire radius, the AC resistance is always greater than its DC value. This increase in the resistance at high frequency will result in an increased voltage division ratio. This conclusion is apparent from the voltage division ratio,

$$\frac{V_1}{V_{out}} = \frac{R_1 + R_{scope}}{R_{scope}} \quad .$$

That is, an increase in R_1 results in an increase in the voltage division ratio, V_1 / V_{out}.

However, the effect of shunt capacitance on the voltage division ratio is more severe at higher resistance values, which has been illustrated in Section 7.3, Figure 28. It is likely that the effective resistance of some chip resistors and carbon composition resistors increases somewhat with high frequency due to skin depth effects, and it is unlikely that this accounts for the experiemental results. The increase in resistance with frequency increases the voltage division ratio and shunt capacitance effect decrease in voltage dividing ratio. These competing effects explain why the measured voltage division ratios do not decrease parabolically as the circuit simulations show, but rather tend to decrease in a somewhat more linear fashion.

7.4.2 Resistors rated for high frequency

To investigate if the resistor itself is responsible for the degradation in probe performance, additional probes, of identical construction to those above, were made using various resistor types which are rated for high frequency. The experimentally determined voltage division ratios are plotted as a function of frequency for these resistors in Figure 32.

The carbon film rod resistor denoted "RF rod" is a commercially available resistor which is specifically rated for use at high frequency. For these preliminary tests, resistor samples with a nominal value of 100 Ω were obtained. A probe with an input resistance of 250 Ω was made. Although the resistor values are too low for the 50 Ω experimental test circuit load, the voltage division ratio does not vary with frequency. This conclusively indicates the resistive component is responsible for a degradation in the performance with increasing frequency of this class of probe. Rod resistors, available from Component General, come in standard sizes to 500 Ω. Values up to 1kΩ can be custom made. A probe was tested with this special order item and is also shown in Figure 32. The Z_0 voltage probe made with the 1kΩ RF rod resistor shows an increase in the voltage division ratio with increasing frequency. The reason for this increase is unclear, but may be due to manufacturing considerations, since this is the highest value of this type of resistor which is available. Figure 32 also shows the voltage division ratio for a thick film chip resistor which is available through State of the Art, Inc. The frequency response is excellent, since no degradation at increasing frequency is apparent.
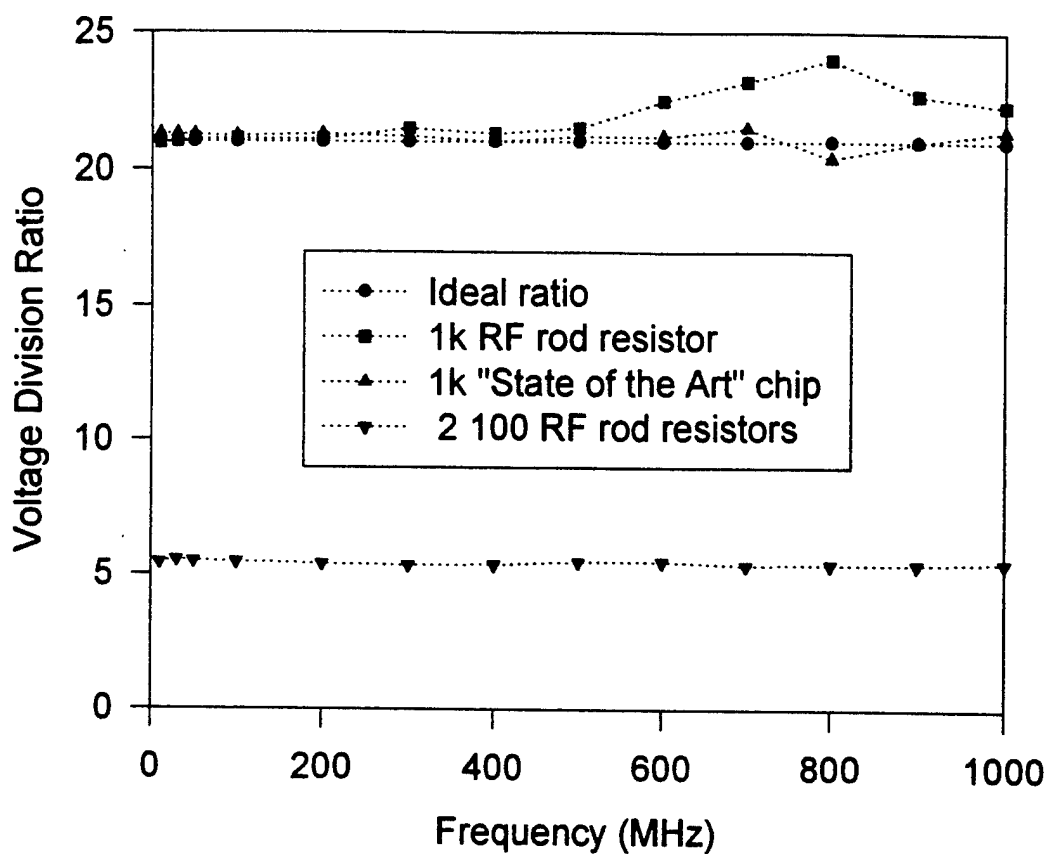
Figure 32. The frequency response of Z_0 voltage probes which are made with resistors which are rated for high frequencies. Note the probe made with two 100Ω RF rod resistors is loading the experimental test circuit, but is included to show the frequency response is excellent.

61

7.5 Comparison of Various Probe Constructions

One of the persistent problems in using Z_0 probes is their mechanical frailty. In an effort to address this problem for some applications, the construction of the probes was investigated. One design increased the mechanical stability of the probe by backing the chip resistor with printed circuit board and epoxy. The response was very good and prompted a look into various probe constructions.

Probe constructions have been previously studied but focused exclusively on the connection of the probe to ground. As expected, inductive ground paths were found to be detrimental to voltage probe operation by altering the effective impedance at high frequency. This is expected because a wire has an internal inductance. The internal inductance of a circular wire of radius, r, and length, s, expressed in meters, is given by

$$L = 0.2 \ s \ [\ln(\frac{4s}{2r}) - 1] \ \mu H \ .$$

The internal inductance of a wire is different than the external inductance which increases as the loop area. The internal inductance of a wire does not have to be in loop, and this internal inductance is the reason that long wire lengths on resistors are undesirable. The equations for rectangular lengths of conductors are different than the above equations, and tend to reduce the inductance of the conductor. This is why straps are desirable for grounding applications where conductor lengths may be long.

A test of the specific construction of voltage probes was conducted. A carbon composition resistor was used to construct two probes; one is a standard construction and the other is a fully shielded probe. The shielded probe covers the resistor with a portion of the solid copper jacket which makes up the outer conductor as illustrated in Figure 33. The extended outer conductor minimizes the connection length to circuit ground and enhances the mechanical strength of the probe. It also affects the stray capacitance to ground in the vicinity of the resistive element.
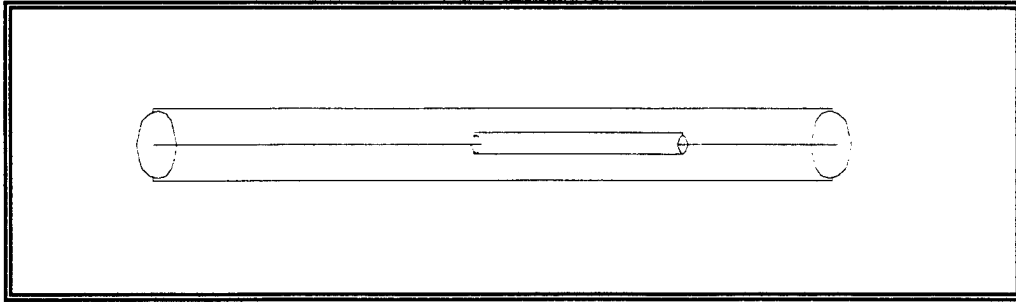
Figure 33. Two Z_0 voltage probes were contructed using carbon composition resistors to evaluate the effect of probe design on its performance. The probe shown here is refered to as the "shielded construction." It was meant to simulate the common practice of pulling the shielding over the resistor.

The frequency response of each of these two probes is shown in Figure 34. The conventionally constructed probe has a decreasing transfer response function as frequency is increased. The shielded probe has a response which degrades rapidly (compared to a similiar conventional probe), then increases again, nearly to its starting ratio. The decrease in the voltage dividing ratio has been identified as being largely the result of capacitive shunting. The rise in voltage dividing ratio has been identified, by a Pspice circuit simulation, as an inductive effect. Thus, this unexpected behavior is a response to the competing behavior of the decrease in effective resistance and increase in reactance with increasing frequency.

To further investigate the effect of probe construction on performance, a series of probes were made using RF rod resistors. The various probes designs are labeled A, B, C, and D. The effect of the various probe designs on the voltage dividing ratio are shown in Figure 35. The various probe designs were mainly an investigation of ways to increase their mechanical stability, but provide information on the importance of characterizing a probe prior to its installation in a DUT.
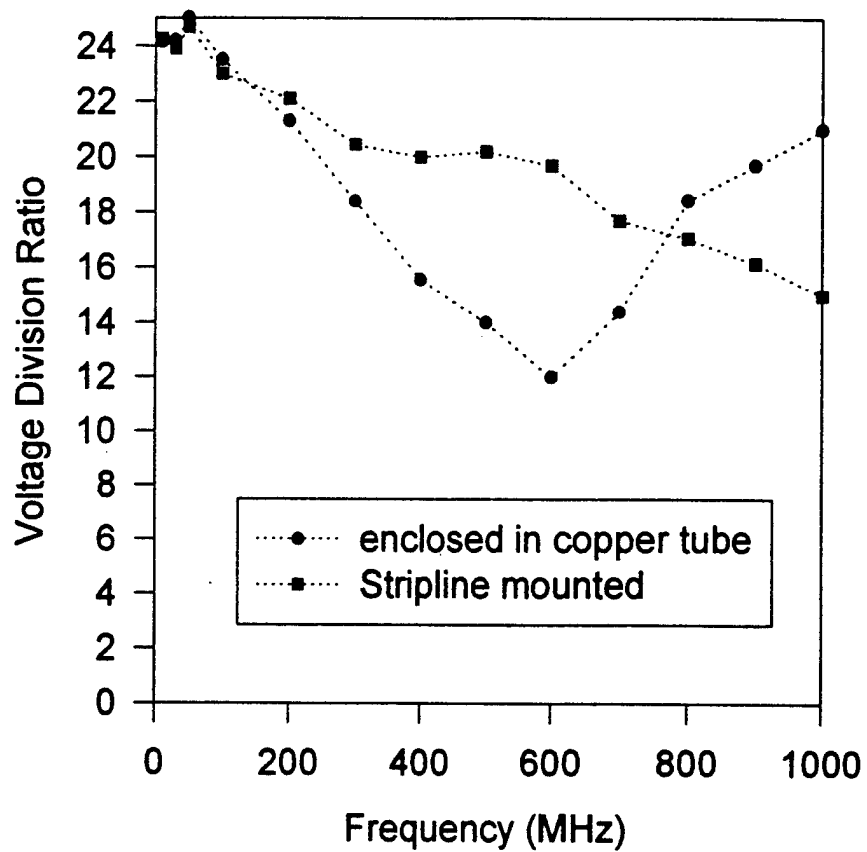
Figure 34. The voltage division ratio of two probes made with carbon composition resistors. One probe is a standard Z0 probe and the other is fully shielded. The fully shielded probe show the effect of the added inductance at higher frequencies.

64
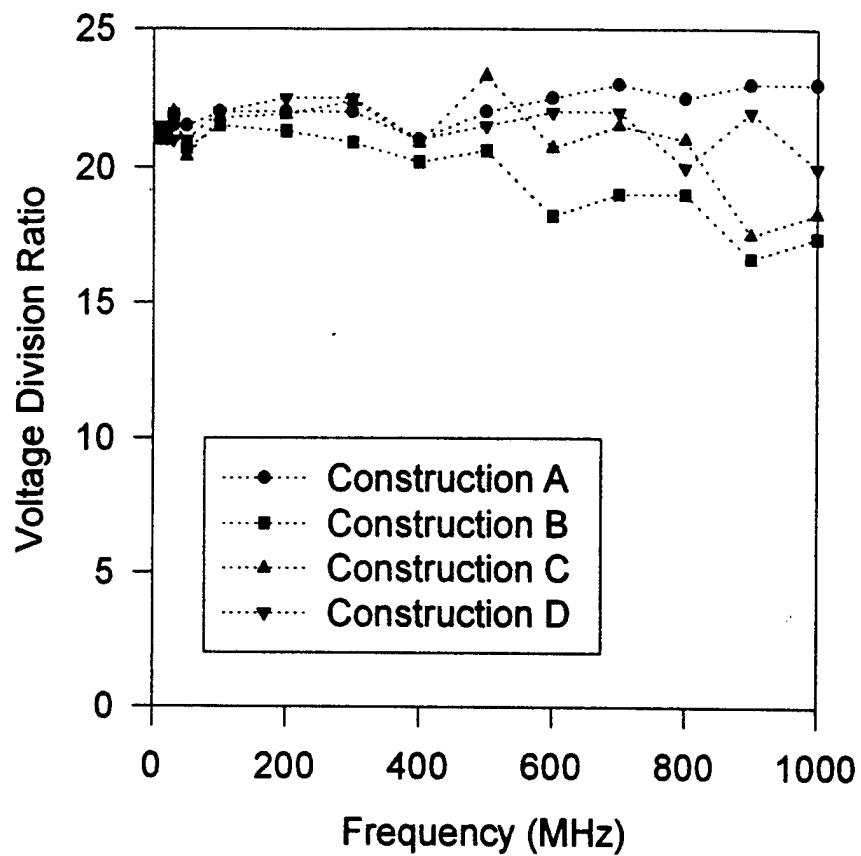
Figure 35. The effect of various probe constuctions on the voltage dividing ratio. A fair amount of discrepancy is evident in the various probe constructions.

8.0   METHODS OF CHARACTERIZING VOLTAGE PROBES: THE TRANSFER FUNCTION

The first step in a direct drive experiment should be the selection and complete characterization of the probes to be used in the experiment. The pretest chores will necessarily include measuring the node impedance and choosing an appropriate probe. Maximum sensitivity will be achieved if the lowest value of input resistance, which does not load the circuit node, is used. Neglect of this pretest task can result in faulty data. It should be noted that a transfer function measurement cannot correct for circuit loading effects because an inappropriately chosen probe will draw excessive current from the circuit under test and perturb circuit operation.

The probes can be characterized in many ways, but one of the most popular techniques for high frequency applications is the transfer function. The transfer function is schematically represented in Figure 36.

$$F(f) \longrightarrow \boxed{T(f)} \longrightarrow G(f)$$
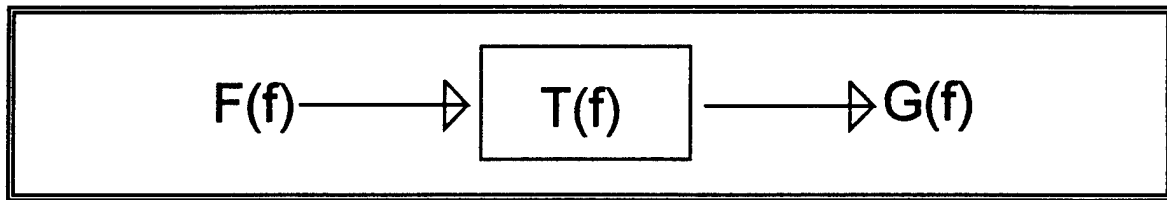
Figure 36.   The transfer function.

The transfer function, T(f), is defined as,

$$T(f) = \frac{G(f)}{F(f)} .$$

where F(f) is the excitation function and G(f) is the response function of the system.

For a voltage probe, the transfer function is a representation of the voltage division ratio. That is, the input voltage, V_I, is the driving function F(f) and the output voltage, V_{out}, is the response function, G(f). Explicitly, the theoretical transfer function is the scenario of a purely resistive probe and can be calculated from

66

$$dB = -20 \ \log(\frac{V_I}{V_{out}}) = -20 \ \log(\ \frac{R_1 + R_{scope}}{R_{scope}} \ )$$

where V_I is the input voltage, V_{out}, is the measured voltage at the analyzer, R_{scope} is the resistance of the analyzer, and is typically 50Ω. The input resistance of the resistive probe is $(R_1 + R_{scope})$.

Thus, the transfer function for a resistive divider probe should be flat and centered about its ideal value as calculated from the above equation. To illustrate the importance of verifying probe characteristics, the transfer function of two probes will be discussed one that has been used in direct drive tests, and one which this team constructed.

8.1   Demonstration of Present High Frequency Probe Operation

The transfer function measurement of a probe which is used in a state of the art direct drive facilitator for use with avionics systems is shown in Figure 37. Citing Figure 37, the 3dB bandwidth of the probe is approximately 700 MHZ. Note that for the 1 kΩ chip resistor probe, designed as in Figure 38, the ideal ratio is -32.26 dB. During the scan frequency of 300 kHz to 3 GHZ, the voltage division ratio changes over 12dB. The rationale for allowing such a large change is that the measured transfer function is used to reconstruct the measured signal, with the contention that the data can be corrected for the probe degradation. This ignored the loading effects from the probe on the signal. From the treatise on signal measurements in Section 4.0, however, it has been shown that circuit loading effects are the result of both reactive and resistive elements.

67

Voltage Probe Transfer Functions
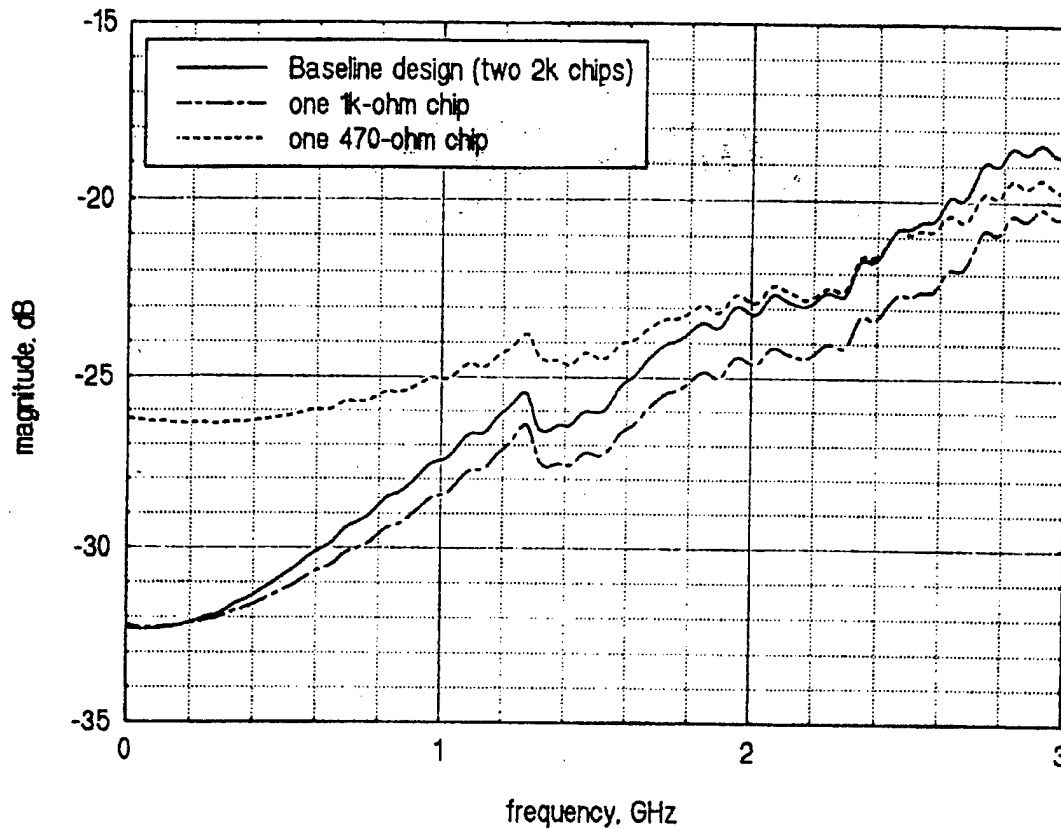
Figure 37. **The transfer function of probes used on a typical direct drive experiment. Note the bandwidth is approximately 700 MHZ. The transfer function changes over 12 dB in the frequency range 300kHz to 3 Ghz.**

The above probe is constructed slightly different than the configuration shown in Section 3.3.2. A 50 Ω resistor is inserted to ground as shown in Figure 39 to minimize the reflections.
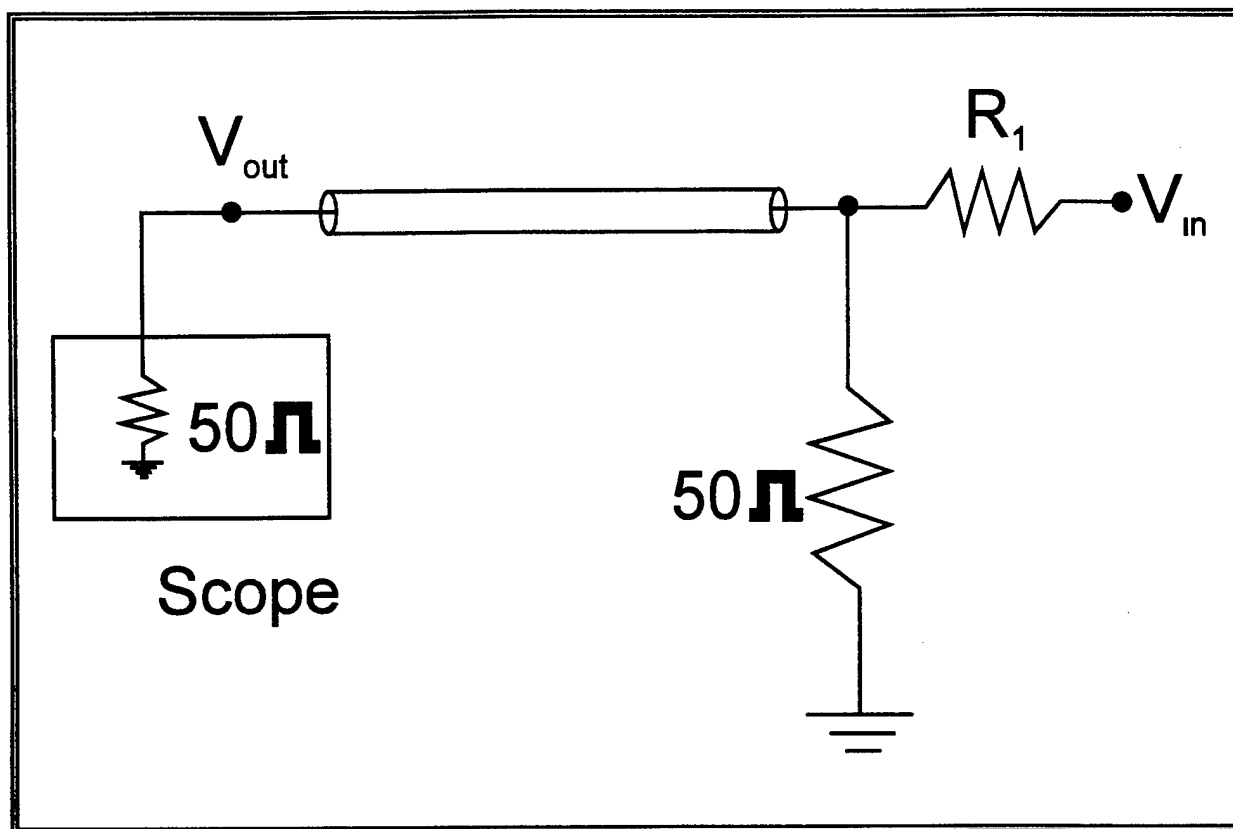
Figure 38. **The schematic of the voltage probes used to obtain the transfer functions of Figure 37.**

The 50 Ω resistor is in parallel with the 50 Ω resistance of the recorder, R$_{scope}$,

$$\frac{V_I}{V_{out}} = \frac{R_1 + R_I}{R_I}$$

where R$_I$ is the equivalent parallel resistance of the 50 Ω resistor and the 50 Ω resistance of the recorder. The addition of the 50 Ω resistor to ground serves to increase the voltage dividing ratio to 41 for a Z$_0$ probe using 1 kΩ resistance at the input. In dB, this voltage dividing ratio corresponds to a transfer function magnitude of ±32.26 dB. Figure 37 indicates the transfer function is located at this line for frequencies below 200 MHZ.

The 2 kΩ chip resistor which was used to construct one of these probes was tested and the voltage dividing ratio was measured. This experimental data is shown in Figure 39.
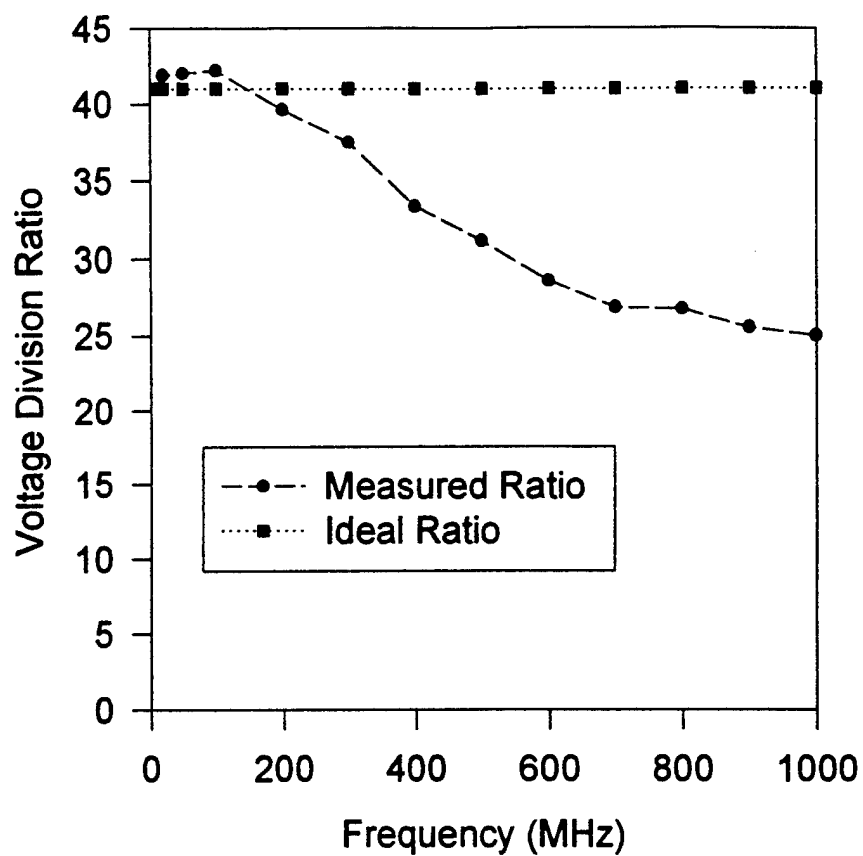
Figure 39. The voltage dividing ratio to 1GHz for the 2 kΩ chip resistor used in a state of the art direct drive experiment. The transfer function for this probe is shown in Figure 37. The ideal voltage dividing ratio is shown to be 41.

70

Figure 39 indicates that the voltage dividing ratio begins to degrade at a frequency of 200 MHZ. Note this degradation is also seen to start at 200 MHZ in the transfer function of Figure 37. The baseline design of two 2 kΩ resistors indicate that this parallel combination degrades in performance faster than a single 1 kΩ resistor. This indicates the degradation is caused by the inherent shunt capacitance of the resistor, since the parallel capacitors combine via a sum.

8.2   Demonstration of Proper High Frequency Probe Performance

The above probe must be compared to one carefully constructed using components rated for high frequency. The prototype probe is made with a Mini-Systems, Inc. (MSI) thick film chip resistor, part number WNR73PS-1001F-NS, with a nominal value of 1kΩ and a 1% tolerance.

For clarity, it should be noted that the frequency response of chip resistors defies universal characterization. Chip resistors are used in application where low inductance is required. The geometry of the chip resistor is inherently low inductance: the current flows through a broad area, and the distance between electrical contacts is short. However, with increasing frequency, the effect of intrinsic capacitance also becomes appreciable. Moreover, as the frequency approaches the microwave range, the current does not flow evenly through the resistive component anymore; the current travels towards the surface. This high frequency behavior serves to degrade the performance of the resistive element in addition to the increased impact of the stray capacitance. Hence, the frequency response of specific chip resistors depends largely on its geometry. To the user, this means that before a resistor is used in testing, its frequency response must be tested.

The MSI thick film chip resistors used in this test operated admirably throughout the frequency range of interest, 300 kHz to 3GHz. The MSI literature rates its thick film resistors to 2 GHz. The voltage division ratio for a probe constructed with this resistor is shown in Figure 40.
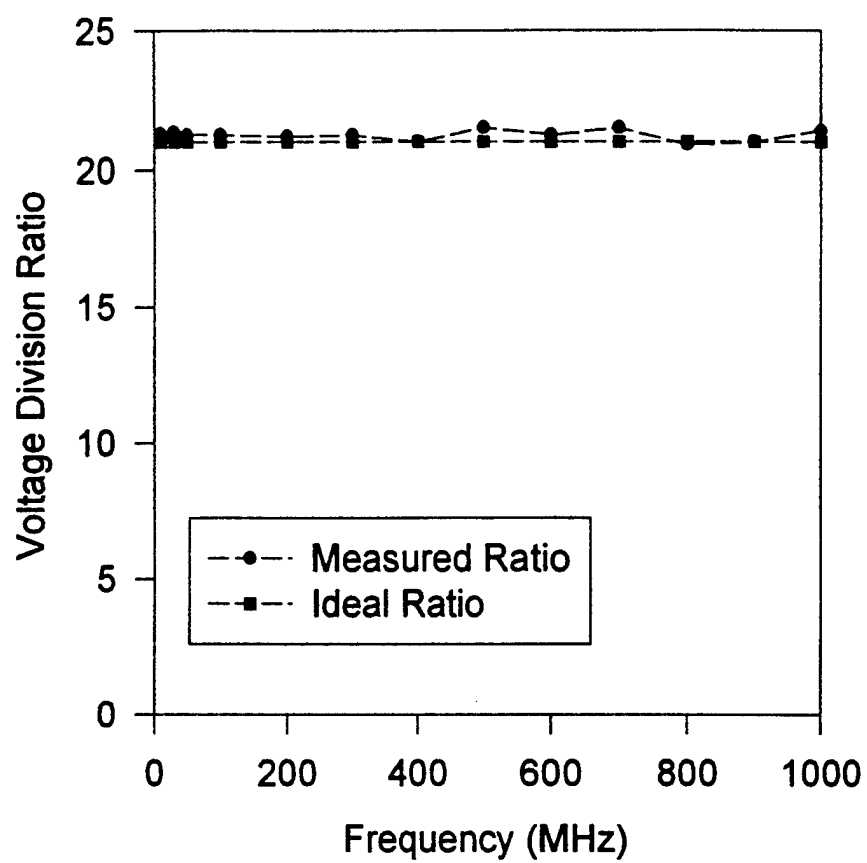
Figure 40. The voltage division ratio, to 1GHz, of the MSI thick film chip resistor.

Figure 40 shows there is negligible degradation in the performance of the thick film chip resistor with frequency. Since transfer functions are the standard way of characterizing a voltage dividing probe in the DIT community, the transfer function was measured using the probe calibration fixture which is discussed in Section 8.4. The transfer function for the MSI thick film chip resistor is shown in Figure 41.

CH2 S$_{21}$ log MAG   2 dB/   REF -27 dB   1: -29.994 dB
447.455 260 MHz
MARKER 1
447.45526 MHz
C2
START   .300 000 MHz   STOP 3 000.000 000 MHz
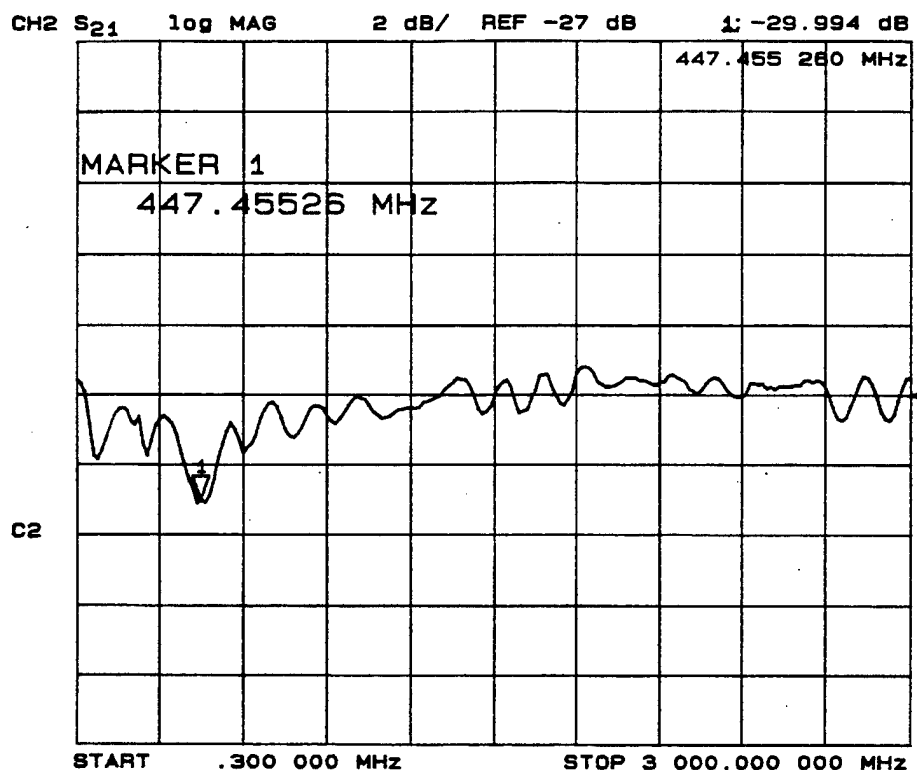
Figure 41.   The transfer function of the voltage probe constructed with the MSI 1 KΩ thick film chip resistor. Note the transfer function is centered about the -26.44dB line, which corresponds to a voltage division ratio of 21.

8.3   Comparison of Transfer Function Measurement Equipment

The transfer function of the probe constructed with the MSI 1kΩ thick film chip resistor was measured using two Hewlett Packard network analyzers. The vector network analyzer was HP model 8753B, and the scalar network analyzer was HP model 8757D. A comparison of data obtained with these two analyzers was performed to determine which yielded better results.

The transfer function obtained with the 8757D scalar network analyzer is shown in Figure 42. The transfer function is centered about the ideal line. Although the probe performance appears acceptable, the maximum deviation is almost 3 dB. It can be assumed that this measurement does not reflect the true transfer function because the transition is not smooth. That is, the frequency response of a resistive probe is determined by the relative importance of the stray capacitance and inductance. If these are small, the transfer function will be flat across the band of interest. Thus, the net change should be smooth with frequency. Near the 3 GHz mark, the transfer function decreases after a net increase. This is an indication that the transfer function measurement is within the accuracy of the scalar network analyzer.

The transfer function obtained with the vector network analyzer is shown in Figure 43. Note that the probe bandwidth cannot be measured since performance degradation is not obvious in the frequency range to 3 GHz. The transfer function shows only slight deviations throughout the frequency range of 300 kHz to 3 GHz. Furthermore, these slight deviations are centered about the theoretical transfer function, located at 26.44 dB.

CRSR   −31.53 dB
585.57 MHz

12 >

2

1

STRT   10.000 MHz   CRSR   585.57 MHz   STOP   3.0000 GHz
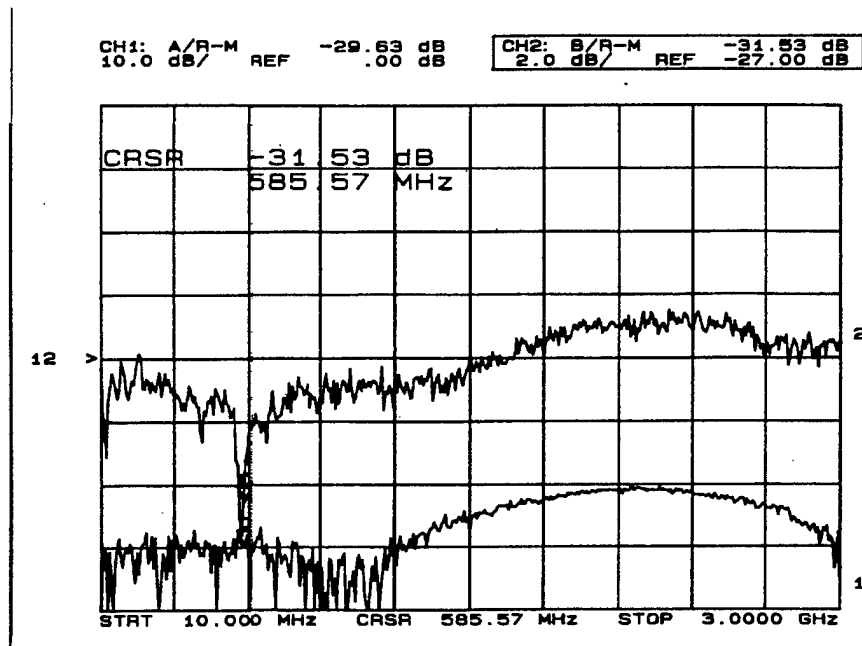
Figure 42.   The upper trace is the transfer function for a 1050 Ω probe obtained with a scalar network analyzer. The frequency range is 10 MHz to 3 Ghz. The lower trace is the return loss measurement.

CH2 S_{21} log MAG   2 dB/   REF −27 dB   1: −29.994 dB

447.455 280 MHz

MARKER 1
447.45526 MHz

C2

START   .300 000 MHz   STOP 3 000.000 000 MHz
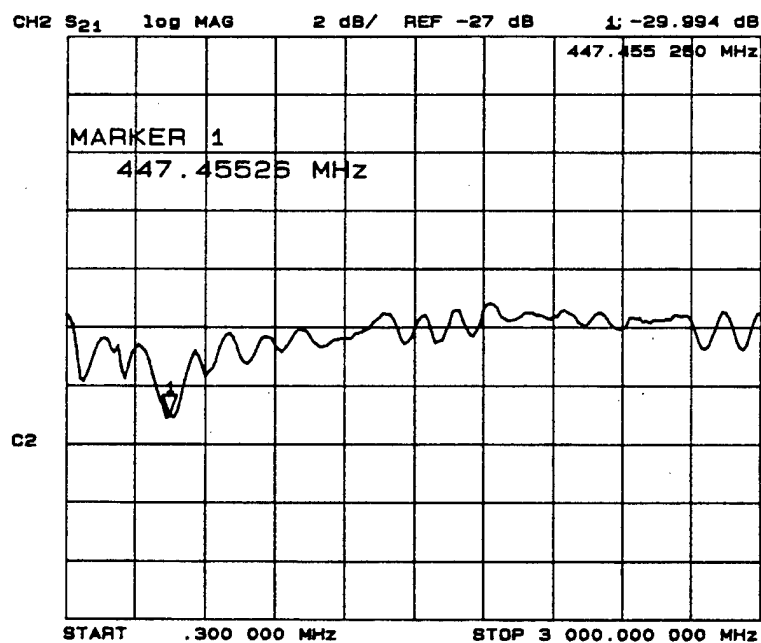
Figure 43.   The transfer function of the same probe as in Figure 42, made with the MSI 1kΩ chip resistor and obtained with the vector network analyzer.

75

The dip in the low frequency portion of the transfer function is attributed to the prototype probe calibration fixture. Evidence for this conclusion is that it remains despite the construction of various probes and is contained in the transfer functions measured with both network analyzers.

This exercise has shown explicitly that the vector network analyzer gives more accurate measurements. This is a well known attribute of vector network analyzers ****, yet is useful because it sets a basis for an engineering judgement despite which analyzer is available.

8.4   Probe Calibration Fixture Design

It has been established that pretest verification of voltage probe performance is critical to obtaining reliable data. To aid in the determination of the voltage probe performance, a calibration fixture has been designed and tested.

The calibration fixture design, shown in Figure 44, is easy to implement and technically elegant in its simplicity and reliablitity. The calibrator consists of a 50Ω microstrip section with one SMA connector on each side. Microstrip is chosen as the transmission line since it is easily accessed electrically for the probe connection, and is resistant to stray reactances. One SMA connector of the fixture is terminated in a 50Ω coaxial resistive termination which is rated for high frequency. The other SMA connector is the RF feed line.

The prinicple of operation of the probe calibation fixture is to provide a matched system with a spatially homogeneous voltage. That is, the matched system has a voltage standing wave ratio (VSWR) which is equal to one. Thus, the voltage at any length along the line is constant. The probe under test may be placed anywhere along the microstrip center conductor, and the transfer function can easily be obtained. It has been experimentally determined that a soldered connection between the probe and the calibration fixture is not necessary to obtain valid transfer functions.

**** Hewlett Packard Hotline, private communication
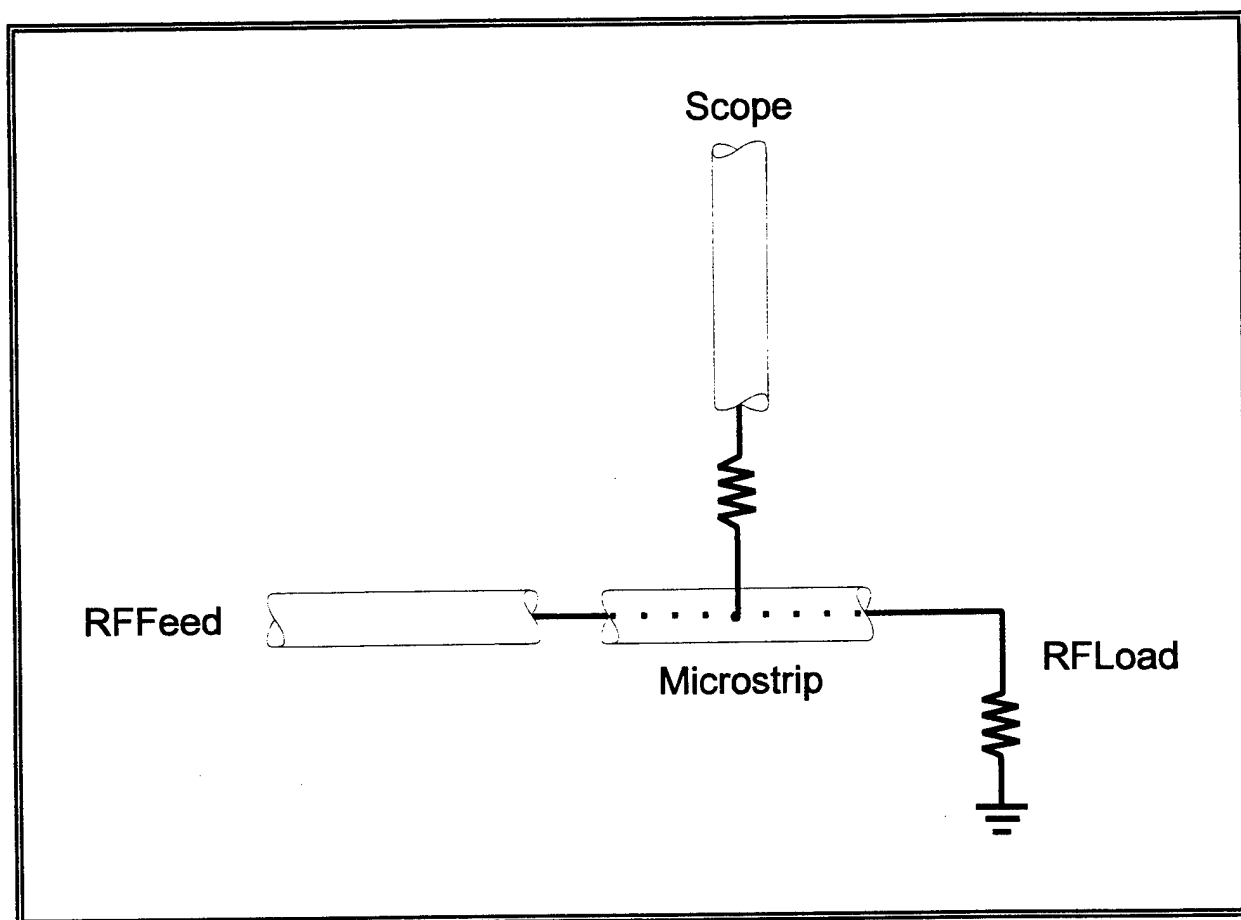
Figure 44. A simple, easy to use, fixture for the calibration and measurement of transfer functions of voltage probes. The probe does not need to be soldered to the fixture to be accurate.

This calibration fixture allows the quick verification of probe performance prior to its installation in a circuit. This simple pretest procedure insures a reliable voltage probe and opens the possibility of meaningful measurements.

9.0 RELEVANT POWER QUANTITIES

In performing direct injection testing, some test engineers measure only the incident power which results in an effect. While this practice can be rationalized, the incident power is not the truly relevant quantity for direct injection testing, as it is in free field testing. Moreover, it can be postulated that energy is the quantity of interest, since it accounts for additional test parameters, such as pulse repetition frequency, pulse duration and illumination time. After all, in free field testing, the relevant quantity is the power on target.

It is a widespread practice in direct injection testing to measure only the incident power. However, since electrical energy from radiation sources and direct voltage injection couple differently into a circuit, the power which is absorbed into circuit allows a direct comparison. This issue will be further investigated in Section 11. After all, the portion of power which is absorbed may result in an "effect". This practice may be a part of the reason why electromagnetic effects vary in power level from one DUT to another.

The absorbed power is related to the circuit parameters of the node of the DUT. For a node impedance, Z_n, the absorbed power, P_a, is related to the incident power, P_{Inc}, by

$$P_a = P_{Inc} \left(1 - |\Gamma|^2\right) \ ,$$

where Γ is the reflection coefficient. The reflection coefficient may be calculated from the formula,

$$\Gamma = \frac{Z_n - Z_0}{Z_n + Z_0} \ ,$$

where Z_0 is the characteristic impedance of the RF feed line, or by experiment. It should be noted that in general, the node impedance, Z_n, is a function of frequency. Thus, the reflection coefficient, Γ is also a function of frequency.

In determining the absorbed power, the exact experimental configuration must be taken into account. For instance, if an isolating resistor is used, the power which is absorbed by the DUT cannot be measured directly by recording the reflected wave since the isolating resistor will

dissipate power. This obstacle can be overcome through calibration and data analysis.

Once the power absorbed by the DUT has been determined, the distribution of the power can be determined by knowledge of the node impedance. The absorbed power is distributed in a two port network according to the magnitude of the complex impedance. Explicitly,

$$P_a = P_d + j \, 4\pi f \, (W_m - W_e) \,,$$

where P_d is the average power dissipated in the circuit and W_m and W_e represent the stored magnetic and electric energy. The node impedance can be equated with expressions for the voltage and current which yields the relation,

$$P_a = \tfrac{1}{2} \, |I|^2 \, Z_n = \tfrac{1}{2} \, |I|^2 \, (R_n + jX_n)$$

Rearranging terms and equating expressions for the absorbed power, yields,

$$Z_n = R_n + jX_n = \frac{P_d + j4\pi f \, (W_m + W_e)}{\tfrac{1}{2} \, |I|^2} \,.$$

The real part of the node impedance is related to the dissipated power, P_d,

$$P_d = \tfrac{1}{2} \, R_n \, I^2 \,,$$

and the imaginary part, X_n, is related to the energy stored in the DUT. Thus, the energy stored in the system is

$$W_m - W_e = \frac{X_n \, |I|^2}{8\pi f} \,,$$

which is positive for an inductive load and negative for a capacitive load.

9.1 Impedance Matching for Maximum Transfer

Since the need to measure absorbed power is established, ways to maximize the absorbed power can be investigated. Various quantities can be maximized depending on the DUT of interest, and it is expected that different circuit types may be sensitive to different quantities. For

instance, the voltage which is transmitted into the asset, V_a, is given by

$$V_a = V_{inc} (1 - \Gamma) \ .$$

Thus, the voltage which is transmitted to the asset is maximized by minimizing the reflection coefficient, Γ.

However, presently, in electromagnetic effects testing, power is generally the scaling quantity. The absorbed power is given by

$$P_a = P_{Inc} (1 - |\Gamma|^2) \ ,$$

and is optimized by minimizing the value of $|\Gamma|^2$.

9.1.1   Impedance Matching for Ultrawideband Excitations

Impedance matching for UWB pulses can be difficult because of the wide range of frequencies that must be accommodated. For applications requiring a bandwidth greater than a single quarter wavelength, multi section transformers can be used. Then the total reflection coefficient is given by the partial reflections of small discontinuities. A full treatment of the theory of small reflections can be found elsewhere[9.1, 9.2]

One method of impedance matching a source impedance, Z_s, to a load impedance, Z_n, is to successively increase the impedance in small steps from Z_s to Z_n. The impedance taper is a stepped impedance transformer with infinitesimal steps, and is commonly used in high power systems. Although high power impedance taper are generally a coaxial gambit, this is not appropriate for use in confined spaces, which frequently occurs in DIT.

A small, low power impedance taper for use with UWB pulses can be easily made using a microstrip transmission line by varying the width of the strip. The geometry of a microstrip line is shown in Figure 45.
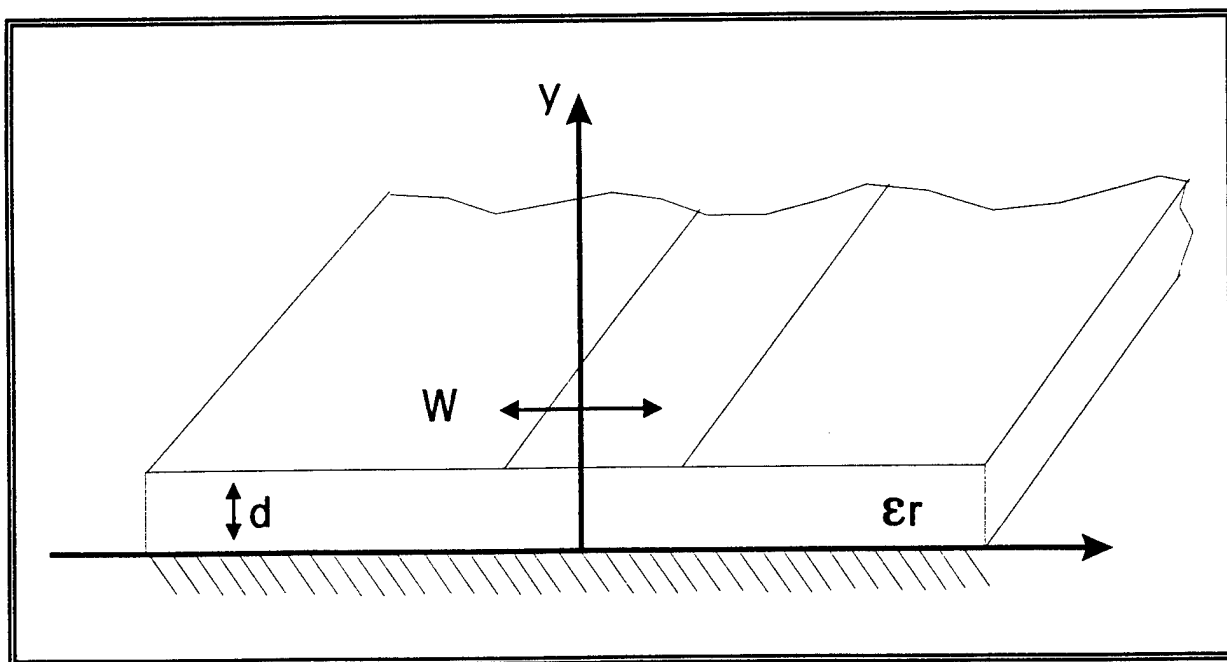
Figure 45. The geometry of a microstrip line.

The impedance of a microstrip line is given as a function of the dimensionless quantity, W/d, by

$$Z_0 = \frac{60}{\sqrt{\epsilon_e}} \ln(\frac{8d}{W} + \frac{W}{4d}) \qquad for \quad \frac{W}{d} \leq 1$$

and

$$Z_0 = \frac{120\pi}{\sqrt{\epsilon_e} [\frac{W}{d} + 1.393 + 0.667 \ln(\frac{W}{d} + 1.444)} \qquad for \quad \frac{W}{d} \geq 1.$$

The quantity ϵ_e is the effective dielectric constant of the microstrip and is given approximately by

$$\epsilon_e = \frac{\epsilon_r + 1}{2} + \frac{\epsilon_r - 1}{2} \frac{1}{\sqrt{1 + 12\frac{d}{W}}}$$

Thus, if the value of the ratio W/d is varied continuously, an impedance transformer can be easily made to transition from the source impedance to the load impedance.

9.2   Impedance Matching for Narrowband Excitations

Impedance matching in narrowband systems is considerably easier than in ultrawideband systems. However, many techniques for impedance matching require prior knowledge of the load and source impedances as well as the frequency. Any change in these parameters requires a new matching fixture. One impedance matching technique, however, is not limited in this way: stub tuning. Moreover, a stub tuner matches a complex impedance conjugately. As previously stated, the absorbed power is maximized when the value of $|\Gamma|^2$ is minimized, which occurs when the system is conjugately matched. In narrowband systems, one of the easiest and most versatile ways to conjugately match a system is through the use of a stub tuner.

9.2.1   Single Stub Tuners

A single stub tuner matches discrete complex impedances at discrete frequencies. Figure 46 shows a schematic diagram of a single stub tuner.
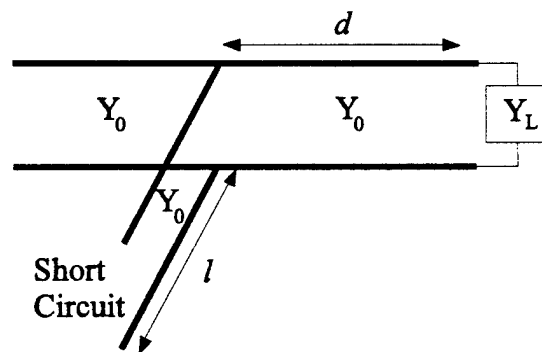
Figure 46.   Single Stub Tuning.[14]

The real part of the impedance is varied by changing the distance of the stub (d) from the complex load. The imaginary part of the impedance is varied by changing the length of the stub (l). The operation of a single stub tuner is easily understood by examining the input impedance of the stub section. At the junction, the impedance looking into the stub section is derived from the input impedance, Z_{input},

$$Z_{input} = Z_0 \frac{Z_L + jZ_0\tan(\beta l)}{Z_0 + jZ_L\tan(\beta l)}$$

where $\beta = 2\pi f/c$, is the wave propagation constant. For a stub of length, l, which is terminated in a short circuit, the load impedance, Z_L is zero. The input impedance of the stub line reduces to

$$Z_{input} = jZ_0\tan(\beta l) \quad .$$

The stub line is in parallel with the input impedance of the load section. Thus, by equating the parallel combination to the line impedance, a relation between the distance to the load, d, the stub length, l, and the load impedance, Z_L, is obtained. The real part of this relation is matched by choosing the distance to the load and the imaginary part is matched by choosing the stub length. However, single stub tuners are suitable for only a small range of frequencies for fixed distances. This limitation is overcome by expanding the single stub concept to multiple stubs.

9.2.2   Triple Stub Tuners

A triple stub tuner can match different configurations of complex impedance and corresponding frequency. It is not feasible to use a single stub tuner for such a purpose because it is difficult to vary the length of line between the load and the stub to match the real part of the load impedance. The combination of stub lengths in the triple stub tuner not only accounts for the imaginary part of the load, but also the real part. There is an adjustable short on each of the three stubs to change the stub length (within the physical constraints of the tuner). The triple stub tuner used for this experiment is shown in Figure 47.
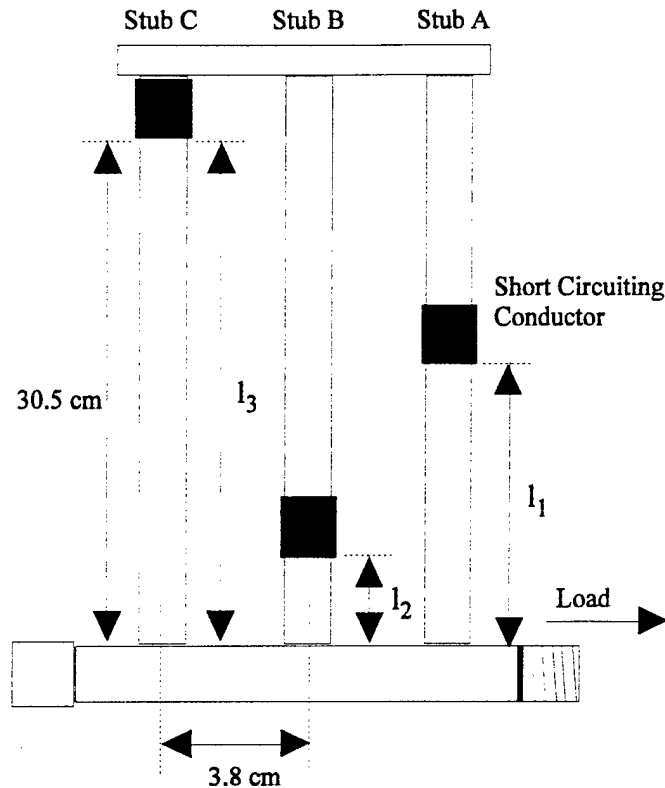
Figure 47. **Triple Stub Tuner Used in Experiment.**

The length of each of the stubs is 30.5 cm (12 inches), based on the maximum distance that the variable shorts can move and not on the total length of the stub. The separation between each stub is 2.8 cm (1.5 inches) as measured from the radial center of two adjacent stubs. There are limitations built into triple stub tuner. The tuner cannot match any impedance at every frequency. The lengths of the stubs and the separation between each stub limit the frequency and impedances that a triple stub tuner can match. Smith Charts make these limitations clear.

A popular way to understand the characteristics of a stub tuner is to analyze it using a Smith Chart. A Smith Chart is shown in Figure 48.
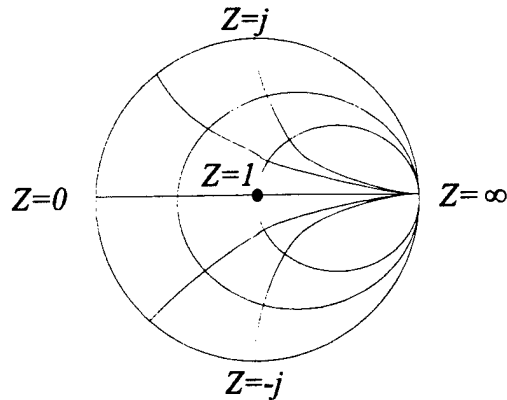
Figure 48.   Smith Chart.

The Smith Chart can calculate the lengths of multiple stubs to match a given impedance. An impedance located at the center of the Smith Chart indicates a perfect match. This corresponds to a normalized impedance of one. The circles are lines of equivalent real impedance and the curved are lines of equivalent imaginary impedance. The circle which stretches from the right side of the chart to the center is termed the 1+jb circle. This is because the real part of the normalized impedance is unity all around this circle. The left side of the chart indicates smaller impedances (larger admittances) and the right side of the chart indicates larger impedances (smaller admittances). Stub lengths are determined by locating the impedance to be matched on the Smith Chart, converting the impedance to an admittance, and then following a series of steps to get to the center of the chart.

If the distance between the radial center of the stubs is 3λ/8 and the stub lengths are at least λ/2, then the stub tuner can match any input impedance.[15] Figure 49 shows what the smith chart looks like for stubs that are 3λ/8 apart. Every circle represents a stub.
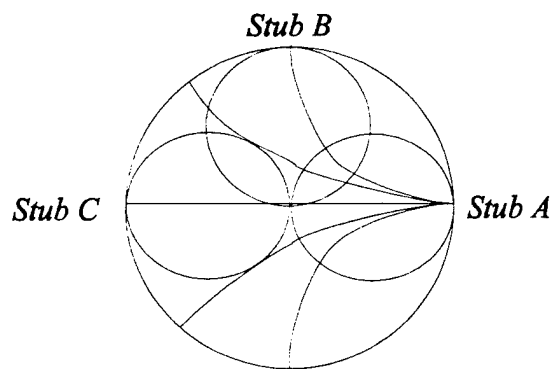
Figure 49. Smith Chart for 3λ/8 stub separation.

One full revolution is half of a wavelength (λ/2) on a Smith Chart. When the stubs are λ/2 apart, there are no possible matches since all of the circles overlap. There is no complex impedance that could be added to an impedance inside of the 1+jb circle to move the impedance out of the 1+jb circle since all of the circles are within each other. The ability to match an impedance is also limited by the length of the stubs on the stub tuner. The longer the stub length, the more impedances that can be matched. The higher the frequency for a given stub length, the more impedances that can be matched. The best matching frequencies can only match every impedance when the wavelength of the frequency being used is no more than λ/2.

9.2.3   Specific Tuner Characteristics

It is very difficult to state specific impedances and frequencies that a triple stub tuner can match, as is explained below, but some observations can be made. The best matching frequencies for any triple stub tuner occur at λ/8, 3λ/8, 5λ/8, etc. The stubs of the tuner tested are 3.8 cm apart and so the corresponding wavelengths that work with the defined stub separations are: 99 MHZ, 300 MHZ, 490 MHZ, etc. Notice that each successive frequency is approximately 200 MHZ greater. Note that the tuner cannot match every impedance for frequencies below 490 MHZ because these lower frequencies have wavelengths such that λ/2 is more than 30.5 cm--the length of the stubs.

86

The worst matching frequencies for any triple stub tuner occur at λ/2, λ, 3λ/2, etc. The frequencies that correspond to these wavelengths for tuner tested are: 390 MHZ, 790 MHZ, 1.2 GHz, etc. Notice that each successive frequency is approximately 400 MHZ greater. These nulls exist within the frequency range of interest but are very narrow and will not make the matching any worse that it would be without the stub tuner. This stub tuner can theoretically match most of the possible input impedances of an asset driven with an UWB pulse (500 MHZ to 3 GHz).

9.2.4 Tuner Characterization Difficulties

It is very difficult to define a parameter space of impedances that a triple stub tuner can match for a given frequency. It is even more difficult to define this parameter space for a frequency range. There are many combinations of stub lengths that can match an impedance at a frequency and one would like to choose the stub lengths that match multiple frequencies well.

Note that the distance in wavelength between each of the stubs will change based upon the frequency being used. This makes it extremely difficult to theoretically determine the best stub lengths to tune frequencies over a large bandwidth. Triple stub tuners are invariably adjusted by trial and error--not by calculation--and so calculations merely demonstrate the general matching conditions that a specific triple stub tuner can achieve.[15] The calculated worst case reflection coefficient for no more than 3 dB of reflection should be

$$\Gamma = 1 - 10^{-\frac{3}{20}} = 0.292$$

or no more than 30% radially from the center point of the Smith Chart.

Figure 50 shows the admittances that cannot be matched for a stub separation of λ/4, 3λ/4, 5λ/4, etc. These admittances translate to higher impedances on the order of three times the characteristic impedance or greater than 150 Ω for a 50 Ω characteristic impedance.
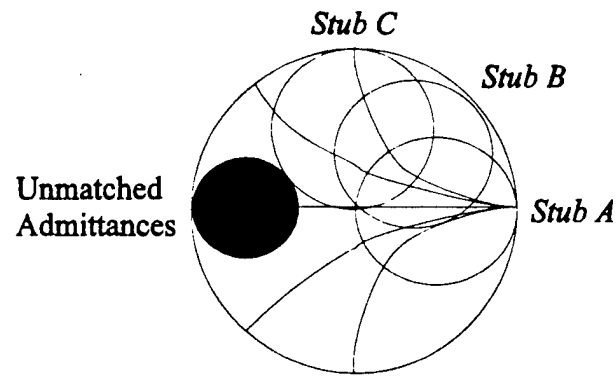
Figure 50.   Unmatched admittances for λ/4 stub separation.

Figure 51 below shows an example of one set of input impedances and Figure 52 shows another.
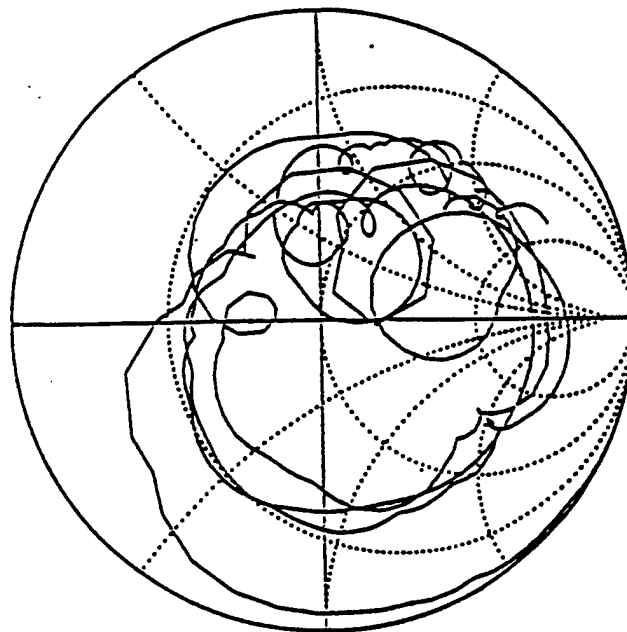
Figure 51.   Input impedance of a test point.

Figure 51 shows the input impedance versus frequency on a Smith Chart for one test point and Figure 52 shows the input impedance for a different test point. The average input impedance in Figure 51 appears to be about 50 Ω while the average input impedance in Figure 52 appears to be about 25+j10 Ω. The input impedance must be measured for every test point so that the absorbed power can be measured and, if necessary, to match the average input impedance. It is wrong to assume that the input impedance of a test point is always 50 Ω--Figure 52 clearly shows that this assumption is not always valid. The triple stub tuner described above is able to match both of these cases fairly well over the specified frequency range.
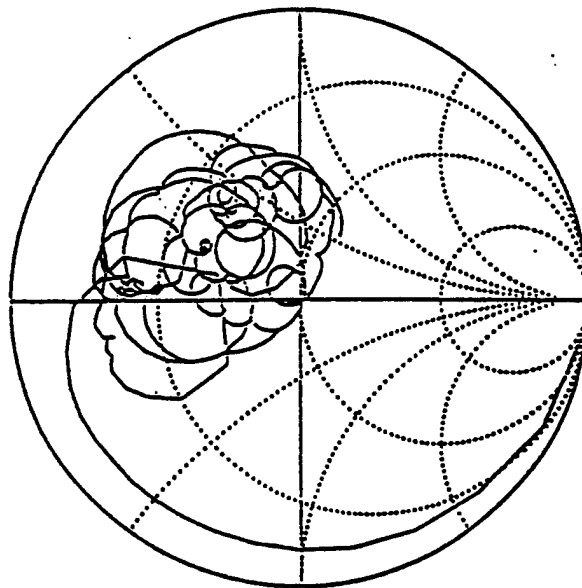
Figure 52.   **Input impedance of another test point.**

10.0 EXPERIMENTS WITH STUB TUNERS FOR NB AND UWB MATCHING

The purpose of this experiment was to determine the bandwidths (BWs) over which the triple stub tuner could inject at least half of the incident power into an asset between 100 MHZ and 3 GHz and to determine if the same bandwidths could be achieved in both narrow band (NB) and ultrawideband (UWB) measurements. A tuner that matches impedances over reasonably large bandwidths causes the asset to absorb more available source power and minimizes the data correction needed to account for an impedance mismatch.

The scope of this experiment was to find the stub tuner positions that result in the largest bandwidths around 100, 200, 300, 400, 500, 600, 700, 800, 900, 1000, 2000, and 3000 MHZ for the asset to absorb at least 50% of the power in one case and 90% of the power in another case. The stub tuner was used in an ultrawideband (UWB) experiment to verify that the specified power levels could still be achieved. Pin 33 of the NATO cylinder was used as the DUT.

10.1 NATO Cylinder Input Impedance

Theoretical calculations of the triple stub tuner lengths can only be done once the load impedance is known for the frequency of interest. Table 5 below lists the input impedances as a function of frequency of the NATO Asset at Pin 33.

Frequency (MHZ)	Real (R)	Imaginary (X)
100	22.45	9.27
200	28.64	4.76
300	114.59	32.01
400	50.89	-6.53
500	59.14	-24.77
600	23.47	-9.22
700	21.69	18.73
800	65.69	51.37
900	58.59	12.36
1000	54.79	-55.14
2000	33.52	25.94
3000	138.42	27.38

Table 5. Input Impedances vs. Frequency of the NATO Asset at Pin 33.

The data above shows that average input impedance of this asset was 56 + j7.18 Ω or about 50Ω. This shows that a normal microwave cable should be close to the best single impedance to match the source impedance to the input impedance of the asset. However, the impedance changes considerably over the frequency range of interest. The stub tuner was used to determine if it could achieve a good impedance match over a broad bandwidth.

10.2   Narrow Band Measurements

A stub tuner was used to illustrate how much of the available power could be inserted into the asset. The experimental setup is shown in Figure 53.

Stub Tuner

Network Analyzer   NATO Asset
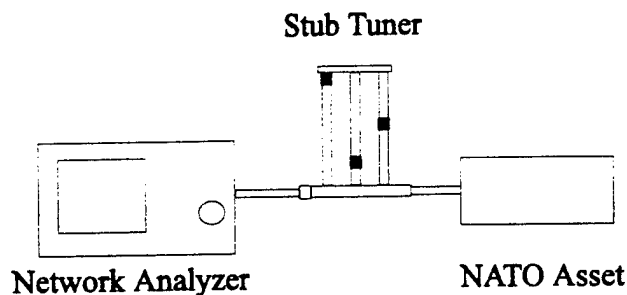
Figure 53.   Narrowband Experimental Setup.

There was approximately six inches of semi-rigid cable between the stub tuner and Pin 33 of the NATO Asset. A HP 8753D Scalar Network Analyzer was used to take a reflection (S11) measurement.

The lengths of the triple stub tuner were varied through guess and check to find widest bandwidths around the frequencies between 100 MHZ and 3 GHz. One common standard of evaluation was chosen and one more strict standard. The more accepted standard was to determine the widest bandwidths that reflected no more than -3 dB of the original signal (S11 less than -3 dB) or in other words that at least half of the power was absorbed by the asset. Table 6 lists the results of this test with extraordinarily large bandwidths in bold numbers.

Shot #	Stop and Start Frequency (MHZ)	Bandwidth (MHZ)	Stub Length (cm)		
			Stub A	Stub B	Stub C
1	150 - 430	280	30.5	20.0	30.5
2	300 - 600	300	12.0	18.0	11.5
3	600 - 840	240	30.5	8.0	30.5
4	840 - 1240	400	6.0	10.0	20.0
5	470 - 1160	690	5.5	5.5	10.0
6	1180 - 2400	1220	14.5	6.5	7.5
7	2500 - 2910	410	12.2	22.0	17.0
8	2700 - 3000	300	12.0	6.5	17.4
9	1000 - 3000	2000	2.2	1.8	1.0
10	450 - 1300	850	7.0	9.0	6.5
11	320 - 950	630	12.0	10.0	11.5

Table 6.   Stub Lengths for S11 < -3 dB Frequency Bandwidths.

These operating bandwidths are specific not only to the asset tested, but also to the test point. The attainable bandwidths for a test point are unique to that test point. The bandwidths listed show that it is possible to use a stub tuner to match impedances over some fairly wide bandwidths (1 GHz) even though the stub tuner is meant to be a narrowband matching device.

Another standard was to determine the widest bandwidths that reflected no more than -10 dB of the original signal (S11 less than -10 dB) or in other words that at least 90% of the power was absorbed by the asset. Table 7 lists the results of this test.

Shot #	Stop and Start Frequency (MHZ)	Bandwidth (MHZ)	Stub Length (cm)		
			Stub A	Stub B	Stub C
12	320 - 450	130	13.5	18.0	11.0
13	450 - 580	130	12.5	15.0	10.5
14	580 - 650	70	15.2	5.2	10.5
15	650 - 690	40	30.5	9.0	4.0
16	680 - 720	40	7.5	6.0	3.5
17	800 - 970	170	1.5	6.0	3.5
18	1040 - 1520	480	3.8	1.5	3.2
19	1200 - 1700	500	3.9	4.0	3.2
20	1900 - 2100	200	2.8	17.8	2.8
21	2900 - 3000	100	0.0	1.8	1.0

Table 7.   Stub Lengths for S11 < -10 dB Frequency Bandwidths.

Large values of stub separation in wavelengths have the disadvantage of a reduced operating bandwidth.[15] In other words, a triple stub tuner can match over broader bandwidths at higher frequencies for a given stub separation. The data in Table 6 and Table 7 show this to be true. Another way to think of this result is that higher frequencies have smaller wavelengths and some integral number of wavelengths has a better chance of interacting with one of the three stubs in such a way that it is matched.

Since it is more difficult to match impedances for the asset to absorb 90% of the power than to absorb 50%, it was expected that the bandwidths attainable for 90% absorption would be smaller than the bandwidths for 50% absorption. Table 6 and Table 7 show this to be true.

10.3   Ultrawideband (UWB) Measurements

The following describes the setup and data that were taken for the UWB test. The stub tuner positions determined through guess and check from the NB test were used in this test to determine if the stub tuner would propagate the same frequency bandwidths in UWB as it did in NB. The experimental setup for the UWB experiment is shown in Figure 54.
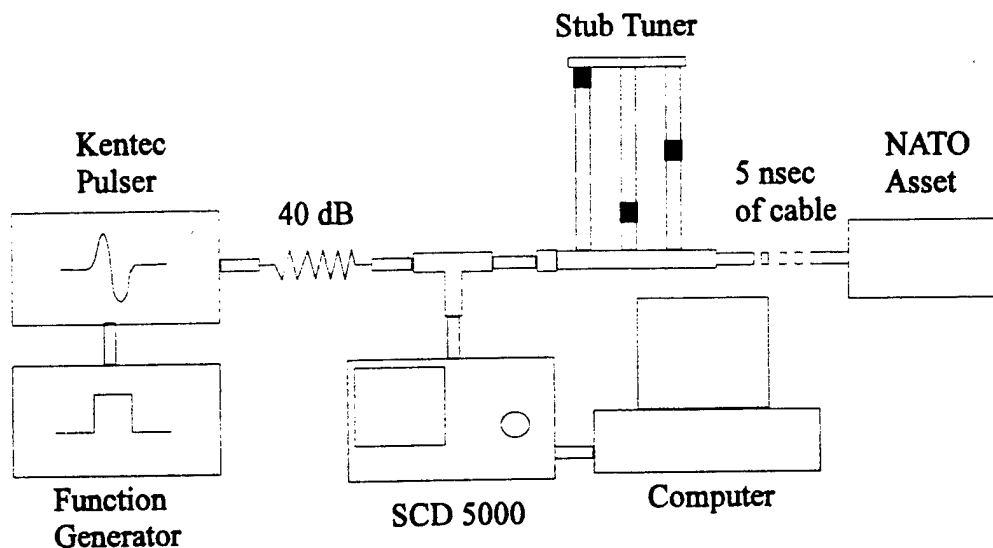
Figure 54.   UWB Experimental Setup.

A Kentec pulser was used to generate the UWB pulse. It has a frequency spectrum with most of the energy between 200 MHZ and 4 GHz. A function generator was used to trigger the pulser. Approximately 40 dB of attenuation was connected to output of the pulser so as not to overdrive the scope and the stub tuner. A digitizing oscilloscope, model SCD 5000 was used to measure the signal that was able to get through the stub tuner. There was 5 feet of cable, which corresponds to a 5 nsec time delay, after the stub tuner so that none of the reflections from the asset were measured. A General Purpose Interface Bus (GPIB) was connected between the scope and the computer to acquire the waveform. The recorded time domain waveform was then imported into the Mathcad software package, where the Fourier transform was performed to obtain the frequency spectrum.

10.3.1   UWB Data

The bandwidths which were transmitted through the triple stub tuner with an UWB pulse is shown in Table 8. They are shown to be very comparable to the NB test. The bolded numbers are extraordinarily large bandwidths.

Shot #	Test Type	Frequency (MHZ)	Bandwidth (MHZ)	Shot #	Test Type	Frequency (MHZ)	Bandwidth (MHZ)
1	UWB	100 - 500	400	12	UWB	400 - 500	100
	NB	150 - 430	280		NB	320 - 450	130
2	UWB	100 - 560	460	13	UWB	350 - 850	**500**
	NB	300 - 600	300		NB	450 - 580	30
3	UWB	620 - 920	300	14	UWB	400 - 850	**450**
	NB	600 - 850	240		NB	580 - 650	70
4	UWB	800 - 1260	460	15	UWB	600 - 900	**300**
	NB	840 - 1240	400		NB	650 - 690	40
5	UWB	450 - 1100	650	16	UWB	600 - 1600	**1000**
	NB	470 - 1160	690		NB	680 - 720	40
6	UWB	2100 -2400	300	17	UWB	700 - 1800	**2100**
	NB	1800 -2400	1220		NB	800 - 970	170
7	UWB	2600 -3000	400	18	UWB		
	NB	2500 -2910	410		NB	1040 - 1520	480
8	UWB	2100 -3000	900	19	UWB	700 - 2200	**1500**
	NB	2700 -3000	300		NB	1200 - 1700	500
9	UWB	950 - 3800	2850	20	UWB	1700 - 2300	**600**
	NB	1000 -3000	2000		NB	1900 - 2100	200
10	UWB	400 - 1300	900	21	UWB	1900 - 2100	200
	NB	450 - 1300	850		NB	2900 - 3000	100
11	UWB	400 - 1000	600				
	NB	320 - 950	630				

Table 8.   Comparison of UWB and NB Bandwidths.

95

Notice that the UWB and NB data compare very well for the first 11 shots but the UWB bandwidths are much larger than the NB bandwidths for shots 12 through 21. This is very odd since shots 12 through 21 had tighter constraints in the NB test. This behavior cannot be explained but it is better than the expected results. This data shows that the triple stub tuner can be used as a broadband impedance matching device.

10.4   Conclusions

Improving the power into the asset is not critical. It is good practice to use resources wisely, however, and cause the asset to absorb as much power as possible. On the other hand, it is critical to know the input impedance of the asset to determine how much power the asset absorbed. Calculating the average input impedance over the frequency range of interest and matching that impedance will transmit more available power into the asset.

10.4.1   NB Measurements

The NB measurements demonstrated that the triple stub tuner can be used to match complex impedances over bandwidths of approximately 500 MHZ for frequencies below 1 GHz and bandwidths of approximately 1 GHz for frequencies above 1 GHz. These bandwidths are exceptional for a narrow band impedance matching device.

It is not feasible to calculate the stub lengths that will match the input impedance of an asset over the desired frequency range. The general matching limitations of the triple stub tuner eliminate some of the possible impedance and frequency configurations, but one must proceed through trial and error to determine the best stub lengths to match the input impedance of the asset over the frequency range of interest. This experiment showed that a triple stub tuner can match frequencies over a broad frequency range.

10.4.2   UWB Measurements

The UWB measurements showed that a triple stub tuner will work with an UWB source. The bandwidths that can be matched in UWB are predicted well by the NB measurements. Even though the attainable bandwidths are less than the bandwidths of typical UWB sources (200 MHZ to 8 GHz), more power is absorbed by the asset and to get more power into the total range of frequencies, different matching bandwidths may be used in different UWB shots.

11.0 CORRELATION BETWEEN POWER LEVELS OBTAINED WITH FREE FIELD HPM TESTING AND DIRECT DRIVE EXPERIMENTS

It is has been documented[2] that good correlation is obtained between the results from directly driving inductive coupling probes along a line and free field HPM testing when the bundle lengths are electrically short ($2\pi L/\lambda \ll 1$). When direct injection testing is conducted by directly driving a voltage signal from a generator into the circuit node, the upset levels are expected to directly correspond to free field testing. This expectation, that the power levels necessary to induce an effect in direct drive experiments and free field testing are equivalent, may be faulty. In this interest, a correlation factor has been derived for the experimental values obtained with direct drive experiments to compare with free field testing.

Direct drive testing is a useful tool for simulating the impinging electromagnetic field incident from a free field source on a subsystem. This may yield valuable information about the nature and frequencies of interest to induce electromagnetic effects; it could also identify critical subsystems. Free field testing is the unequivocal demonstration of an electromagnetic effect on a DUT. Direct injection testing is a simulation tool, and, thus, it is the responsibility of the experimenter conducting direct drive tests to adjust the data to correlate to free field power levels. However, as part of this technical effort, it has been recognized that free field radiation penetrates into an electronic system differently than a voltage signal. Thus, a quick look model has been developed to investigate the magnitude of the difference.

It should be noted that while the one port circuit model is appropriate for a direct drive test, it is inappropriate for a free field test scenario. In free field testing, the impinging radiation enters into multiple ports simultaneously. Thus, the one port analysis for which this correlation factor is based is subject to experimental conditions. Namely, the signal is injected directly into a circuit node through a transmission line which may also involve an isolating resistor. The correlation factor can be used to predict free field power levels to induce an effect in a subsystem, but the reverse is not true. That is, the correlation factor cannot be used with free field power levels to predict direct injection power levels.

The crux of the correlation issue may be the node impedance to ground of the circuit under test. This impedance affects the power absorbed into the node of the DUT in both free field and direct injection excitation. Since the absorbed power is the quantity which produces an electromagnetic effect, by equating the power absorbed in a free field test and a direct injection test, a correlation factor between the two can be derived. Presently, the correlation between free field power levels and direct injection power levels is assumed to be 1:1. However, by modeling the electromagnetic effects test by transmission lines, which is valid for high frequencies, the correlation factor is shown to vary over two orders of magnitude.

The model for a direct drive experiment is shown in Figure 55. A source is connected to the DUT with a transmission line of characteristic impedance, Z_0. The circuit node, which is connected in the diagram to the transmission line has an impedance to ground, $Z_n(f)$, which is generally a function of frequency.
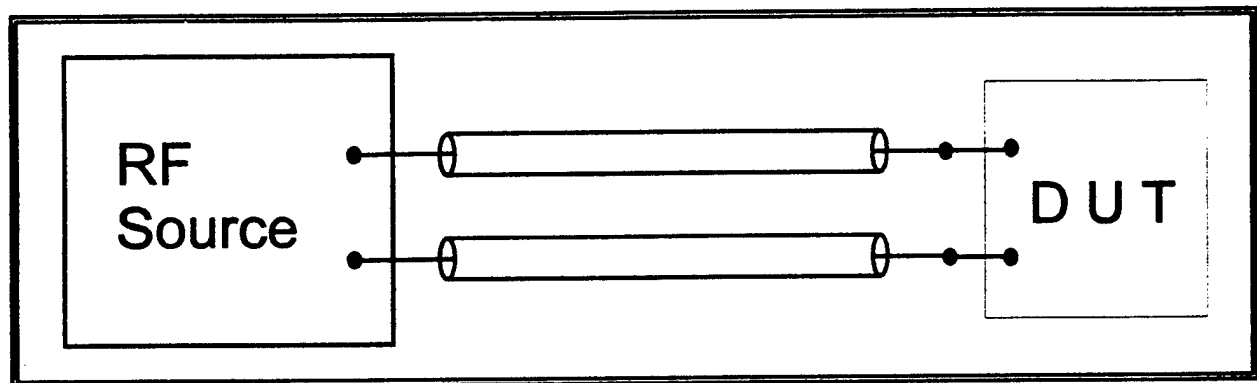
Figure 55. **One port circuit model for a signal being injected into a node of the DUT in a direct injection test. The absorbed power is the quantity of interest.**

For simplicity, assume the transmission line is electrically matched to the source impedance. The reflection coefficient, Γ^{DD}, for the direct drive circuit is given by,

$$\Gamma^{DD} = \frac{Z_n(f) - Z_0}{Z_n(f) + Z_0} \; .$$

98

The absorbed average power, P_A, is related, in a general sense, to the incident power, P_{inc}, by,

$$P_A = P_{inc} (1 - |\Gamma|^2) \ .$$

where Γ is the reflection coefficient. Thus, the power absorbed into the circuit in the direct injection test is fully determined by the reflection coefficient, $\Gamma^{DD}(f)$.

A similar expression can be derived for free field testing. The experimental setup for a free field test is shown in Figure 56. The electromagnetic wave is radiated through the antenna, which impinges a plane wave on the device under test (DUT).

Figure 56. **The experimental setup of a free field test.**

If the HPM source is set sufficiently far from the DUT, and the frequency of the excitation is such that

$$\frac{c}{f} \ll d \ ,$$

99

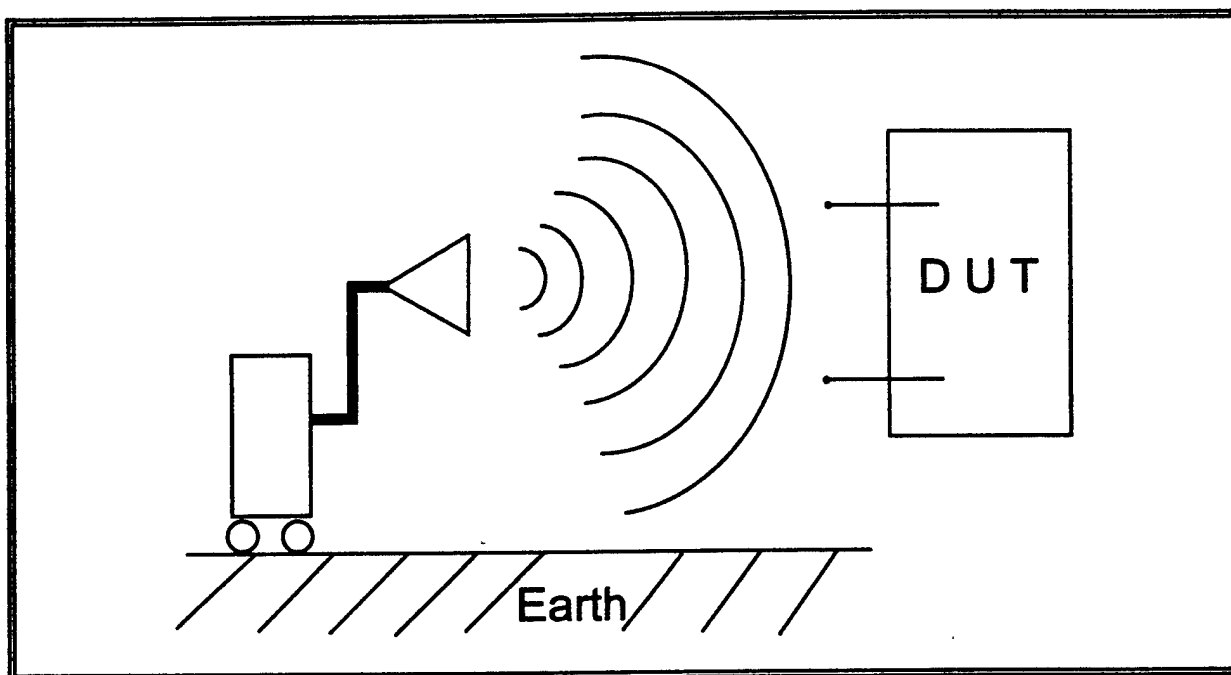where d is the distance between the radiating antenna and the DUT, the experimental setup may be modeled as shown in Figure 57.
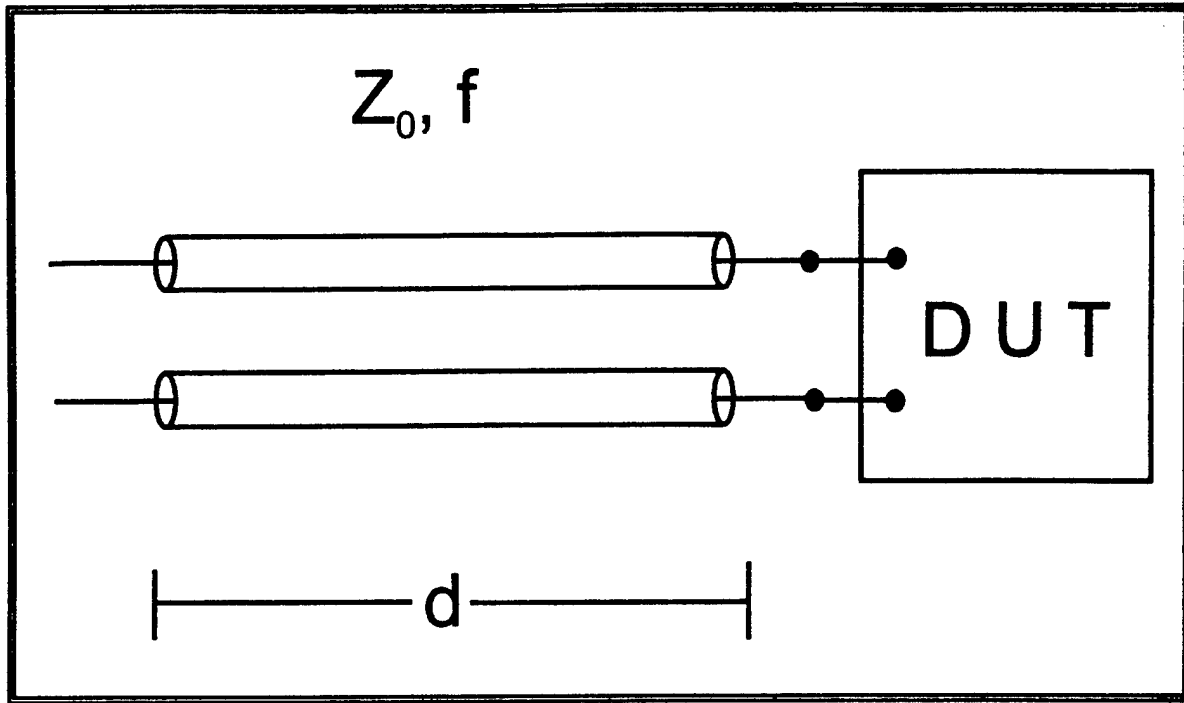
Figure 57. **The equivalent model of the free field experimental setup of Figure 2, coupling into a two port circuit, under the condition, c/f << d.**

The radiated HPM signal is represented by a lossless transmission line with characteristic impedance, $Z_0^{Air} = 377 \ \Omega$. The reflection coefficient, Γ^{FF}, for the equivalent circuit is given by,

$$\Gamma^{FF} = \frac{Z_n(f) - Z_0^{Air}}{Z_n(f) + Z_0^{Air}} \ .$$

The node impedance, $Z_n(f)$ is the same under each type of excitation. Thus, the reflection coefficients, Γ^{FF} and Γ^{DD} are not equal if Z_0^{Air} and Z_0 are different. This implies that the power absorbed into the asset at the insertion node is different for direct injection and free fields testing, for equivalent incident powers. Thus, for numerically different reflection coefficients, Γ^{FF} and Γ^{DD}, the absorbed power is different for the two experiments. .

Recognizing that the absorbed power is the relevant quantity for comparison, since the

absorbed power results in an effect, leads directly to a correlation factor. Equating the expressions for the absorbed power for free field and direct drive tests, one obtains the following relation,

$$P_{inc}^{FF} = P_{inc}^{DD} \left[\frac{1 - |\Gamma^{DD}|^2}{1 - |\Gamma^{FF}|^2} \right] \ .$$

Thus, the correlation factor for direct drive experiments is expressed as,

$$Correlation \ Factor = \frac{1 - |\Gamma^{DD}|^2}{1 - |\Gamma^{FF}|^2} \ .$$

When $Z_n(f)$ for the node under test has been measured, the reflection coefficients, Γ^{FF} and Γ^{DD}, can be computed. To illustrate the effect this correction factor can have on the comparison of experimental results, let $Z_n(f)$ and Z_0 be constant 50 Ω impedances. Thus, the reflection coefficient for the direct drive setup in this matched case is 0. The correction factor is calculated from the above expression as

$$Correlation \ Factor = \frac{1}{1 - \left(\dfrac{50 - 377}{50 + 377} \right)} = 2.4 \ .$$

The variation of the correlation factor changes dramatically with the load impedance. Suppose $Z_n(f)$ is a real number which does not vary with frequency. The magnitude of the correlation factor changes with this load impedance as shown in Figure 58.
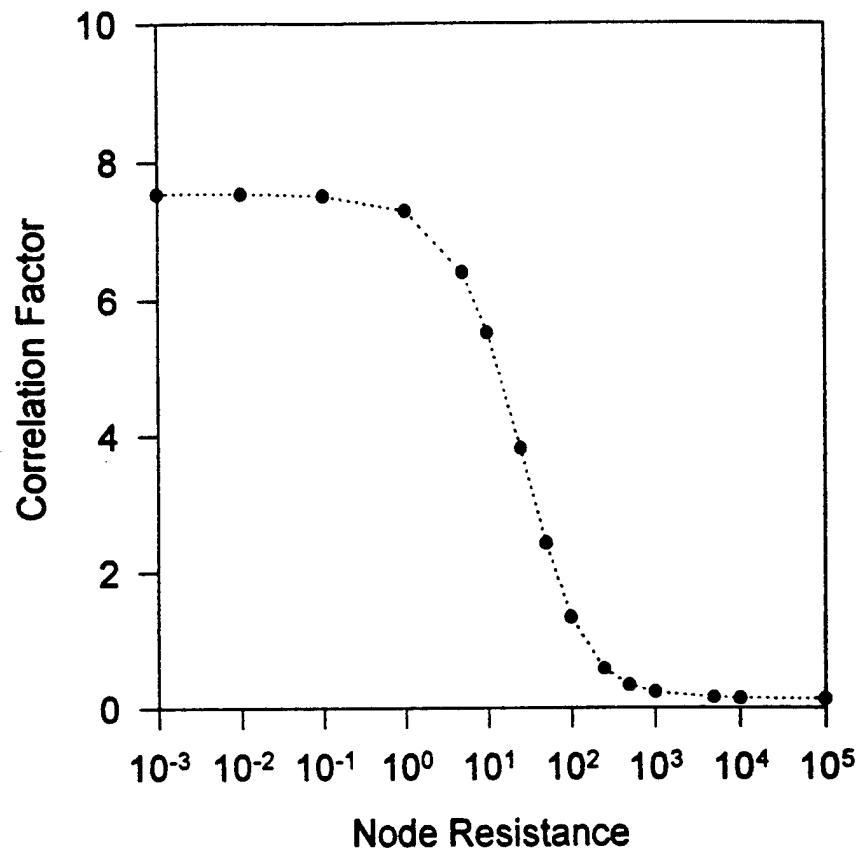
Figure 58.   The variation of the correlation factor when the node has a real constant load impedance. The correlation factor changes from 7.5 at 10^{-3} Ω to 0.13 at high resistance. The range in the correlation factor holds when the load also has a reactive component.

In general, the load impedance is a complex quantity. If both Z_0^{Air} and Z_0 are real, the expression for the correlation factor for a general complex load can be expressed as,

$$Correlation\ Factor = \frac{Z_0}{Z_0^{Air}} \frac{|Z_n(f)|^2 + 2Z_0^{Air}Re(Z_n(f)) + (Z_0^{Air})^2}{|Z_n(f)|^2 + 2Z_0 Re(Z_n(f)) + (Z_0)^2}$$

where $Re(Z_L(f))$ is the real part of the complex impedance, $Z_L(f)$.

The derived equation for the correction factor shows a range from 0.13 to over 7.5 when the node impedance is purely resistive. This range is applicable in the general case of a complex node impedance also. It should be noted that if a resistive isolation is used between the direct drive source and the node of the DUT, the above equations must be rederived based on the power absorbed. The correlation factor will allow for an improved prediction of the power levels necessary in free field testing to induce electromagnetic effects that are comparable to those obtained via simulation from direct drive tests.

12.0 CONCLUSIONS

Direct injection testing is an economical simulation tool for free field electromagnetic effects testing. It is particularly useful to identify susceptible subsystems and new electromagnetic effects prior to a full scale free field test. However, as the frequencies of interest have increased, the validity of data obtained with direct injection has become unreliable. We have identified and addressed several key procedural and diagnostic reasons for the unreliability of the data.

Typically, during a direct injection measurement, the voltage at various nodes is monitored. However, the parameters of the voltage probes are currently not being chosen in conjunction with the parameters of the circuit under test. This can result in drawing excessive current from the circuit and a loss of probe sensitivity. Maximum probe sensitivity is attained when the input resistance of the voltage probe is chosen to be ten times the resistance of the node under test at the test frequency. This, of course requires that the impedance of the node under test be measured prior to probe selection.

Moreover, the voltage probes which are commonly used have long been known to degrade with increasing frequency. The degradation in performance with increasing frequency has been identified as being mainly due to capacitive coupling over the resistive element. The effects of intrinsic capacitance and inductance in voltage dividing probes have been investigated by circuit simulation of the equivalent probe circuit. A decrease in the voltage dividing ratio is identified as a shunt capacitive effect and an increase in the metric with inductive effects. It is desirable to minimize the shunt capacitance of voltage probes for two reasons. First, capacitive effects determine the bandwidth of the voltage probe and thus, degrades its performance, even within the bandwidth. Secondly, the voltage probe can also capacitively load the circuit under test. The effects of capacitively loading the circuit manifest differently for wideband and narrowband systems, which is documented in the text.

Preliminary experimental results document the effect of the impedance of the device under test on narrowband excitations. The measured voltage dividing ratio varies wildly in the frequency range of 10 MHz to 1 GHz. The cause of the variation in the metric is the establishment of standing waves caused by an impedance mismatch in the system. An

experiment was devised to evaluate the performance of the voltage probe with frequency, exclusive of the circuit under test. By changing the type of resistor used in the voltage dividing probes, probe transfer function which show no degradation in performance with frequency to 3 GHz have been demonstrated. Coaxial transmission lines have been used in the past as voltage probes. This technique shows an excellent frequency response, but must be used with care, since the likelihood of circuit loading is greatly increased due to the low input impedance.

In addition to measuring techniques, it was found that many test engineers have been measuring the incident power necessary to induce an electromagnetic effect. While this is a valid measurement when conducting free field testing, the absorbed power is the truly relevant measurement for direct injection testing. Techniques for increasing the absorbed power in direct injection testing for narrowband and wideband direct drive testing are outlined. Moreover, this treatment of the absorbed power has lead to the an order of magnitude calculation of a correlation factor for use with direct injection data. A thorough treatment for the derivation of a correlation factor will allow for an improved correlation between free field measurements for electromagnetic effects testing, and its simulation from DIT.

13.0 RECOMMENDATIONS FOR FUTURE RESEARCH

This effort was conducted so as to address, specifically, the problems associated with performing direct injection testing on very compact electronic systems. Thus, the restrictions on the construction of the voltage probe were severely limited and the goal was to improve the frequency response of the design presently in use. This task was successfully accomplished, and exceeded the requirements. However, when the physical size limitation is relaxed, the possibility for other voltage probes designs should be investigated. For instance, there is some questions as to the best method to ground the voltage dividing probes to the system ground. It is known that a low inductance connection is desirable, but a well documented method of doing so in complex electronic systems has not been investigated. Moreover, as the frequencies of interest is increased, good system grounding topology becomes increasingly important.

This effort raised the issue of the correlation between free field testing and direct injection testing. Currently, the power levels for upset, obtained by direct injection, are combined with coupling crosssections to obtain an equivalent free field power density. The validity of this practice needs to be examined fully. The brief treatment accorded here to this topic quantified the difference in the coupling of free field radiation and direct voltage signal injection to a node in an unrealistically simple model.

Typically, power levels for upset at a given frequency are quoted as the relevant quantities. However, notably for ultrawideband signals, the peak power does not reflect the pulse parameters; the pulse width, pulse repetition frequency, duty cycle and burst duration are critical parameters. Similarly, for narrowband signals, the burst duration is a critical parameter. To account for these variables, the total energy may be a more useful scaling parameter for electromagnetic effects testing.

References

[1] J. W. Adams, J. Cruz, and D. Melquist, "Comparison Measurements of Currents Induced by Radiation and Injection," Trans. Electromag.Compat., Vol. 34, no. 3, pp. 360-362, Aug, 1992.

[2] D. A. Hill, "Currents Induced on Multiconductor Transmission Lines by Radiation and Injection," Trans. Electromag.Compat., Vol. 34, no. 4, pp. 445-450, Nov, 1992.

[3] V. Peckham, "Requirements and Specifications for a High Frequency Direct Drive Coupler," Kaman Sciences Corp., DC-TR-8006.405-1, June, 1990.

[4] Pulse Generators, Radiation Laboratory Series, G.N. Glasoe and J.V. Lebacqz, Eds., McGraw Hill, New York, pp. 670, 1948.

[5] Joe Weber, Oscilloscope Probe Measurements, Tektronix Measurement Series, Tektronix, Inc., 1969.

[6] Harold Kinley, "Test Equipment Loading Effects," Technically Speaking, Mobile Radio Technology, pg. 8, May, 1996.

[7] H. N. Lavally, T.J. Kearns, and R.N. Randall, "Electromagnetic Testbed Aircraft (EMPTAC) Test #8 Report," UIE-TR-93-0018, August, 1993.

[8] William H. Hayt, Jr. and Jack E. Kemmerly, Engineering Circuit Analysis, McGraw-Hill 1978.

[9] S. S. Haykin, Active Network Theory, Addison Wesley Publishing Co., 1970.

[10] Walter E. McAbel, Measurement Concepts, Tektronix Measurement series, Tektronix, Inc., 1969.

[11] Steven D. Swift, "Build the Fast Pulser Scope Calibrator," Electronics Now, October, 1996.

[12] T. S. Bowen, J. E. Lawrence, and J. Bolme, "Direct Injection Test Report for the SNR Cylinder," Phillips Laboratory, April, 1993.

[13] R. E. Collin, Foundations for Microwave Engineering, McGraw-Hill, N.Y., 1966.

[14] David M. Pozar, Microwave Engineering, Addison-Wesley, 1990.

[15] R. Chipman, Schaum's Outline of Theory and Problems of Transmission Lines, McGraw-Hill Book Co.

DISTRIBUTION LIST

AUL/LSE
Bldg 1405 - 600 Chennault Circle
Maxwell AFB, AL 36112-6424   1 cy

DTIC/OCP
8725 John J. Kingman Rd, Suite 0944
Ft Belvoir, VA 22060-6218   2 cys

AFSAA/SAI
1580 Air Force Pentagon
Washington, DC 20330-1580   1 cy

PL/SUL
Kirtland AFB, NM 87117-5776   2 cys

PL/HO
Kirtland AFB, NM 87117-5776   1 cy

Official Record Copy
PL/WSM/ATTN: Maj Paul R. Barré   3 cys

PL/WSME/Lt Eric Johnson
Kirtland AFB, NM 87117-5776   1 cy

PL/WSME/Mr Hector Del Aguila
Kirtland AFB, NM 87117-5776   1 cy

PL/WSME/Dr Greg Nelson
Kirtland AFB, NM 87117-5776   1 cy

PL/WSME/Mr Steve Langdon
Kirtland AFB, NM 87117-5776   1 cy

PL/WSME/Mr Sam Guiterrez
Kirtland AFB, NM 87117-5776   1 cy

Fiore Dinustries, Inc
c/o Bill Miera, Dr Lehr, Mr Sizemore   3 cys
5301 Central Ave NE, Suite 900
Albuquerque, NM 87108

PL/WSMA/Dr Tracey Bowen
Kirtland AFB, NM 87117-5776   1 cy